New developments in medical imaging

The potential and clinical applications in otolaryngology and head and neck disease

Sylvia Louise van Egmond

New developments in medical imaging

The potential and clinical applications in otolaryngology and head and neck disease

Sylvia Louise van Egmond

New developments in medical imaging
The potential and clinical applications in otolaryngology and head and neck disease

ISBN: 9789090316710

Design and lay-out: Wendy Schoneveld || www.wenzid.nl
Printed: ProefschiftMaken || Proefschiftmaken.nl

The author gratefully acknowledges the financial support for publication of this thesis by: Afdeling KNO-Heelkunde, LUMC, Leiden | PENTAX B.V. | Mylan Healthcare B.V. ZEISS | EmiD audiologische apparatuur | Michel Keijzerfonds/Patiëntenvereniging HOOFD HALS | Dos Medical B.V. | Atos Medical B.V. | MediTop Medical Products | ALK

New developments in medical imaging:

The potential and clinical applications in otolaryngology and head and neck disease

Nieuwe ontwikkelingen in medische beeldvorming:

Het potentieel en de klinische toepassingen bij keel-,neus- en oorheelkunde en ziekte van het hoofd hals gebied
(met een samenvatting in het Nederlands)

Proefschrift

ter verkrijging van de graad van doctor aan de Universiteit Utrecht
op gezag van de rector magnificus, prof.dr. H.R.B.M. Kummeling,
ingevolge het besluit van het college voor promoties
in het openbaar te verdedigen op
maandag 20 mei 2019 des middags te 2.30 uur

door

Sylvia Louise van Egmond

geboren op maandag 14 september 1981
te De Bilt

Promotoren: Prof. dr. C.H.J. Terhaard
Prof. dr. W. Grolman

Copromotor: Dr. L.M. Janssen

Table of Contents

APPENDICES

CHAPTER 1

General Introduction

THE HISTORY OF MEDICAL IMAGING

Medical imaging began in 1895 with the discovery of the X-ray by German professor of physics Wilhelm Conrad Roentgen. He was working with an early cathode ray tube called a Crooke's-Hittorf tube, when he noticed that the invisible rays were able to penetrate tissues (like skin or muscle) better than others (like bone or metals). Nearly two weeks after his discovery, he took the very first picture of his wife's hand using X-rays. For his discovery and scientific work he was awarded the first Nobel Prize in 1901. Film replaced glass plates for visualizing radiographic images in the mid-1920s . The original X-ray films had to go to a wet developer process in a dark room. As the X-ray beam became more powerful, "fluoroscopy" became possible. In the 1920s, radiologists began giving patients radio-opaque barium as a swallow and taking films as the barium passed through the gastrointestinal tract. In the 1940's X-ray tomography was introduced. Tomography is from the Greek word *"tomos"* meaning "slice" or "section" and *"graphia"* meaning "describing". By rotating an X-ray tube, only a 'tomogram' or slice of tissue stayed in focus without the surrounding tissues being seen. In the earliest days, a head x-ray could require up to 11 minutes of exposure time. Now, modern x-rays images are made in milliseconds and the x-ray dose currently used is as little as 2% of what was used for that 11 minute head x-ray 100 years ago. Furthermore, modern x-rays have significantly more spatial resolution and contrast detail. This improved image quality allows the diagnosis of smaller pathology that could not be detected with older technology.

In the 1950s, nuclear medicine came into play. One of the most clinically relevant studies for oncology is positron emission tomography (PET) scanning. An isotope emits positively charged electrons, called positrons. These positrons combine with a local electron and annihilate, emitting two photons in opposite directions. By noting the arrival time of the two photons at the detectors around the patient ("coincidence detection"), the source of emission can be localized in space. Most PET is based on a positron-emitting isotope of fluorine (F-18) that is incorporated into a glucose analog called fluorodeoxyglucose (FDG). Since glucose uptake is increased in most cancers, FDG PET especially has its clinical application in primary and metastasized malignancies. When the metabolic, low resolution, information of PET is combined with the high spatial resolution of CT, PET CT has a wide clinical applicability, e.g. for tumor localization, regional or distant metastatic spread, biopsy localization, identification of recurrent disease or radiotherapy.

In 1967 Sir Godfrey Hounsfield in England invented the first commercially viable computed tomography (CT) scanner. Hounsfield used gamma rays (and later x-rays).

X-rays that are not absorbed, reflected, or refracted as they pass through the body are picked up by a detector attached to a special rotating frame. Together with a digital computer, detailed cross sectional images of objects can be created. The first clinical CT scanners were installed between 1974 and 1976. Early CT units produced basic images on a 64x64 matrix. The first CT scanner by Hounsfield took several hours to acquire the raw data for a single scan and more than 24 hours to reconstruct these data into single images. Today's multi-slice CT systems can collect up to 4 slices of data in about 350 ms and reconstruct a 512 x 512-matrix image from millions of data points in less than a second. Iodinated contrast agents are used with CT since they block X-rays based on their density compared with that of normal tissue.

Magnetic Resonance Imaging MRI also evolved during the 1970s and is regarded to be invented by Paul C. Lauterbur, a Professor of Chemistry at the State University of New York, in September 1971. Peter Mansfield of Nottingham, England, further developed the utilization of gradients in the magnetic field. He developed the echo-planar technique, which allows images to be produced in seconds and later became the basis for fast MR imaging. Both were awarded a Nobel prize in 2003. MRI was originally called 'NMRI' (nuclear magnetic resonance imaging). MRI makes use of the magnetic properties of certain atomic nuclei. Most often, hydrogen atoms are used, because it is so abundant in de human body - water constitutes about two-thirds of the human body weight- and because its nucleus (a single photon) has a property known as spin. The hydrogen nuclei behave like compass needles that are partially aligned by a strong magnetic field in the scanner. The exact resonance frequency depends on the local value of the magnetic field. The nuclei can be rotated using radio waves, and they subsequently oscillate in the magnetic field while returning to equilibrium. Simultaneously they emit a radio signal. This is detected using antennas (coils), localizing the signal in space. By varying the parameters of the radiowave pulse sequence, different contrasts may be generated between tissues based on the relaxation properties of the hydrogen atoms in the tissues. By advanced computer processing, it is possible to build up a three-dimensional image that reflects the chemical structure of the tissue, including differences in water content and in movements of the water molecules. This results in a very detailed image of the area of interest. The advantages of MRI over other imaging modalities include absence of ionizing radiation, superior soft tissue contrast resolution, high-resolution imaging, and multiplanar imaging capabilities. In head and neck oncology, the superior soft tissue contrast resolution of MRI compared to CT has its benefits for skin carcinoma's, salivary gland tumors, paraphayngeal space tumors. Also, MRI can discriminate tumor from mucous retention in nasal cavity/sinus tumors, it can identify perineural and intracranial tumor spread,

it can detect early bone invasion due to an altered bone marrow signal and MRI has superior tumor delineation in the soft tissues of the head and neck, including oral cavity carcinomas.

Development in MRI techniques is evolving very fast. In 1980s and 1990s, superconducting magnets became common, initially at 1.5 Tesla (measure of magnetic field strength). Nowadays, MRI units as high as 7 Tesla are in clinical use. To put things in perspective, the earth's magnetic field is .00005 Tesla. Thus a 7 T magnet has a field strength 140.000 times stronger than that of the earth. Even higher magnetic fields up to 17.6 Tesla are available, but only for scanning ex vivo or scanning of animals [1].

The sensitivity of MRI to motion also allows us to image microscopic water motion ("diffusion imaging"). Le Bihan published an article in Radiology in 1986, which describes this diffusion weighted imaging (DWI) technique [2]. Nowadays, MR DWI has a wide range of clinical use. Since the 1990's, diffusion weighted imaging (DWI) sequences have proven to be a valuable tool for gathering information of cellular density of human tissues. Diffusion weighted MRI is based on the random, microscopic movement of water and other small molecules due to thermal collisions, the Brownian motion. In a perfectly homogeneous medium, diffusion is random and isotropic. But since the human body is a complex environment, existing of intra- and extracellular compartments, water molecules can experience a difference in diffusion. In extracellular environments, they experience relative free diffusion. In intracellular compartments, diffusion is more restricted. Even more in pathological processes with an increased cellular proportion, for example high grade malignancies. Therefore, DW MRI adds functional information about tissue density to the anatomical information gathered by conventional MRI sequences. It is easy to implement and adds very little time to standard MR examination protocols. The parameter "*b* value" decides the diffusion weighting and is expressed in s/mm^{2}. Diffusion is qualitatively evaluated on trace images and quantitatively by the parameter called apparent diffusion coefficient (ADC). Tissues with restricted diffusion are bright on the trace image and hypointense on the ADC map.
DW MRI had great potential for the differentiation of head and neck abnormalities, especially the detection of malignancy [3]. Differences in ADC can differentiate squamous cell carcinoma from lymphoma and benign neck disease from regional metastasis. Wang et al reported that ADC less than 1.22×10^{-3} mm^2/s has 86% predictive accuracy for malignancy with 84% sensitivity and 91% specificity [4]. It can also be a helpful in selection of the appropriate location for biopsy or, after (chemo)radiation, discriminate between residual or recurrent tumor versus post-treatment changes [5].

APPLICATIONS OF IMAGING IN EAR NOSE AND THROAT DISEASE

Benign otolaryngology disease

Middle ear

The middle ear is an air-filled space, located between the external ear canal and the cochlea [figure 1]. Sound vibrations are conducted from the eardrum to the oval window (the entrance of the cochlea in the inner ear) by the ossicular chain, including the malleus, incus and stapes. The middle ear acts as an amplification system. Both the difference in surface area between the ear drum and the oval window, as well as the ossicular lever (from malleus to incus) results in a sound pressure gain. This pressure gain corrects for the mismatch in impedance between the low-impedance air and the high-impedance liquid of the cochlea. For the tympanic membrane to have maximal mobility, the air pressure within the middle ear must equal that of the external environment. The Eustachian tube acts as a pressure release valve to adjust the middle ear pressure. A negative pressure in the middle ear can lead to retraction of the ear drum.

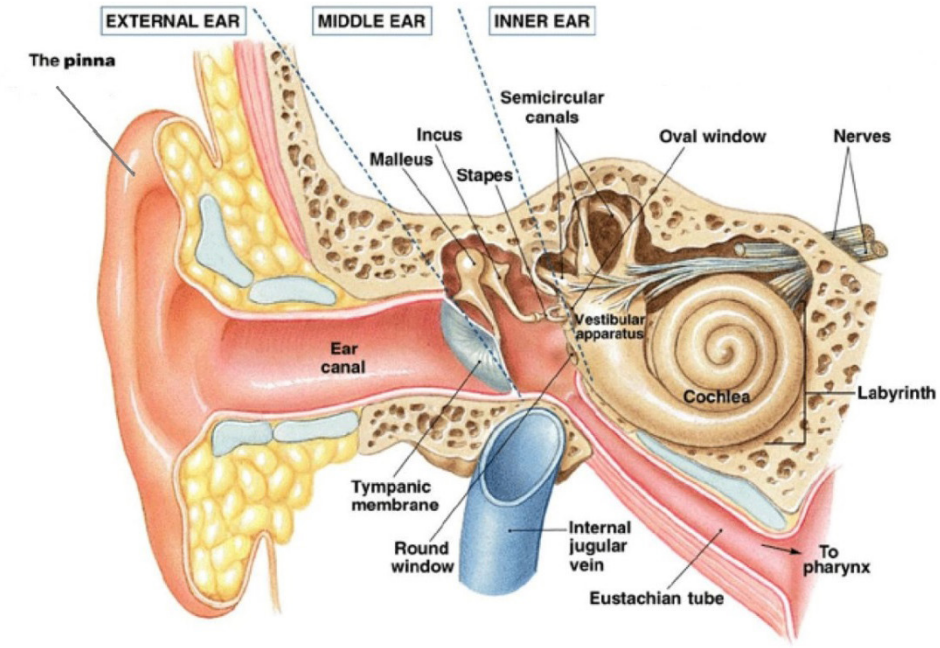

Figure 1: anatomy of the middle- and inner ear

When the eardrum is retracted or as a result of injury to the eardrum (perforation of surgical manipulation) a middle ear cholesteatoma can occur. This is a benign skin-lined cyst, consisting of keratin within a sac of squamous epithelium. Cholesteatoma can be congenital or acquired. The congenital form is usually identified behind a normal looking ear drum. The acquired form begins at the margin of the eardrum and invades the middle ear and mastoid, potentially causing damage to the ossicles and/or other surrounding structures. As a result, patients can present with a combination of conductive hearing loss (a diminished conduction of sound waves in the ear), ear drainage and/or granulation tissue in the ear canal/middle ear which is unresponsive to therapy, and/or vertigo (dizziness caused by functional deficits of the labyrinth). If left untreated, cholesteatoma has the potential to cause major complications, including sigmoid sinus thrombosis, epidural abscess or meningitis.

When a cholesteatoma cannot be removed through otoscopy on the Out Patient Department (OPD), it warrants surgical exploration. Middle ear cholesteatoma surgery is traditionally divided into canal-wall-up (CWD) or canal-wall-down (CWD) surgery, depending on whether the posterior canal wall is preserved. After a CWD procedure, an open mastoid cavity remains which requires regular follow up visits for removal of wax accumulation. Other drawbacks are water intolerance, infections, difficulty in fitting a hearing aid (when necessary) and vertigo due to temperature changes through water or air [6]. The cavity is usually easy to inspect and recurrent cholesteatoma can be detected and removed on clinical otoscopy. Adversely, after CWU surgery, the canal wall remains intact, preserving the anatomy, but blocking the view of the middle ear and mastoid cavity. CWU cases are therefore associated with a higher risk of residual (up to 36%) and recurrent (up to 18%) disease than CWD cases [7]. In case of CWU surgery, a staged or 'second-look' procedure, that is planned months to years after the first operation, is advocated to detect residual or recurrent cholesteatoma, and, in case of absence of cholesteatoma, to reconstruct the ossicular chain and restore hearing.

A third type of surgery involves reconstruction or repair of the posterior ear canal wall combined with obliteration of the mastoid cavity. The various reconstruction and repair methods use cartilage,

bone, fascial and muscle grafts or synthetic material. This technique is demonstrated to significantly lower the residual and recurrence rates of cholesteatoma while keeping the original posterior canal wall intact as well [Harris]. An analysis of 640 patients identified a failure rate of between 5.3% and 20% [6]. Because of the recent surgical shift to this type of surgery, results are based on a much smaller patient group compared with the open or canal wall up surgery groups. The positive results of the obliteration surgery implies that cholesteatoma surgery can become a one stage procedure including both resection of the cholesteatoma and reconstruction of the hearing. This

has significant gain for the patient but also for hospital health care resources. But also urges the need for reliable diagnostic imaging to detect residual or recurrent disease, which would be otherwise detected during a second look procedure.
When a CT scan is performed, a grey mass in the middle ear can be seen, with erosion of the scutum (a sharp bony spur formed by the superior wall of the external auditory canal and the lateral wall of the tympanic cavity). However, a CT cannot discriminate between granulation tissue and cholesteatoma. Diffusion Weighted (DW) MRI can. Cholesteatomas are hyperintense on DWI images compared with Cerebro Spinal Fluid (CSF) and brain parenchyma. Debate is whether this is caused by diffusion restriction or by a T2 shine-through effect [8,9,10]. The T2 shine-through effect is caused by the bright signal of epidermoid cysts on standard T2-weighted images.
Our **clinical question** was to evaluate the diagnostic accuracy of DW for the detection of primary and/or residual or recurrent cholesteatoma. In the latter, DW MRI may avoid the need for second look surgery and advocate a one stage surgery including hearing restoration with or without mastoid obliteration.

Inner ear

The inner ear, including the cochlea and labyrinth, is a complex structure. Images of the inner ear anatomy are shown in figure 2. Whereas the middle ear acts as an amplification system for sound waves, the inner ear is a sensorineural receptor organ, converting an acoustic waveform into an electrochemical stimulus that can be transmitted to the Central Nervous System (CNS). Pathology of the cochlea or the signaling pathway beyond the cochlea, along the 8th cranial nerve or other areas of the central auditory system can result in sensorineural hearing loss (SNHL). Depiction of the cochlea in more anatomical detail has its benefits for accurate diagnosis, localization of pathology and surgical planning. Obtaining normative measurements of normal and pathological variants of the cochlea can especially help in patients that suffer from severe SNHL and are eligible for cochlear implant surgery.
Twenty percent of SNHL patients show some degree of inner ear malformation [11]. When a malformation is present, the surgical procedure carries a higher risk for complications such as Cerebro Spinal Fluid gusher. Also, a different surgical approach and electrode type may be chosen to ensure an atraumatic insertion and optimal position of the electrodes in the scala tympani, as this directly effects electroacoustic stimulation and therefore hearing outcome [12].
SNHL can also be caused by partial or total cochlear obliteration. This can be a result of meningitis-induced labyrinthitis which can cause fibrotic or osseous obliteration of the cochlear lumen, or a result of temporal bone fracture. Detection of obliteration is crucial for cochlear implant surgery planning. And may not be seen on CT [13]. In these

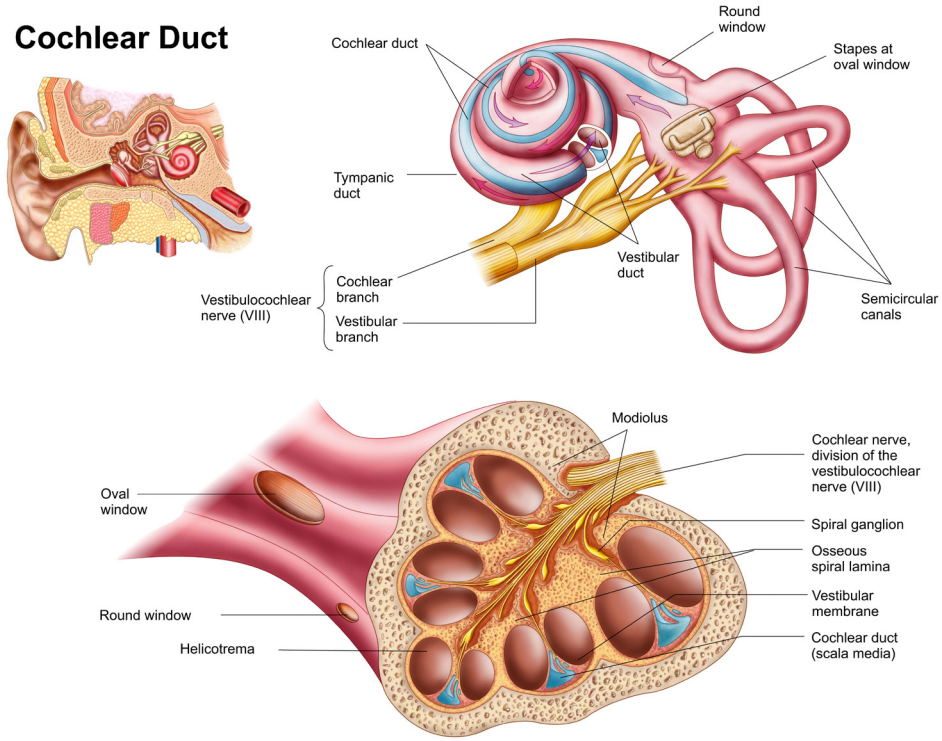

Figure 2: Inner ear anatomy

cases, surgical approach can include a split array electrode, inserting two separate arrays through different cochleostomies. Besides cochlear malformations and partially patent cochleas, MRI can assess other morphologic cochlear variants and its influence on electrode position and hearing outcome.

Another application of MRI of the inner ear is the imaging of endolymphatic hydrops (EH). Endolymphatic hydrops is an abnormal anatomical finding in which the endolymphatic space is distended into areas that are normally occupied by perilymphatic space [figure 3]. EH can result in progressive loss of audiovestibular function. Patients with EH can present with the classical triad of episodic vertigo, fluctuating hearing loss and tinnitus. In addition, a sense of fullness in the ear can be present. As the clinical diagnosis can be difficult, especially in cases of atypical symptoms, reliable imaging can be of additional value [14]. To classify endolymphatic hydrops, both endolymphatic and perilymphatic spaces have to be depicted in sufficient detail. Various scanning protocols have been attempted with both intratympanic and

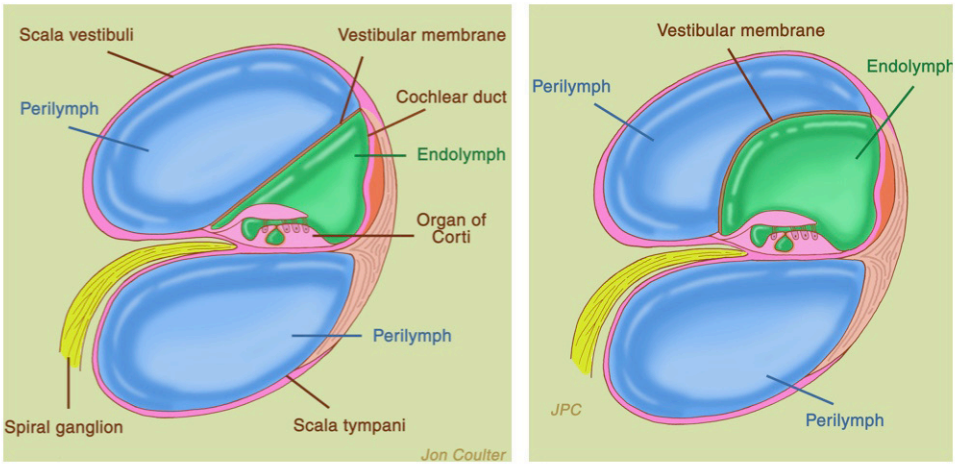

Figure 3: Endolymphatic hydrops in the inner ear

intravenous injection of Gadolinium, with different scanning sequences (including subtraction of positive endolymph images and positive perilymph images) and with different gadolinium administration, including time intervals between gadolinium administration and scanning, and differing Gadolinium dosage [15]. Up to now, 3 Tesla MRI performed at 4 hours post-intravenous gadolinium with 3D-FLAIR sequences seems most useful, but EH grading remains difficult [16].

The implementation of 7.0 Tesla magnetic resonance imaging (MRI) for human use has the potential to further advance spatial resolution beyond that of 1.5T and 3T.

Our **clinical question** is therefore if 7 Tesla MRI can result in a better depiction of the membranous structures of the inner ear, than 3 Tesla MRI. This can have its benefits in accurate diagnosis, localization of pathology and surgical planning (in case of cochlear implant surgery).

Malignant otolaryngology disease

Early glottic carcinoma

Laryngeal cancer (meaning cancer of the voice box) generally arises from the mucosal surface [figure 4]. It can therefore be easily detected by direct laryngoscopy (inspection of the larynx by flexible or rigid endoscope) and endoscopic biopsy (tissue sampling) to confirm the diagnosis. In most tumors, however, cross sectional imaging has a complementary role and is of importance to evaluate deep submucosal extension, for example paraglottic extension, pre-epiglottic extension and cartilage erosion/destruction.

Invasion of laryngeal cartilages, for example, affects the T(tumor) classification and is generally associated with a lower response to radiation therapy and a higher risk of tumor recurrence. For larger (T2-4) laryngeal carcinomas, CT and MRI are well accepted diagnostic tools. However, their role in early stage glottic carcinoma remains limited.
Glottic laryngeal cancer, confined to one or both vocal cords, generally present as a small lesion with low tumor volume. Reported local control rates for endoscopic laser excision and radiotherapy are equally high (71%-95%). Therefore functional outcome is the main outcome parameter [17]. The main factor that prohibits the systematic evaluation and pooling of data is the uncertainty of tumor comparability, due to an absence of a standardized method that accurately measures tumor extent and depth. MRI has the potential to achieve this, with the advantages of lack of ionizing radiation, greater inter-tissue contrast, and multiplanar imaging capabilities.
Our **first clinical goal** was therefore to review the diagnostic value of (the currently used) 1.5 and 3 Tesla MRI in pre-therapeutic staging of primary early stage (T1 and T2) glottic carcinoma. And **second**, to assess the feasibility of the clinical use of a dedicated 3 Tesla MRI protocol for small laryngeal lesions and a 7 Tesla MRI protocol, including structural assessment of technical image quality and visibility of the tumor.

Primary staging of head and neck cancer; neck metastases
Lymph node involvement is the most important prognostic indicator for survival of patients with head and neck cancer (HNC). Detection of lymph node metastases with optimal imaging techniques is therefore crucial to initiate adequate treatment resulting in the most favorable prognostic outcome. Diagnostic accuracy of CT alone, for the clinically node negative neck is insufficient. Reported sensitivity on a per neck basis of the latest review on this topic was 52% (95% confidence interval 39% - 65%) [18]. On CT and MRI, size and morphology of lymph nodes are used to assess for metastatic nodal disease, such as maximal cross-sectional dimensions more than 10-15 mm or central necrosis. However, metastatic disease can be present in morphologically normal lymph nodes. FDG PET-CT has the ability to combine the metabolic, low resolution of PET with the high spatial resolution of CT. PET-CT mainly has its clinical applicability in head and neck malignancies. In about 25% of patients with proven metastatic neck disease and Cancer of Unknown Primary origin (CUP), following routine clinical work-up, PET-CT can identify the primary tumor location [19]. Furthermore, PET-CT has demonstrated a high detection rate of distant metastatic disease and synchronous cancer, higher than chest X-ray or chest CT [20]. In radiotherapy planning, PET-CT decreases the inter- and intra-observer variability and increases the conformity to real tumor boundaries. It is able to achieve a more precise definition of Gross Tumor Boundaries [21]. [18]FDG-PET is also able to detect residual tumor disease or early recurrences. A pitfall, however, is the presence of inflammation, eg induced by radiation therapy, leading to false positive results.

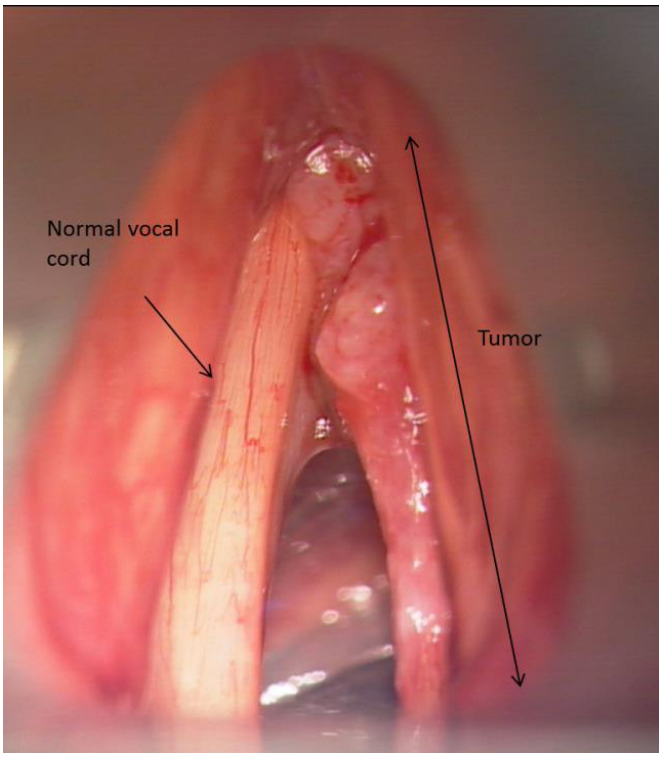

Figure 4: Endoscopic photo of an early glottic carcinoma of the right vocal cord

Three meta-analyses, published in 2008, 2013 and 2015, have evaluated FDG-PET (Kyzas 2008), or FDG PET-CT (Yonkui 2013 and Sun 2015) for the detection of regional node metastasis in patients with primary head and neck cancer [22,23,24]. PET-CT had a high diagnostic accuracy and an improvement for per-neck-level sensitivity of 20% compared to conventional imaging (CT/MRI). PET-CT thus might be beneficial for the initial staging of nodal disease. However, FDG-PET-CT findings must be interpreted with caution. Reactive lymph nodes can have variable FDG avidity. And FDG PET-CT may fail to detect cystic necrotic lymph nodes, that can be more easily seen on CT or MRI.
The role of FDG-PET in routine clinical work-up is not yet established. In case of primary radiation, histopathological verification cannot be obtained. But correct judgement of nodal metastases remains of vital importance for nodal target volume definition. False-positive nodes lead to overtreatment, while false-negative nodes lead to regional recurrence or distant failure. Second, smaller radiation fields using IMRT, allow tissue sparing, but could also lead to more marginal failures.

Therefore, we performed a retrospective study of patients treated with primary radiation or chemoradiation therapy for head and neck cancer. **Clinical goals** were to analyze the influence of FDG-PET/CT versus CT alone on defining nodal target volume definition. Second, to analyze the long-term clinical results. And, third, in case of nodal recurrences, to relate the location of nodal recurrence to the radiation regional dose distribution and to determine if these recurrences are located in the high dose field, elective dose field or outside the radiation field.

REFERENCES

1. De Jong MC, de Graaf P, Pouwels PJW, et al. 9.4T and 17.6T MRI of Retinoblastoma: Ex Vivo evaluation of microstructural anatomy and disease extent compared with histopathology. *J Magn Reson Imaging*. 2018;47(6):1487-1497.

2. Le Bihan D, Breton E, Lallemand D, et al. MR imaging of intravoxel incherent motions: application of diffusion and perfusion in neurologic disorders. *Radiology.* 1986;161(2):401-7.

3. Baliyan V, Das CJ, Sharma R, Gupta AK. Diffusion weighted imaging: Technique and applications. *World J Radiol.* 2016;8(9):785-798.

4. Wang J, Takashima S, Takayama F, et al. Head and neck lesions: characterization with diffusion-weighted echo-planar MR imaging. *Radiology.* 2001;220:621–630.

5. Schouten CS, de Graaf P, Alberts FM, et al. Response evaluation after chemoradiotherapy for advanced nodal disease in head and neck cancer using diffusion-weighted MRI and 18F-FDG-PET-CT. *Oral Oncol.* 2015;51:541–547.

6. Harris AT, Mettias B, Lesser TH. Pooled analysis of the evidence for open cavity, combined approach and reconstruction of the mastoid cavity in primary cholesteatoma surgery. J *Laryngol Otol.* 2016;130:235–241.

7. Tomlin J, Chang D, McCutcheon B, Harris J. Surgical Technique and Recurrence in Cholesteatoma: A Meta-Analysis. *Audiol Neurotol*. 2013;18:135–142.

8. Schaefer PW, Grant PE, Gonzalez RG. Diffusion-weighted MR imaging of the brain. *Radiology* 2000:217;331-45.

9. Vercruysse JP, De Foer B, Pouillon M, et al. The value if diffusion-weighted MR imaging in the diagnosis of primary acquired and residual cholesteatoma: a surgical verified study of 100 patients. *Eur Radiol* 2006;16:1461-67

10. De Foer B, Vercruysse JP, Bernaerts A, et al. *Neuroradiology.* 2007;49:841-48.

11. Sennaroglu L. Cochlear implantation in inner ear malformations: a review article. *Cochlear Implants Int.* 2010;11:4-41.

12. Sennaroglu L, Sarac S, Ergin T. Surgical results of cochlear implantation in malformed cochlea. *Otol Neurotol*. 2006;27:615-23.

13. Lewer RM, Bertuleit H, Wittkugel O, Freitag HJ. Indications for imaging the inner ear with CISS-MRI. *Laryngorhinootologie*. 1999;78(8):417-20.

14. Gurkov R, Pyyko I, Zou J, Kentala E. What is Meniere's disease? A contemporary re-evaluation of endolymphatic hydrops. *J Neurol*. 2016;263(Suppl 1):S71–S81.

15. Lingam RK, Connor SEJ, Casselman JW, Beale T. MRI in otology: applications in cholesteatoma and Meniere's disease. *Clinical Radiology.* 2018; 73(35-44).

16. Sano R, Teranishi M, Yamazaki M, Isoda H, Naganawa S et al. Contrast enhancement of the inner ear in magnetic resonance images taken at 10 minutes or 4 hours after intravenous gadolinium injection. *Acta Otolaryngol*. 2012;132(3): 241-6.

17. Van Loon Y, Sjogren E, Langeveld T et al. Functional outcomes after radiotherapy or laser surgery in early glottic carcinoma: A systematic review. *Head Neck.* 2012;34(8):1179-89.

18. Liao LJ, Lo WC, Hsu WL, Wang CT, Lai MS. Detection of cervical lymph node metastasis in head and neck cancer patients with clinically N0 neck-a meta-analysis comparing different imaging modalities. *BMC Cancer.* 2012;12:236.

19. De Bree R. The real additional value of FDG-PET in detecting the occult primary tumour in patients with cervical node metastases of unknown primary tumour. *Eur Arch Otohinolaryngol.* 2010;267:1653-1655.

20. Rohde M, Nielsen A, Johansen J, et al. Head-to-Head Comparison of Chest X-Ray/ Head and Neck MRI, Chest CT/Head and Neck MRI, and ^{18} F-FDG PET/CT for Detection of Distant Metastases and Synchronous Cancer in Oral, Pharyngeal, and Laryngeal Cancer. *J Nucl Med.* 2017;58:1919-1924.

21. Farina E, Martina F, Castellucci P, et al. ^{18}F-Fdg-PET-guided planning and RE-planning (Adaptive) Radiotherapy in Head and Neck Cancer: Current state of Art. *Anticancer Res.* 2017;37(12):6523-6532.

22. Kyzas PA, Evangelou E, Denaxa-Kyza D, Ioannidis JP. 18F-fluorodeoxyglucose positron emission tomography to evaluate cervical node metastases in patients with head and neck squamous cell carcinoma: a meta-analysis*. J Natl Cancer Inst.* 2008;100:712–20.

23. Yongkui L, Jian L, Wanghan Jingui L. 18FDG-PET/CT for the detection of regional nodal metastasis in patients with primary head and neck cancer before treatment: a meta-analysis. *Surg Oncol.* 2013;22:e11–16.

24. Sun R, Tang X, Yang Y, Zhang C. 18FDG-PET/CT for the detection of regional nodal metastasis in patients with head and neck cancer. A meta-analysis. *Oral Oncol* 2015;51:314–20.

OUTLINE OF THIS THESIS

Since the start of medical imaging, techniques have been evolving rapidly. Both acquisition and reconstruction of data are far less time-consuming, spatial resolution increases, MRI units as high as 7 Tesla are in clinical use and new techniques, for example diffusion weighted MRI, are becoming standard of care for varying clinical indications.
In daily clinical practice, it has to be taken into account what imaging modality or imaging protocol will give the most accurate information to answer your clinical question. We have encountered various clinical problems, both for (benign) middle and inner ear disease, as well as for (malignant) laryngeal and metastastic neck disease. For these clinical problems, we have tried to evaluate the most accurate diagnostic tools and evaluate its feasibility in daily Otolaryngology practice.

Benign otolaryngology disease

First, focusing on benign otolaryngology disease, we have systematically evaluated the diagnostic value of non-EPI Diffusion Weighted MRI for the detection of both primary, residual and recurrent cholesteatoma. A reliable imaging method could avoid the need for second look surgery and advocate a one stage surgery including hearing restoration with or without mastoid obliteration **(chapter 2).**
With the evolvement MRI techniques, nowadays, the implementation of ultrahigh-field 7 Tesla MRI for human use, had the potential to further advance spatial resolution beyond that of 1.5 and 3 Tesla. This could result in potential advantages in the depiction of the membranous structures of the inner ear. In **chapter 3**, we explored the maximum potential of 7 Tesla for depiction of the inner ear ex vivo by scanning a human head specimen with ultrahigh resolution, independent of scan duration. Second aim was to reduce scan duration, leading to a scan protocol, suitable for clinical practice. In **chapter 4**, we compared the depiction of the inner ear structures at 7 Tesla and 3 Tesla images by scanning healthy volunteers.

Malignant otolaryngology disease

Focusing on malignant otolaryngology disease, the higher spatial resolution of higher magnetic fields also has its potential benefits in the depiction of small laryngeal lesions. In early glottic cancer, accurate assessment of tumor extension, including depth infiltration, is of great importance for both staging, therapeutic approach and systematic comparison of data. In **chapter 5**, we performed a systematic review of literature to assess the diagnostic value of MRI in pre-therapeutic staging of primary early stage (T1 and T2) glottic carcinoma. Reported MRI protocols appeared to be suboptimal for small

laryngeal lesions. In **chapter 6**, we therefore did a prospective feasibility study with a 3 Tesla scanning protocol, specifically adjusted for small laryngeal lesions and a 7 Tesla protocol. Acquisition difficulties, technical image quality and visibility of the tumor was assessed.

Concerning other head and neck cancers, imaging also places a vital role. The presence of neck metastasis is the most important prognostic factor of the disease. Accurate diagnostic imaging, including the neck status, is therefore of vital importance in staging and treatment planning. The role of 2-[18F]-fluoro-2-deoxy-D-glucose (FDG)-positron emission tomography (PET)/computed tomography (CT) in routine diagnostic staging remains controversial. In case of discordance between FDG-PET and CT, a compromise has to be made between the risk of false positive FDG-PET and the risk of delaying appropriate salvage intervention. Second, with intensity modulated radiation therapy (IMRT), smaller radiation fields allow tissue sparing, but could also lead to more marginal failures. In **chapter 7**, we retrospectively studied 283 patients with head and neck carcinoma scheduled for radiotherapy between 2002 and 2010. We analyzed the influence of FDG-PET/CT versus CT alone on defining nodal target volume definition and evaluated its long-term clinical results. Second, the location of nodal recurrences was related to the radiation regional dose distribution.

Table 1: Overview of performed studies and its anatomical region

	Inner ear	Middle ear cholesteatoma	Early glottic carcinoma	Neck metastases
CT				
3T MRI				
7T MRI				
DW MRI				
PET-CT				

Chapter 2
Chapter 3 and 4
Chapter 5 and 6
Chapter 7

SECTION ONE

Benign otolaryngology disease; middle- and inner ear

CHAPTER 2

A Systematic Review of Non-Echo Planar Diffusion-Weighted Magnetic Resonance Imaging for Detection of Primary and Postoperative Cholesteatoma

Otolaryngology–Head and Neck Surgery. 2016; 154(2) 233–240.

Sylvia L. van Egmond
Inge Stegeman
Wilko Grolman
Mark C. J. Aarts

ABSTRACT

Objective

To investigate the diagnostic value of non–echo planar diffusion-weighted magnetic resonance imaging (DW MRI) for primary and recurrent/residual (postoperative) cholesteatoma in adults (>18 years) after canal wall up surgery.

Data Sources

We conducted a systematic search in PubMed, Embase, and Cochrane up to October 22, 2014.

Review methods

All studies investigating non–echo planar DW MRI for primary and postoperative cholesteatoma were selected and critically appraised for relevance and validity.

Results

In total, 779 unique articles were identified, of which 23 articles were included for critical appraisal. Seven articles met our criteria for relevance and validity for postoperative cholesteatoma. Four studies were additionally included for subgroup analysis of primary cases only. Ranges of sensitivity, specificity, positive predictive value, and negative predictive value yielded 43%-92%, 58%-100%, 50%-100% and 64%-100%, respectively. Results for primary subgroup analysis were 83%-100%, 50%-100%, 85%-100%, and 50%-100%, respectively. Results for subgroup analysis for only postoperative cases yielded 80%-82%, 90%-100%, 96%-100%, 64%-85%, respectively. Despite a higher prevalence of cholesteatoma in the primary cases, there was no clinical difference in added value of DW MRI between primary and postoperative cases.

Conclusion

We found a high predictive value of non–echo planar DW MRI for the detection of primary and postoperative cholesteatoma. Given the moderate quality of evidence, we strongly recommend both the use of non-echo planar DW MRI scans for the follow-up after cholesteatoma surgery, and when the correct diagnosis is questioned in primary preoperative cases.

INTRODUCTION

Due to the locally aggressive nature of primary cholesteatoma, with often permanent damage to the middle ear and its surrounding bony structures, its early detection, as well as residual or recurrent disease, is of great importance. In the last decade, the development of diffusion-weighted magnetic resonance imaging (DW MRI) techniques has resulted in better diagnostic performance in the detection of primary and recurrent cholesteatoma. A large number of studies have reported on this
modality, with better performance of the newer non–echo planar imaging (non-EPI) technique than the EPI technique. Non-EPI algorithms are less susceptible to magnetic interface artifacts and provide better image quality and better spatial resolution, with reported cholesteatoma detection rates of only 2 mm.[1] MRI techniques are rapidly evolving, with improvements in quality and speed of data acquisition.[2] Following a systematic review of Aarts et al in 2010, we perform diffusion-weighted MRI on a regular basis.[1] However, false-positive and false-negative results are encountered. Since 2010, several studies have reported on the high diagnostic performance of non-EPI algorithms. With this systematic review, we aim to evaluate the results of non–echo planar (non-EP) diffusion-weighted imaging (DWI) sequences for the detection of primary and postoperative cholesteatoma.

METHODS

Search Strategy

We conducted a systematic search in PubMed, Embase, and Cochrane up to October 22, 2014. A syntax was designed with synonyms for non-EP DW MRI (determinant) and cholesteatoma (outcome; Figure 1). Reporting of our data is done according to the PRISMA statement.[3]

Study Selection

Screening of publications was performed by at least 2 authors independently (S.L.E., I.S.). Any difference in opinion was resolved by consensus. Duplicates were removed from the retrieved articles. Title, abstract, and, ultimately, the full text of potentially eligible articles were screened with criteria shown in Figure 2. A thorough analysis of selected articles was made, and their bibliographies were analyzed to identify any additional articles that could be relevant for this review.

We included patients with primary and postoperative cholesteatoma. Since the diagnostic value of magnetic resonance might differ in these patients, as a result of

APPENDIX

A. Pubmed search

("mri"[Title/Abstract] OR "magnetic resonance imaging"[Title/Abstract] OR "dw mri"[Title/Abstract] OR "mri dwi"[Title/Abstract] OR "dwi"[Title/Abstract] OR "diffusion weighted imaging"[Title/Abstract] OR "diffusion magnetic resonance imaging"[Title/Abstract] OR "diffusion magnetic resonance imaging"[MeSH Terms] OR "magnetic resonance imaging"[MeSH Terms]) AND (cholesteatom* OR "cholesteatoma"[MeSH Terms] OR "cholesteatoma, middle ear"[MeSH Terms])

B. Embase search

(mri:ab,ti OR 'magnetic resonance imaging':ab,ti OR 'dw mri':ab,ti OR 'mri dwi':ab,ti OR 'dwi':ab,ti OR 'diffusion weighted imaging':ab,ti OR 'diffusion magnetic resonance imaging':ab,ti OR 'diffusion weighted imaging'/exp OR 'diffusion weighted imaging' OR 'nuclear magnetic resonance imaging'/exp OR 'nuclear magnetic resonance imaging') AND (cholesteatom*:ab,ti OR 'cholesteatoma'/exp

C. Cochrane search

'MRI' OR 'magnetic resonance imaging' OR 'MRI DWI' OR 'DW-MRI' OR 'diffusion magnetic resonance imaging' OR 'diffusion weighted imaging' OR Diffusion Magnetic Resonance Imaging (MeSH descriptor) OR Magnetic Resonance Imaging (MeSH descriptor) AND cholesteatoma OR cholesteatomas OR cholesteatomata OR cholesteatomatous OR Cholesteatoma (MeSH descriptor)

Figure 1: Search syntax

changed anatomy and the presence of postoperative soft tissue in the tympanic cavity, we performed an additional subgroup analysis.

Concerning postoperative cholesteatoma, our primary objective was to include only patients after canal wall up (CWU) surgery. CWU surgery is associated with a higher incidence of residual or recurrent disease, which may not be evaluated adequately on clinical examination alone. Articles reporting on both techniques were included only when CWU data could be separately analyzed. When the method of primary surgery (CWU or canal wall down [CWD]) was not specifically reported, the authors were contacted for further information. Since non-EP DWI has shown more promising results

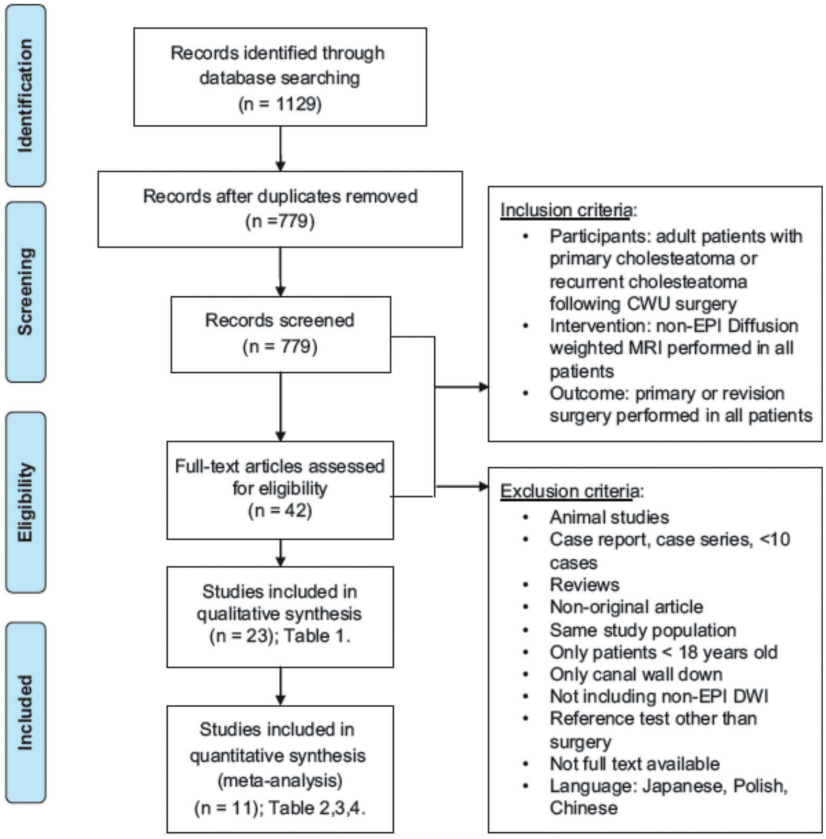

Figure 2: Flow diagram of search strategy and screening of publications. CWU, canal wall up; DWI, diffusion-weighted imaging; EPI, echo planar imaging; MRI, magnetic resonance imaging.

than EP DWI, we included only studies using non-EP DWI sequences. Concerning outcome, surgery as a reference standard had to be available for all patients.

Critical Appraisal of Included Studies

On the basis of predefined criteria, articles were critically appraised for relevance and validity. Data collected included study design, number of primary and recurrent episodes, and standardization and adequate reporting of non-EP DWI protocol and surgical procedures, including presence or absence of surgical intervention following negative DW MRI results. The interval between DW MRI and surgery was reported, as well as blinding of radiologists to the surgical outcome. Missing data were scored as adequate if all consecutive patients underwent both DW MRI and surgery.

Missing data were considered inadequate if patients were excluded a priori on the basis of incomplete data (DW MRI or surgical data).

Data Extraction and Statistics

To evaluate the diagnostic value of non-EP DW MRI, positive predictive value (PPV), negative predictive value (NPV), sensitivity (SN), and specificity (SP) were extracted from eligible articles or, when not described, calculated (when possible) from the original data. Subsequently, subgroup analysis of primary and postoperative cholesteatoma was done.

RESULTS

Search Strategy and Study Selection

Our search strategy yielded 779 unique publications (Figure 2). After title and abstract screening, 42 articles were left for full-text assessment, of which 20 were excluded for various reasons. Cross-reference checking yielded 1 additional article. This resulted in a total of 23 eligible studies. [4-26]

Critical Appraisal

Appraisal of 23 eligible studies is presented in Table 1. All studies were case series or cohort studies; 17 of 23 studies were prospective. The number of episodes varied between 8 (suitable for review) and 120. The mean number of episodes of all 23 studies was 39. We initially excluded 14 studies on the basis of relevance. [13-26] Five studies included CWU and CWD procedures, of which the CWU data could not be extracted.[13,17,20,24,26] In another 5 studies, the authors could not be contacted, and operative technique (CWU or CWD) could not be specified with certainty.[14,15,16,19,21] Seven studies were excluded because not all patients received surgery as a reference standard, and the radiologic findings could therefore not be confirmed.[18,20-25] Of these 14 excluded studies, 5 were eligible for subgroup analysis of primary cholesteatoma only (reported with "p" in Table 1).[13-17] Following appraisal of relevance, 9 studies were eligible for quantitative analysis of primary and recurrent cholesteatoma, and 5 were eligible for subgroup analysis of primary cases only. Following assessment for validity, 2 additional articles were excluded for primary and recurrent cases,[11,12] and 1 was excluded for primary subgroup analysis. [17] The main reason of exclusion was that not all patients with positive and negative DW MRI results underwent surgical intervention and/or missing data were not mentioned. This resulted in a total of 7 studies included for final quantitative analysis of primary and recurrent cases [4-10] and 4 studies for subgroup analysis of primary cases only.[13-16]

Data Extraction and Statistics

Study characteristics are shown in Table 1. The 7 selected studies included a total of 223 episodes, of which 69 were primary cases and 154 were analyzed for recurrent/residual cholesteatoma. Additionally, 87 episodes (of 4 studies) were included for primary subgroup analysis only. There were differences in technique among studies with regard to timing of MRI relative to surgery and imaging protocols. The calculated diagnostic value of DW MRI is presented in Figure 2. The ranges for SN, SP, PPV, and NPV were 43%-92%, 58%-100%, 50%-100%, and 64%-100%, respectively, for the whole patient population respectively (Table 2). Kasbekar et al reported a relatively low diagnostic value of DW MRI as compared with other studies.8 The PROPELLER sequence used in that study was not able to detect cholesteatoma <4 mm, comparable to EP DWI results.

The PPV and NPV are shown in Figure 3, with wide variation in NPV. Studies by Akkari et al and Khemani et al reported particularly low NPVs.4,9 Two studies could not be plotted because of absence of positive DW MRI findings and unknown prevalence.8,10 The added value of non-EP DW MRI for a positive result (PPV minus prevalence) ranged from 20% to 39%. The added value for a negative result (NPV minus [1 minus prevalence]) ranged from 38% to 55%.

In the primary cholesteatoma subgroup analysis, SN, SP, PPV, and NPV were 83%-100%, 50%-100%, 85%-100%, and 50%-100%, respectively (Table 3). The added value for a positive result (PPV minus prevalence) in primary cases varied between 10% and 44%. The added value for a negative result (NPV minus [1 minus prevalence]) in primary cases varied between 36% and 56%.

In postoperative patients analyzed for residual/recurrent disease, only 2 studies could be plotted. SN, SP, PPV, and NPV in these 2 studies were 80%-82%, 90%-100%, 96%-100%, and 64%-85%, respectively (Table 4). The added value for a positive result (PPV minus prevalence) in recurrent cases was 22% to 55%. The added value for a negative result (NPV minus [1 minus prevalence]) in recurrent cases only was 30% to 38%.

Table 1: critical appraisal of relevance and validity

Author	Publication year	Primary/Rec chol after CWU	Non-EPi DWI MRI	Surgical reference	**Total relevance**	No. Total episodes	No. recurrent or residual cases	Study design	Standardized DW MRI	Type Non-EPI DW MRI	Surgery when MRI + AND -	Standardized surgery	Interval MRI to surgery	Blinding	Missing data	**Total Assessment**
Akkari[4]	2014	●	●	●	●	95#	81	CS-P	●	HASTE	●	●	Mean 4m	●	●	++
Alvo[5]	2014	●	●	●	●	16	0	CS-P	●	HASTE	●	●	<2m	●	●	++
Vaid[6]	2013	●	●	●	●	31	11	CS-P	●	SSTSE	●	●	?	●	●	++
Cavaliere[7]	2014	●	●	●	●	16	0	CS-P	●	MSTSE	●	●	+/- 29d	●	○	+
Kasbekar[8]	2011	●	●	●	●	19	16	CS-P	●	PROPELLER	●	●	+/-1.5m	●	?	+
Khemani[9]	2011	●	●	●	●	38	38	CO-P	●	HASTE	●	●	0-6m	●	○	+
Dhepnorrarat[10]	2009	●	●	●	●	8 (22)	8	CS-P	●	HASTE	●	●	<6m	●	○	+
Majithia[11]	2012	●	●	●	●	24	0	CS-P	●	HASTE	○	●	Median 3m	●	○	+/-
De Foer[12]	2010	●	●	●	●	120	63	CS-R	●	SSTSE	○	●	<2m	●	?	+/-
Profant[13]	2012	○	●	●	**	33	(17)	CO-P	●	HASTE	●	●	0-169d	●	●	-/p++
Sharifian[14]	2012	?	●	●	*	35	16	CS-P	●	HASTE	●	●	<4m	●	●	-/p++
Nagai[15]	2008	?	●	●	*	56	18	CO-P	●	FASE	●	●	?	●	●	-/p++
Huins[16]	2010	?	●	●	*	32	18	CO-P	●	HASTE	●	●	0-12m	●	○	-/p+
Migirov[17]	2014	○	●	●	**	50	23	CS-R	○	HASTE + PROPELLER	○	●	2w-6m	?	○	-
Velthuis[18]	2014	●	●	○	○	48	48	CO-R	●	HASTE	○	●	14-527d Mean 108d	●	●	-

Table 1: continued

Author	Publication year	Primary/Rec chol after CWU	Non-EPi DWI MRI	Surgical reference	**Total relevance**	No. Total episodes	No. recurrent or residual cases	Study design	Standardized DW MRI	Type Non-EPI DW MRI	Surgery when MRI + AND -	Standardized surgery	Interval MRI to surgery	Blinding	Missing data	**Total Assessment**
Lingam[19]	2013	?	●	●	○	71	71	CO-R	●	HASTE	●	●	Median 5.4m	●	○	-
Dremmen[20]	2012	○	●	○	○	51 (56##)	51	CO-R	●	MSTSE	○	●	?	●	●	-
Ilica[21]	2012	?	●	○	○	11 (21)	4	CO-P	●	HASTE	○	●	<1m	●	?	-
Mateos-Fernandez[22]	2012	●	●	○	○	54	21	CS-P	●	PROPELLER	○	●	?	●	○	-
El Mogy[23]	2011	●	●	○	○	32(42)	11	CS-P	●	PROPELLER	○	?	?	●	?	-
Pizzini[24]	2010	○	●	○	○	28 (30)	11	CS-R	●	HASTE	●	●	<6m	●	●	-
Lehmann[25]	2009	?	●	○	○	10 (35)	10	CS-P	●	PROPELLER	○	●	?	●	●	-
Dubrulle[26]	2006	○	●	●	○	24	24	CO-P	●	Fast SE	●	●	<5m	●	●	-

Categories: ● Accurate , ○ Not Accurate , ? Unknown
* CWU or CWD not known with certainty, authors could not be reached. Only included for primary subgroup analysis.
** canal wall up and down results could not be separately analyzed in de recurrent/residual group. Only suitable for primary subgroup analysis.
# Exclusion of 2 patients with CWD after contact with author.
Exclusion of 5 children
CO Cohort Study, CS Case Serie
p Assessment of validity for primary subgroup analysis
SE = Spin Echo, FASE = Fast Advanced Spin Echo, HASTE = Half-Fourier Acquired Single-shot Turbo spin-Echo, PROPELLER = Periodically Rotated Overlapping ParallEl Lines with Enhanced Reconstruction Sequence, SSTSE = Single Shot Turbo Spin Echo, MSTSE = Multi Shot Turbo Spin Echo

Table 2: results of 7 selected studies (primary and post-operative cases)

	MR+	MR-	Chol+	Chol-	Sensitivity	Specificity	PPV% (CI)	NPV% (CI)	Prevalence	Kappa
Akkari[4]	68*	27	72*	23	88 (77-95)	86 (64-97)	95 (86-99)	69 (48-86)	75 (65-83)	n.a.
Alvo[5]	9	7	10	6	90 (56-100)	100 (54-100)	100 (66-100)	86 (42-100)	63 (36-84)	0.88 (0.64-1.00)
Vaid[6]	17	14	19	12	89 (67-98)	100 (73-100)	100 (80-100)	86 (57-98)	61 (42-78)	n.a.
Cavaliere[7]	11	5	12	4	92 (61-99)	100 (40-100)	100 (71-100)	80 (29-97)	75 (47-92)	?
Kasbekar[8]	?	?	7	12	43-71	58-92	50-75	73-78	?	0.39
Khemani[9]	24	14	28	10	82 (63-94)	90 (55-100)	96 (79-100)	64 (35-87)	74 (57-86)	n.a.
Dhepnorrarat[10]	0	8	0	8	n.a	100 (63-100)	n.a.	100 (63-100)	0 (0-40)	n.a.

* Correction of study numbers after contact with the author (2 patients after canal wall down)

Table 3: subgroup analysis of primary cases only

	MR+	MR-	Chol+	Chol-	Sensitivity % (CI)	Specificity % (CI)	PPV% (CI)	NPV% (CI)	Prevalence % (CI)
Alvo[5]	9	7	10	6	90 (56-100)	100 (54-100)	100 (66-100)	86 (42-100)	63 (36-84)
Vaid[6]	13	7	14	6	92	100	100	85	70 (46-87)
Cavaliere[7]	11	5	12	4	92 (61-99)	100 (40-100)	100 (71-100)	80 (29-97)	75 (47-92)
Profant[13]	13	3	12	4	92 (61-99)	50 (8-92)	85 (55-98)	67 (12-95)	75 (47-92)
Sharifian[14]			16		93-100	100	100	80-100	?
Nagai[15]	25	10	30	5	83 (65-94)	100 (48-100)	100 (86-100)	50 (19-81)	86 (69-95)
Huins[16]	12	2	12	2	100 (73-100)	100 (19-100)	100 (73-100)	100 (19-100)	56 (56-97)

Table 4: subgroup analysis of post-operative cases only

	MR+	MR-	Chol+	Chol-	Sensitivity % (CI)	Specificity % (CI)	PPV% (CI)	NPV% (CI)	Prevalence % (CI)
Vaid[5]	4	7	5	6	80	100	100	85	45 (18-75)
Khemani[8]	24	14	28	10	82 (63-94)	90 (55-100)	96 (79-100)	64 (35-87)	74 (57-86)
Dhepnorrarat[9]	0	8	0	8	n.a.	100 (63-100)	n.a.	100 (63-100)	0 (0-40)

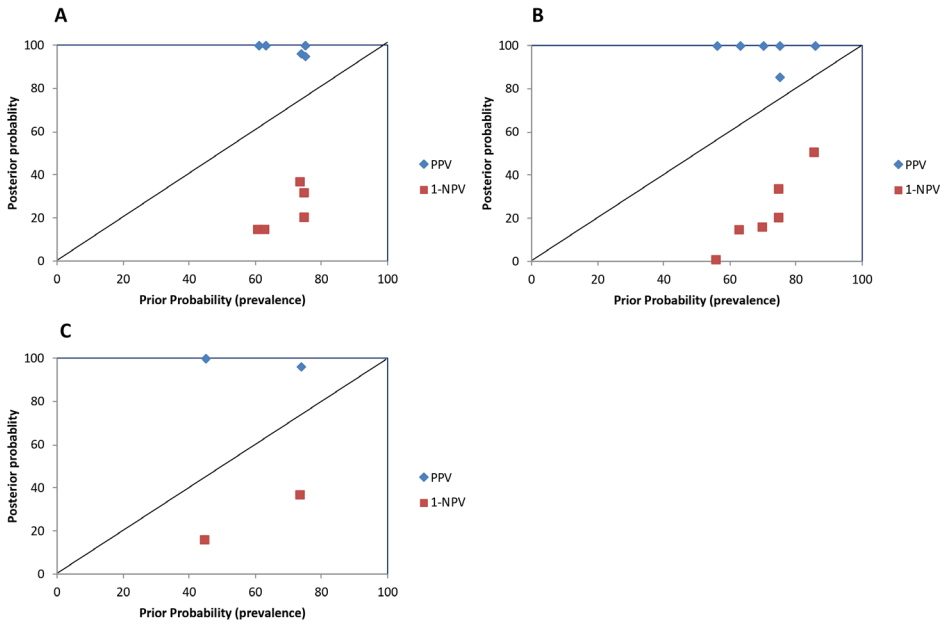

Figure 3: Comparison of pretest probability (prevalence of cholesteatoma) and posttest probability for positive predictive value (PPV) and negative predictive value (NPV) diffusion-weighted magnetic resonance imaging findings: a, primary and postoperative cases (Table 2); b, primary cases (Table 3); c, postoperative cases (Table 4).

DISCUSSION

In this systematic review, we investigated the diagnostic value of non-EP DW MRI for the detection of primary and recurrent cholesteatoma after previous CWU surgery in adult patients. As stated earlier, non-EPI sequences are less susceptible to magnetic interface artifacts than the previously used EPI sequences, which is of great importance in the temporal bone, where air, bone, tissue, and fluid lie in close proximity to one another. Non-EPI sequences also have a better spatial resolution, providing improved image quality with a short acquisition time.

Our results show overall high PPV and NPV of the non- EP DW MRI technique for postoperative cholesteatoma; ranges of SN, SP, PPV, and NPV yielded 43%-92%, 58%-100%, 50%-100%, and 64%-100%, respectively. The added value of non-EP DW MRI for a positive result (PPV minus prevalence) ranged from 20% to 39%. The added value for a negative result (NPV minus [1 minus prevalence]) ranged from 38% to 55%. Despite

a higher prevalence of cholesteatoma in the primary cases, there was no clinical difference in added value of DW-MRI between primary and postoperative cases.
The findings in this study are comparable to the high PPV and NPV reported for non-EP DW MRI in a previous systematic review.27 We included only 2 of 8 previously reviewed non-EP DWI studies by Jindal; the other 6 studies were excluded. Two studies focused on the pediatric population; 2 studies included patients without surgery as a reference standard; and in 2 studies, CWU and CWD could not be separately analyzed. Of 23 eligible studies assessed in our review, 16 were published after the previous systematic review. Jindal reported SN, SP, PPVs, and NPVs of 91%, 96%, 97%, and 85%, respectively. This is in accordance with our results, with the exception of the moderate diagnostic value reported by Kasbekar et al. The overall SN and the SN in the postoperative subgroup analysis were slightly lower than previously reported.
In this review, we included only studies after CWU. Since there are a number of studies reporting on the value of DW MRI for evaluation of cholesteatoma, we were able to narrow our inclusion criteria. Specifically, 14 studies were excluded for further analysis due to lack of a description of the primary surgery (CWU vs CWD), the inclusion of both adults and pediatric patients, or a lack of a surgical reference standard for confirmation of radiologic findings. A recent meta-analysis of surgical technique demonstrated a 3-times-greater likelihood of recurrence with CWU surgery than CWD surgery.28 After CWU surgery, residual cholesteatoma is reported to be as high as 35%, with recurrence in 8% of cases.[29] Following CWD surgery, clinical evaluation becomes more important, and diagnostic impact of DW MRI may differ.

When our results are interpreted, several limitations need to be considered. First, there was a large difference in methodology and study populations within and between the included studies (eg, different slice thicknesses and imaging techniques, variable parameters and protocols). Therefore, the studies were too heterogeneous to pool. Second, wide variations existed in the time between MRI scanning and second-look surgeries, with a range of 0 to 18 months. A large delay could lead to more false negatives, due to recurrence over time.28 Third, some studies included only patients with a high suspicion for recurrence based on clinical findings. This selection bias could have increased the pretest probability, leading to an overestimation of the PPV and underestimation of NPV. We therefore calculated the added value, based on prevalence (Figure 3). Fourth, most studies showed a high prevalence of cholesteatoma. This was due to the fact that patients with negative MRI findings were excluded from the study, patients were asymptomatic and refused routine reexplorative surgery, or patients were lost to follow-up. This could lead to selection bias. Dhepnorrarat et al, for example, included only 22 of 48 patients from the database, since 26 did not receive second-look

surgery or the interval between MRI and surgery exceeded 6 months.[10] Of the 22 study patients, 14 patients already underwent CWD surgery. We therefore excluded these 14 patients, leaving only 8 patients suitable for review. These missing data were often not well described (Table 2).
Furthermore, in 9 studies, not all patients were treated surgically on the basis of positive or negative MRI results. [11, 12, 17, 18, 20, 21, 22, 23, 25.] Although this is concordant with clinical practice, it is an important confounding factor. Workup bias cannot be precluded. Asymptomatic patients may have very small residual lesions that are more likely to be missed by MRI, resulting in false-negative MRI results. This could also explain the high percentage of recurrent cholesteatoma in some studies. We therefore excluded these studies in our quantitative analysis.

Accounting for the limitations mentioned above and the number and type of studies included in this review (case series and cohort studies), our results are based on a moderate level of evidence.30 Despite these limitations, the clinical value of the results remains high. This systematic review supplements available evidence that supports radiologic follow-up with non-EP DW MRI. When DW MRI is performed as a primary diagnostic test for follow-up in patients with a history of cholesteatoma and CWU surgery, the risks of unnecessary invasive second-look procedures may be avoided (including hearing loss, vertigo, and surgical trauma to the facial nerve and/or chorda tympani), with potential for cost savings as well. It should, however, again be emphasized that in clinical practice, due to the presence of false-negative results in small cholesteatomas (<2 mm) and the clinical implications of growing cholesteatomas, non-EP DW MRI has to be repeated within a certain interval.

CONCLUSION

In this study, we found a high predictive and added value of non-EP DW MRI for primary and postoperative cholesteatoma. However, heterogeneity among studies prevents pooling of data. Also, several limitations of study methodology could affect the interpretation of the results. However the clinical relevance of the included studies is high. Therefore, despite of moderate quality of evidence, we strongly recommend the use of non-EP DW MRI as a primary diagnostic tool in cases of suspected primary or recurrent (postoperative) cholesteatoma.

REFERENCES

1. Aarts MC, Rovers MM, van der Veen EL, Schilder AG, van der Heijden GJ, Grolman W. The diagnostic value of diffusion weighted magnetic resonance imaging in detecting a residual cholesteatoma. *Otolaryngol Head Neck Surg*. 2010;143:12-16.

2. Nitz WR.Fast and ultrafast non-echo-planar MR imaging techniques. *Eur Radiol*. 2002;12:2866-2882.

3. Moher D, Liberati A, Tetzlaff J, Altman DG: PRISMA Group. Preferred reporting items for systematic reviews and meta analyses: the PRISMA statement. *BMJ*. 2009;339:b2535.

4. Akkari M, Gabrillargues J, Saroul N, et al. Contribution of magnetic resonance imaging to the diagnosis of middle ear cholesteatoma: analysis of a series of 97 cases. *Eur Ann Otorhinolaryngol Head Neck Dis*. 2014;131:153-158.

5. Alvo A, Garrido C, Salas A, Miranda G, Stott CE, Delano PH. Use of non-echo-planar diffusion-weighted MR imaging for the detection of cholesteatomas in high-risk tympanic retraction pockets. *AJNR AM J Neuroradiol*. 2014;35:1820-1824.

6. Vaid S, Kamble Y, Vaid N, et al. Role of magnetic resonance imaging in cholesteatoma: the Indian experience. *Indian J Otolaryngol Head Neck Surg*. 2013;65(suppl 3):485-492.

7. Cavaliere M, Di Lullo AM, Caruso A, et al. Diffusionweighted intensity magnetic resonance in the preoperative diagnosis of cholesteatoma. *ORL J Otorhinolaryngol Relat Spec.* 2014;76:212-221.

8. Kasbekar AV, Scoffings DJ, Kenway B, et al. Non echo planar, diffusion-weighted magnetic resonance imaging (periodically rotated overlapping parallel lines with enhanced reconstruction sequence) compared with echo planar imaging for the detection of middle-ear cholesteatoma. *J Laryngol Otol*. 2011;125:376-380.

9. Khemani S, Lingam RK, Kalan A, Singh A. The value of nonecho planar HASTE diffusion-weighted MR imaging in the detection, localisation and prediction of extent of postoperative cholesteatoma. *Clin Otolaryngol*. 2011;36:306-312.

10. Dhepnorrarat RC, Wood B, Rajan GP. Postoperative nonecho-planar diffusion-weighted magnetic resonance imaging changes after cholesteatoma surgery: implications for cholesteatoma screening. *Otol Neurotol*. 2009;30:54-58.

11. Majithia A, Lingam RK, Nash R, Khemani S, Kalan A, Singh A. Staging primary middle ear cholesteatoma with non-echoplanar (half-Fourier-acquisition single-shot turbo-spin-echo) diffusion-weighted magnetic resonance imaging helps plan surgery in 22 patients: our experience. *Clin Otolaryngol*. 2012;37:325-330.

12. De Foer B, Vercruysse JP, Bernaerts A, et al. Middle ear cholesteatoma: non-echo-planar diffusion-weighted MR imaging versus delayed gadolinium-enhanced T1-weighted MR imaging—value in detection. *Radiology*. 2010;255:866-872.

13. Profant M, Slavikova K, Kabatova Z, Slezak P, Waczulikova I. Predictive validity of MRI in detecting and following cholesteatoma. *Eur Arch Otorhinolaryngol*. 2012;269:757-765.

14. Sharifian H, Taheri E, Borghei P, et al. Diagnostic accuracy of non-echo-planar diffusion-weighted MRI versus other MRI sequences in cholesteatoma. *J Med Imaging Radiat Oncol*. 2012;56:398-408.

15. Nagai N, Tono T, Matsuda K, Toyama K, Kawano H, Kodama T. Value of non echo-planar diffusion-weighted magnetic resonance imaging in the detection of middle ear cholesteatomea. *Mediterr J Otol*. 2008:197-202.

16. Huins CT, Singh A, Lingam RK, Kalan A. Detecting cholesteatoma with non-echo planar (HASTE) diffusion-weighted magnetic resonance imaging. *Otolaryngol Head Neck Surg*. 2010;143:141-146.

17. Migirov L, Wolf M, Greenberg G, Eyal A. Non-EPI DW MRI in planning the surgical approach to primary and recurrent cholesteatoma. *Otol Neurotol*. 2014;35:121-125.

18. Velthuis S, van Everdingen KJ, Quak JJ, Colnot DR. The value of non echo-planar, diffusion-weighted magnetic resonance imaging for the detection of residual or recurrent middle-ear cholesteatoma. *J Laryngol Otol*. 2014;128:599-603.

19. Lingam RK, Khatri P, Hughes J, Singh A. Apparent diffusion coefficients for detection of postoperative middle ear cholesteatoma on non-echo-planar diffusion-weighted images. *Radiology*. 2013;269:504-510.

20. Dremmen MH, Hofman PA, Hof JR, Stokroos RJ, Postma AA. The diagnostic accuracy of non-echo-planar diffusion-weighted imaging in the detection of residual and/or recurrent cholesteatoma of the temporal bone. *Am J Neuroradiol*. 2012;33:439-444.

21. Ilica AT, Hıdır Y, Bulakbasxı N, et al. HASTE diffusion-weighted MRI for the reliable detection of cholesteatoma. *Diagn Interv Radiol*. 2012;18:153-158.

22. Mateos-Fernandez M, Mas-Estelles F, de Paula-Vernetta C, Guzman-Calvete A, Villanueva-Marti R, Morera-Perez C. The role of diffusion-weighted magnetic resonance imaging in cholesteatoma diagnosis and follow-up: study with the diffusion PROPELLER technique. *Acta Otorrinolaringol Esp*. 2012;63:436-442.

23. El Mogy SA, Mazroa JA, El Ghaffar MA, El Mogy MS, El Mogy IS. Evaluation of acquired cholesteatoma with PROPELLER diffusion imaging. *Egypt J Radiol Nucl Med*. 2011;42:9-17.

24. Pizzini FB, Barbieri F, Beltramello A, Alessandrini F, Fiorino F. HASTE diffusion-weighted 3-Tesla magnetic resonance imaging in the diagnosis of primary and relapsing cholesteatoma. *Otol Neurotol*. 2010;31:596-602.

25. Lehmann P, Saliou G, Brochart C, et al. 3T MR imaging of postoperative recurrent middle ear cholesteatomas: value of periodically rotated overlapping parallel lines with enhanced reconstruction diffusion-weighted MR imaging. *Am J Neuroradiol*. 2009;30:423-427.

26. Dubrulle F, Souillard R, Chechin D, Vaneecloo FM, Desaulty A, Vincent C. Diffusion-weighted MR imaging sequence in the detection of postoperative recurrent cholesteatoma. *Radiology*. 2006;238:604-610.

27. Jindal M, Riskalla A, Jiang D, Connor S, O'Connor AF. A systematic review of diffusion-weighted magnetic resonance imaging in the assessment of postoperative cholesteatoma. *Otol Neurotol*. 2011;32:1243-1249.

28. Tomlin J, Chang D, McCutcheon B, Harris J. Surgical technique and recurrence in cholesteatoma: a meta-analysis. *Audiol Neurotol*. 2013;18:135-142.

29. Wilson KF, Hoggan RN, Shelton C. Tympanoplasty with intact canal wall mastoidectomy for cholesteatoma: long-term surgical outcomes. *Otolaryngol Head Neck Surg.* 2013;149:292-295.

30. Guyatt GH, Oxman AD, Vist GE, et al; for the GRADE Working Group. GRADE: an emerging consensus on rating quality of evidence and strength of recommendations. *BMJ.* 2008;336:924.

CHAPTER 3

Ex vivo and in vivo imaging of the inner ear at 7 Tesla MRI

Otology Neurotology. 2014;35(4):725-9

Sylvia L. van Egmond
Fredy Visser
Frank A. Pameijer
Wilko Grolman

ABSTRACT

Hypothesis

The implementation of 7.0 Tesla magnetic resonance imaging (MRI) for human use has the potential to further advance spatial resolution beyond that of 1.5T and 3T. This could result in potential advantages in the depiction of the membranous structures of the inner ear.

Background

The inner ear is particularly challenging to visualize at 7T. Where the signal-to-noise ratio will scale linear with the field strength, the proximity of the inner ear to the cerebrospinal fluid, nerves, and bone can lead to susceptibility banding artifacts and signal loss at the interface between the inner ear and its surroundings.

Methods

A human head specimen as well as 2 healthy volunteers underwent MRI at a 7 Tesla scanner. First aim was to scan with ultrahigh resolution, independent of scan duration. Second aim was to reduce scan duration. The final step was to develop a scanning protocol suitable for clinical practice, based on previous information from ex vivo imaging.

Results

Both in and ex vivo, large objects like the cochlear basal turn, vestibule, and semicircular canals were visualized clearly. The nerves were depicted in more detail in vivo. The interscalar septum was visible in all images. A prolonged acquisition time ex vivo showed more detail of the scala tympani and vestibuli. However, the scala media was never visible, even with maximal resolution.

Conclusion

Although inhomogeneities remain present, maximum resolution scanning ex vivo as well as scanning in vivo at 7T MRI resulted in clear depiction of the major membranous structures of the inner ear.

INTRODUCTION

High-resolution magnetic resonance imaging (MRI) of the inner ear with a heavily weighted 3D fast spin-echo sequence has been optimized successfully with acceptable imaging time for 1.5 and 3 Tesla [1,2]. These sequences provide excellent imaging of the nerves within the internal auditory canal (IAC) and the fluid within the labyrinth. However, improved visualization with detection of endolymphatic vesicles of the inner ear might permit new insights in the diagnosis and treatment of labyrinthine disease and can be useful for clinical application in cochlear implantation. The implementation of 7.0 Tesla (7T) MRI for human use has the potential to further advance spatial resolution beyond that of 1.5T and 3T. 7 Tesla has already been used to produce high-definition images of various anatomical areas [3,4]. In the ENT region, the human parotid gland and duct have already been imaged with satisfactory results, although the facial nerve could only be depicted close to the skull base [5].

The inner ear is particularly challenging to visualize at 7T. Whereas the signal-to-noise ratio (SNR) increases linearly with field strength, susceptibility image artifacts result in signal loss, especially at the interface between air dense bone and cerebrospinal fluid (CSF). Spin echo based sequences show a low sensitivity to the magnetic field fluctuations induced by these susceptibilities.

However, spin echo is extreme sensitive to RF transmission field (B1+) variations because of standing wave properties in human tissue. Both susceptibility and B1+ variations will scale linear with the main magnetic field. Where the SNR increase is a clear advantage, the sensitivity to field-induced artifacts makes visualization and localization challenging at 7T. To our knowledge, imaging of the inner ear at 7T has not yet been reported. The aim of this study was to overcome these challenges and to optimize sequences for in vivo imaging of the inner ear at 7T. We present the first ex vivo and in vivo images of the inner ear at 7T and explore its potential advantages in the depiction of the membranous structures of the inner ear.

MATERIALS AND METHODS

One undissected adult human head specimen was obtained. The head was fixed 8 hours postmortem in 4% phosphatebuffered formalin. The specimen and 2 healthy volunteers underwent MRI at a 7 Tesla scanner (Phillips Achieva, The Netherlands) using a transmit/receive (T/R) volume coil in combination with a 32-channel receive coil (Nova Medical).

First aim was to scan with ultrahigh spatial resolution, independent of scan duration and technique. Different settings were applied. Optimal sequence parameters were as follows: 3D fast field echo (FFE), TR/TE 25/65 ms, flip angle 20 degrees, field of view (FOV) 140 x 140 x 22.5 mm, 150 transverse slices, imaging matrix of 960 x 960, resulting in an acquisition voxel size of 0.15 x 0.15 x 0.15 mm. Total scan duration was 4 hours 5 minutes (Scan 1).
In working toward the clinical setting, the second aim was to reduce scan duration. This resulted in an optimal sequence of 3D FFE, TR/TE 19/4.2 ms, flip angle 20 degrees, FOV 150 x 150 x 38 mm, 38 transverse slices, imaging matrix of 600 x 600, resulting in an acquisition voxel size of 0.25 x 0.25 x 0.25 mm. Acquisition time was 57 minutes 53 seconds (Scan 2).
With further reduction of scan duration, the aim of scanning was to accomplish an optimal contrast to noise ratio instead of optimal spatial resolution. This resulted in an optimal turbo spin echo sequence: 3D TSE, TR/TEequiv 3200/156 ms, turbofactor 100, FOV 150 x 150 x 38 mm, 95 contiguous transverse slices, imaging matrix of 376 x 376, resulting in an acquisition voxel size of 0.4 x 0.4 x 0.4 mm. Acquisition time was 29 minutes 26 seconds (Scan 3).
The final step was to develop a scanning protocol suitable for clinical practice, based on previous information from ex vivo imaging. Two healthy volunteers were scanned. TR and TE sequences were comparable with our clinically applied settings. The highest spatial resolution was found with the following parameters: 3D TSE, TR/TEequiv 5541/134, turbofactor 51, FOV 150 x 150 x 31 mm, 50 contiguous transverse slices, imaging matrix of 300 x 300, resulting in an acquisition voxel size of 0.5 x 0.5 x 0.5 mm. Acquisition time in vivo was 14 minutes 2 seconds. Finally, with SENSE acceleration, scan duration was reduced to 7 minutes 31 seconds with sequence parameters:
3D TSE, TR/TE 6009/205, turbofactor 100, SENSE factor 1.7, FOV 150 x 150 x 31 mm, 63 contiguous transverse slices, imaging matrix of 300 x 300, resulting in an acquisition voxel size of 0.5 x 0.5 x 0.5 mm.

Most important focus for imaging of the inner ear was the cochlea, not the labyrinth. Using multi planar reformat (MPR), all images were reconstructed in the axial, coronal, and sagittal planes and reviewed by a head and neck radiologist.
Concerning radiofrequency safety of ultrahigh-field MRI, the specific absorption rate (SAR) distributions are based on a model. The most conservative 7T head model was applied to ensure not exceeding both the average SAR over the head or body (SARw.h.) and the maximum SAR weighted over 10 g of tissue (SARmax, 10g) as defined by the International Electrotechnical Commission (IEC) regulations [6,7].

RESULTS

In both ex vivo and in vivo imaging, the cochlea could be clearly demonstrated. Figure 1 shows a coronal oblique image through the cochlea. None of the volunteers experienced any clinically relevant side effects. In one volunteer, transient vertigo was reported, besides the well-known external factors such as acoustic noise and examination duration [8].

Qualitative Analysis of Ex Vivo Images

In maximal resolution imaging as well as with shorter acquisition time, large objects like the cochlear basal turn, vestibular aqueduct, vestibule, and semicircular canals were clearly visualized (Figure 2, A and B). The interscalar septum was visible in all images (Figure 3, B and C).

A prolonged acquisition time showed more detail of the scala tympani and vestibuli. The scala media was never visible, even with maximal resolution. Membranous structures, including Reissner's membrane and the macula, could not be detected. The vestibular aqueduct, which can usually only be seen on 3T when enlarged, could be demonstrated on each ex vivo scan (Figure 4, AYC). A drawback of scanning ex vivo was the lack of fluid in the internal auditory canal (IAC) resulting in insufficient visualization of the facial nerve and the 3 branches of the vestibulocochlear nerve. Although in one ex vivo scan with medium resolution, the more proximal situated genu of the facial nerve could be clearly seen (Figure 5). The nerves were viewed in a sagittaloblique plane reconstructed perpendicular to the IAC (Figure 6, A and B).

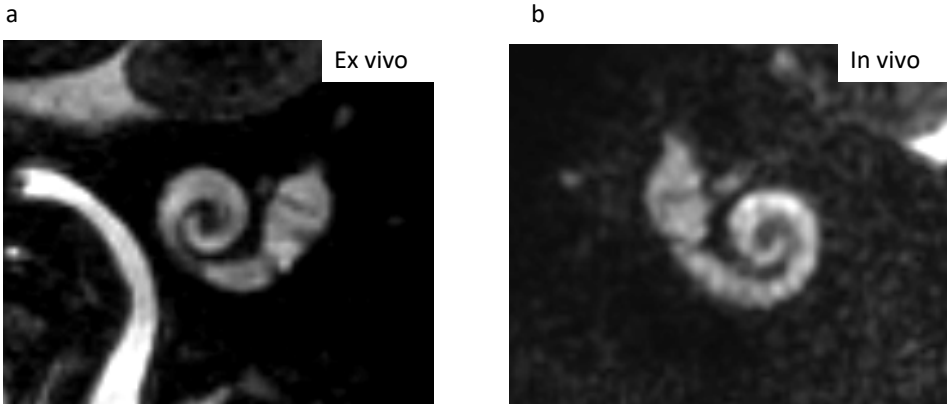

Figure 1: Coronal oblique image (Stenvers view) through cochlea. A: Scan duration: 4 hours 5 minutes. B: Scan duration: 7 minutes 31 seconds.

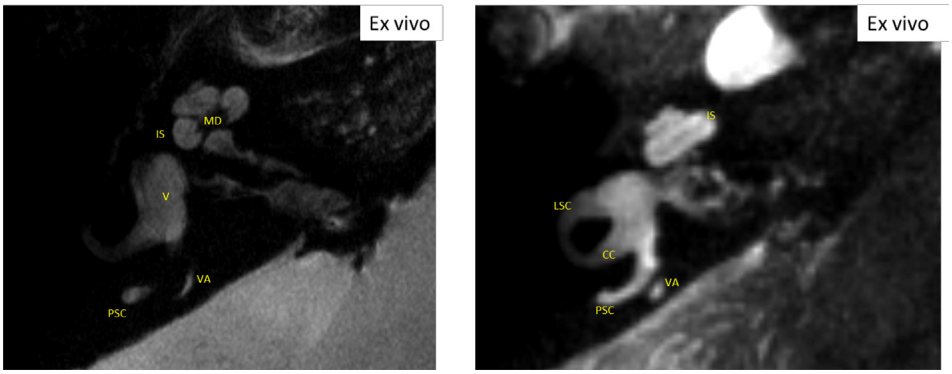

Figure 2: A: Axial maximal intensity projection (MIP) reconstruction of 1.0-cm slice thickness. Scan duration: 4 hours 5 minutes. B: Axial MIP reconstruction of 3.0 cm slice thickness. Scan duration: 29 minutes 26 seconds.

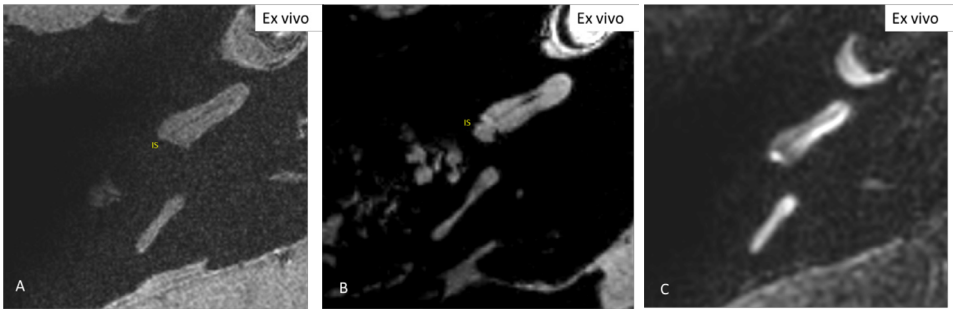

Figure 3: The basilar membrane was clearly visible at all ex vivo scans. A: Scan duration: 4 hours 5 minutes. B: Scan duration: 57 minutes 53 seconds. C: Scan duration: 29 minutes 26 seconds.

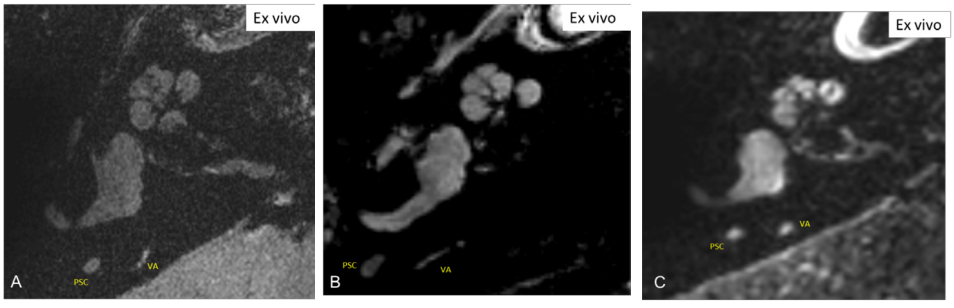

Figure 4: The vestibular aqueduct could be demonstrated on each ex vivo scan. A: Scan duration: 4 hours 5 minutes. B: Scan duration: 57 minutes 53 seconds. C: Scan duration: 29 minutes 26 seconds.

Qualitative Analysis of In vivo Images

In vivo, we were able to visualize most anatomic parts. However, because we focused on the cochlea and IAC with maximum signal intensity, the vestibule and semicircular canals were depicted with less detail (Figure 7). The interscalar septum and modiolus were clearly visible. Membranous structures, including Reissner's membrane and the macula could not be detected. The vestibular aqueduct was not visible on 7T in vivo. In vivo, all 4 nerves were visualized perfectly in both volunteers (Figure 6B). Anatomic structures could be depicted equally on both in vivo scans and was not dependent on scan duration.

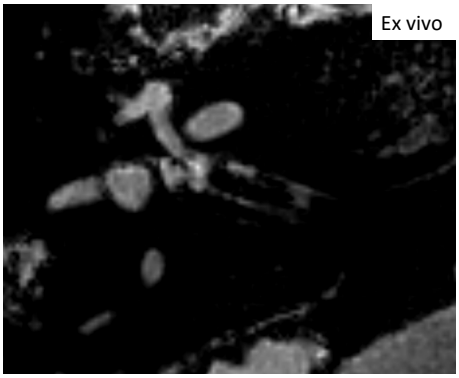

Figure 5: Genu of facial nerve. Scan duration: 57 minutes 53 seconds.

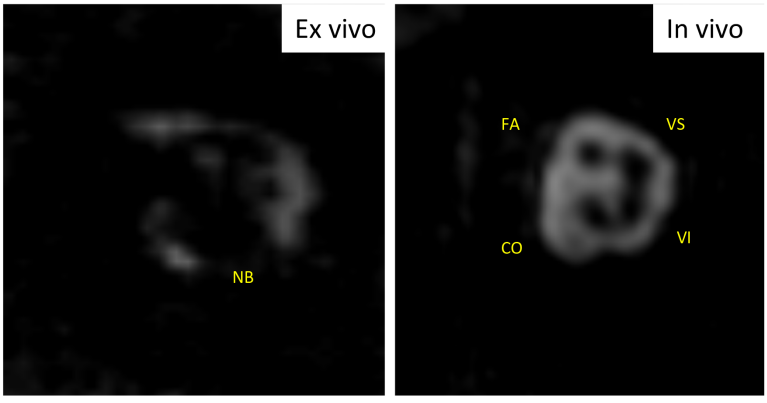

Figure 6: A: Because of the absence of cerebrospinal fluid ex vivo, the nerve bundles are hardly visible. Scan duration: 29 minutes 26 seconds. B: Optimal display of the 4 separate nerve bundles in vivo. Scan duration: 7 minutes 31 seconds.

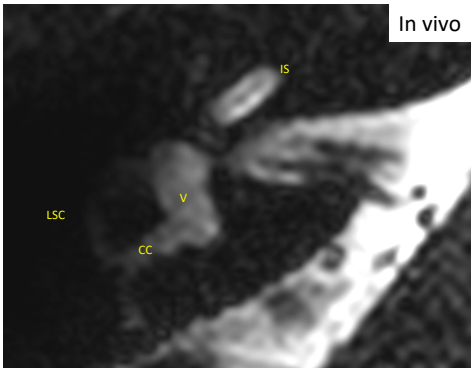

Figure 7: Axial reconstruction. Because we focused on the cochlea and IAC with maximum signal intensity, these are clearly depicted. Because of increasing loss of signal, the vestibule is only moderately depicted, whereas the semicircular canals are hardly visible. Scan duration: 7 minutes 31 seconds.

DISCUSSION

3T MRI of the inner ear, now widely used in the clinical setting, grossly depicts the osseous labyrinth (including semicircular canals and vestibule), the fluid in the cochlea (including cochlear modiolus and interscalar septum), and the 4 nerve bundles in the internal auditory canal. Although the basilar membrane is clearly visible, separating the scala tympani and the scala vestibuli, Reissner's membrane and scala media cannot be depicted on 3T [9].

The initial results on this study demonstrate that high resolution 7T MRI of the inner ear is possible. Overall, all structures visible on 3T could be visualized on 7T. However, no additional membranous structures could be depicted on 7T. Because we focused on the cochlea and IAC with maximum signal intensity, the labyrinth was depicted with less detail.

Ex vivo, we noticed a moderate depiction of the IAC including all 4 nerves because of a lack of fluid in this specific area. On the contrary, a surplus of fluid in the area of the vestibular aqueduct probably resulted in appearance of this structure. On in vivo images, the aqueduct could not be visualized, which is consistent with literature and findings on 3T, only showing the vestibular aqueduct in large vestibular aqueduct syndrome (LVAS), one of the most common inner ear abnormalities reported.
The membranous labyrinth is only 12 mm high and can only be examined in detail when submillimetric (thickness, *e*7 mm) images are used. At 7T, settings applied in 1.5T

and 3T have to be strongly adjusted to optimize image quality [2]. The specific absorption rate (SAR) is higher, and susceptibility artifacts are more pronounced in 7T than at 3T or 1.5T, especially in proximity to the bony skull base and air-filled areas. In our study, this resulted in a good visualization of the cochlea, the focus of maximal intensity, with diminished quality of the labyrinth in vivo.

At 7T, the SAR scales quadratically with field strengths. Because of radiofrequency (RF) standing wave properties in human tissue, the maximum applicable SAR value will depend heavily on the geometry of the part of the body that is exposed to the RF energy and on the exact location and geometry of the RF source. Consequently, this affects the voxel size and maximum acquisition time in vivo. The initial voxel size of 0.15 mm in maximal resolution diminished to a voxel size of 0.5 mm in vivo. Kraff et al. has described depiction of the facial nerve close to the brain stem with 0.6 mm isotropic voxel size [5]. The acquisition time in vivo varied between approximately 7 and 14 minutes, not including 2 to 3 minutes for proper adjustment of frequency, transmitter voltage as well as 3D shim, which had to be performed manually before each examination. Quality of images with different acquisition times was similar.

Concerning side effects, transient vertigo was reported by 1 volunteer. This is consistent with Theysohn et al. who reported vertigo as the most pronounced sensation at 7T, with 5% of patients rating it as very unpleasant [8]. It was the most frequently reported sensation during movement in the 7T field, especially when moving headfirst into and out of the 7T bore. However, vertigo was rated less annoying than the exam duration (statistically significantly different) or, to a lesser degree, noise. Although the number of side effects is increased at 7T compared with 1.5T, 7T was well tolerated by the majority of subjects and is considered a safe procedure [8]. Further improvement of inner ear imaging at 7T could be achieved by developing dedicated surface coils for the inner ear region, reducing the distance between the coil and the inner ear, and gaining maximum SNR in the cochlea with reduction of overall SAR to the patient.

CONCLUSION

To our knowledge, this report is the first to describe imaging of the inner ear at 7T in volunteers. The acquisition time was approximately 10 minutes. Although inhomogeneities remain present, maximum resolution scanning ex vivo and scanning in vivo resulted in clear depiction of the major membranous structures. Of course, further studies are needed to further optimize image quality, with possible application of dedicated surface coils.

Abbreviations

PSC: Posterior Semicircular Canal
VA: Vestibular Aqueduct
CC: Common Crus
LSC: Lateral Semicircular Canal
IS: Interscalar Septum
MD: Modiolus
V: Vestibule
SSC: Superior Semicircular Canal
CA: Crista Ampullaris
CO: Cochlear Nerve
VS: Superior Vestibular Nerve
VI: Inferior Vestibular Nerve
FA: Facial Nerve
NB: Nerve Bundles

REFERENCES

1. Naganawa S, Ito T, Fuktsu H et al. MR imaging of the inner ear: comparison of a three-dimensional fast spin-echo sequence with use of a dedicated quadrature-surface coil with a gadolinium-enhanced spoiled gradient-recalled sequence. *Radiology* 1998;208(3):679-85.

2. Naganawa S, Koshikawa T, Fukatsu H, Ishigaki T, Aoki I, Ninomiya A. Fast recovery 3D fast spin-echo MR imaging of the inner ear at 3 T. *AJNR Am J Neuroradiol.* 2002;23(2):299-302.

3. Heverhagen JT, Bourekas E, Sammet S, et al. Time-of-flight magnetic resonance angiography at 7 Tesla. *Invest Radiol*. 2008;43:568–73.

4. Kollia K, Maderwald S, Putzki N, et al. First clinical study on ultra-high-field MR imaging in patients with multiple sclerosis: comparison of 1.5 T and 7 T. *AJNR* 2009;30:699–702.

5. Kraff O, Theysohn JM, Maderwald S, et al. High-resolution MRI of the human parotid gland and duct at 7 Tesla. *Invest Radiol*. 2009;44(9):518-24.

6. International Electrotechnical Commission. International Standard. Medical electrical equipement. Part 2–33: Particular requirements for the safety of magnetic resonance equipement for medical diagnosis. Edition 2.2. 60601-2-33 Geneva: International Electrotechnical Commission; 2008. p 33–35.

7. Collins CM, Liu W, Wang J et al. Temperature and SAR calculations for a human head within volume and surface coils at 64 and 300 MHz*. J Magn Reson Imaging.* 2004;19(5):650-6.

8. Theysohn JM, Maderwald S, Kraff O, et al. Subjective acceptance of 7 Tesla MRI for human imaging. *Magma* 2008;21:63–72.

9. Casselman JW, Offeciers EF, De Foer B et al. CT and MR imaging of congenital abnormalities of the inner ear and internal auditory canal. *Eur J Radiol.* 2001;40(2): 94-104.

CHAPTER 4

In vivo imaging of the inner ear at 7 Tesla MRI; Image evaluation and comparison with 3 Tesla

Otology Neurotology. 2015;36(4):687-93.

Sylvia L. van Egmond
Fredy Visser
Frank A Pameijer
Wilko Grolman

ABSTRACT

Objective

The implementation of 7T magnetic resonance imaging for human use has the potential to further advance spatial resolution beyond that of 3T. This could result in potential advantages in the depiction of the membranous structures of the inner ear. The inner ear is particularly challenging to visualize at 7T because of its anatomic location, which can lead to susceptibility banding artifacts and signal loss.

Study Design

Three healthy volunteers underwent magnetic resonance imaging at 3T and 7T scanner. At 7T, a unilateral dielectric pad was used for image optimization. Scan duration therefore doubled to a total of 15 minutes at 7T.

Methods

The depiction of 10 anatomic parts of the inner ear was evaluated by two independent readers using a four-point grading scale.

Results

The interscalar septum, utricular macula, and the nerve bundles in the internal auditory canal were visualized more clearly at 7T.

Conclusion

Although reduction of image artifacts remains challenging, especially at 7T, all structures depicted at 3T could be depicted at 7T. Image quality for some anatomic structures was superior at 7T. Further improvement of image quality could be achieved by developing dedicated surface coils and by technical advancement in B1 shimming and dedicated radiofrequency pulses.

INTRODUCTION

Up to now, magnetic resonance imaging (MRI) of the membranous structures of the inner ear has been aimed at the detection of normal fluid signal intensity within the bony labyrinth at 1.5T and 3T imaging. As yet, MRI in the clinical setting has not been able to show smaller membranous structures of the inner ear, such as the basilar membrane/interscalar septum, Reissner's membrane, and macula. Microimaging techniques do have the ability to visualize the cochlear duct (scala media), but its clinical impact is not of importance [1].

Improved visualization with detection of endolymphatic vesicles of the inner ear might permit new insights in the diagnosis and treatment of labyrinthine disease and can be useful for clinical application in cochlear implantation. Up to now, advances in higher-field strength MR systems have significantly improved the resolution of inner ear structures, but the major labyrinthine structures can still not be resolved on clinical scanners. Application of 7T MRI with an increased signal-to-noise ratio (SNR) has already demonstrated diagnostic benefits in various anatomic areas, including high-resolution breast cancer imaging and myocardial tissue characterization [2,3]. Capabilities of 7T are especially suited for neuroapplications, in which the increase in SNR and the enhanced sensitivity to susceptibility have allowed a more detailed microanatomic depiction of various structures and microvascularity. This offers potential benefits for diagnostics, surgical planning, and therapy monitoring.

However, visualization of the inner ear at 7T is particularly challenging. Its close proximity to the bony skull base and air-filled areas can lead to substantial signal loss at the interface between the inner ear and its surroundings because of severe inhomogeneities in both B0 (main magnetic field) and B1 (radiofrequency [RF] field).

In this study, we present in vivo images of the inner ear at 7T and compare its ability with 3T for depiction of the membranous structures of the inner ear.

MATERIALS AND METHODS

During an initial series of scans with a human cadaver head, optimal scanning sequence parameters were formulated [4]. Ex vivo, an isotropic voxel size of 0.15 mm could be achieved in prolonged acquisition time, up to 4.5 hours. However, in vivo scanning only allows a short acquisition time to pursue maximum clinical applicability as well as optimal safety measures during 7T scanning.

Concerning RF safety of ultrahigh-field MRI, the most conservative 7T head model was applied. This is to ensure not to exceed specific absorption rate distributions as defined

by the International Electrotechnical Commission regulations [5]. The in vivo use of 7T and 3T was approved by the institutional review board for a maximum of three volunteers for this pilot project.

Three healthy volunteers underwent MRI at a 7T scanner (Phillips Achieva, The Netherlands) using a Transmit/Receive (T/R) volume coil in combination with a 32-channel receive coil (Nova Medical). A dielectric pad was placed next to the ear of interest. Three sequential three-dimensional (3D) turbo spin echo scans were acquired, all with minor adjustments. The TR and TE sequences were comparable to our clinically applied settings. The highest spatial resolution was found with the following parameters: 3D turbo spin-echo, TR (repetition time)/TE (echo time) 6,009/205 milliseconds, turbofactor 100, SENSE factor 1.7, field of view 150 x 150 x 31 mm, 63 contiguous transverse slices, imaging matrix of 300 x 300, signal average 1, resulting in an acquisition isotropic voxel size of 0.5 x 0.5 x 0.5 mm, scan duration 7 minutes 31 seconds. Right and left ears were scanned successively after replacing the dielectric pad to the contralateral ear.

Subsequently, the three volunteers were scanned at a 3T scanner (Phillips Achieva) using an eight-channel sensitivity encoding (SENSE) head coil. Hospital routine sequence protocol was applied with two strong T2-weighted fast spin-echo (FSE) 3D sequences in transverse and oblique planes. Acquisition time for both sequences was 4 minutes 32 seconds, with a total of 9 minutes 4 seconds. Parameters were TR/ TRequiv 2, 000driven/198 milliseconds, turbofactor 54, field of view 130 x 130 x 25 mm, 50 slices, imaging matrix of 276, signal average 1, resulting in a (nonisotropic) voxel size of 0.5 x 0.6 x 1.0 mm.

The entire volume data set was reconstructed in the axial, coronal, and sagittal planes. All 3T and 7TMR images of the six inner ears scanned were independently reviewed by a dedicated head and neck radiologist and one of the researchers (Ear Nose and Throat resident). Complete blinding was not possible because 7T scans only displayed one inner ear, whereas 3T scans visualized both inner ears. A total of 10 anatomic structures were evaluated on 3T and on 7T, including all semicircular canals; lateral semicircular canal (LSC), posterior semicircular canal (PSC), and superior semicircular canal (SSC), as well as the vestibule (V), the utricular macula (UM), the vestibular aqueduct (VA), the four nerve bundles (NBs) in the internal auditory canal (IAC), the cochlear modiolus (CM), the interscalar septum (IS), and Reissner's membrane using a four-point grading scale (3, clearly demonstrated/good; 2, demonstrated/fair; 1, demonstrated but unclear/ poor; 0, not demonstrated). In the literature, image quality

is usually graded on a three-point scale [6,7]. However, this does not include the possibility that a defined structure cannot be depicted.

We defined clearly demonstrated or good as complete visualization, demonstrated or fair as incomplete visualization with only minor defects, and demonstrated but unclear or poor as incomplete visualization with major defects.

Table 1: *Evaluation of visualization of anatomical parts.*

Evaluated anatomical structures	3 Tesla		7 Tesla	
	Right ear	Left ear	Right ear	Left ear
Vestibule	3.00 (0.00)	3.00 (0.00)	3.00 (0.00)	3.00 (0.00)
Lateral semicircular canal	3.00 (0.00)	3.00 (0.00)	2.67 (0.52)	3.00 (0.00)
Posterior semicircular canal	3.00 (0.00)	3.00 (0.00)	3.00 (0.00)	3.00 (0.00)
Superior semicircular canal	3.00 (0.00)	3.00 (0.00)	2.67 (0.52)	2.67 (0.52)
Utricular macula	1.33 (0.82)	1.33 (0.52)	2.33 (0.52)	2.17 (0.75)
Cochlear modiolus	3.00 (0.00)	3.00 (0.00)	3.00 (0.00)	3.00 (0.00)
Interscalar septum	2.67 (0.52)	2.83 (0.41)	3.00 (0.00)	3.00 (0.00)
Reissner's membrane	0.33 (0.52)	0.17 (0.41)	0.00 (0.00)	0.33 (0.52)
Four nerve bundles	2.00 (0.00)	2.00 (0.00)	3.00 (0.00)	3.00 (0.00)
Vestibular aqueduct	0.00 (0.00)	0.00 (0.00)	0.33 (0.00)	0.00 (0.00)

4-point grading scale (0:not demonstrated, 1:demonstrated but unclear, 2: demonstrated, 3: clearly demonstrated). Values are expressed as mean (SD).

RESULTS

The results of image evaluation are summarized in Table 1. All presented figures give comparable views of 3T and 7T imaging. Figures are presented in axial view. At 3T, the labyrinth was *clearly demonstrated* in all volunteers (Figs. 1, 2). At 7T, in three out of six ears, visualization of the semicircular canals was scored as *fair* by both readers. The V at 7T was *clearly demonstrated*.

The UM was better visualized at 7T, although depiction varied between different scans. The CM was clearly depicted on both field strengths. The IS of the basal turn was clearly visualized on both 3T and 7T, but depiction of the mid and apical turn was better at 7T (Figure 3). Reissner's membrane was rated as *demonstrated but unclear* at both 7T and 3T, identifying the scala media, although interrater agreement was 100% at 7T but 0% at 3T.

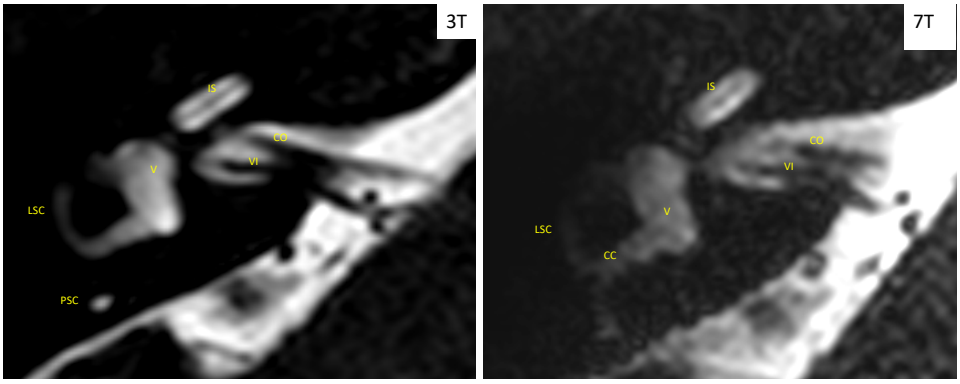

Figure 1: Axial view of vestibule (V), lateral semicircular canal (LSC), and interscalar septum (IS) of the basal cochlear turn. CO indicates cochlear nerve; VI, inferior vestibular nerve; PSC, posterior semicircular canal.

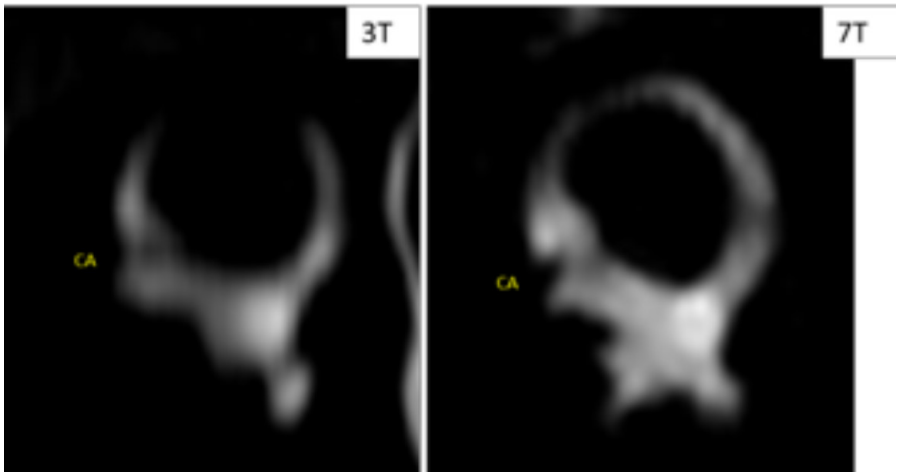

Figure 2: Oblique (Pöschl) view of the superior semicircular canal. CA indicates crista ampullaris.

The four NBs, including the facial nerve and the three branches of the vestibulocochlear nerve, situated in the IAC, were clearly visualized in reconstructed images made perpendicular to the IAC (Figure 4). Image quality of 7T imaging was considered superior. All six ears were scored by the readers as *clearly demonstrated* at 7T. At 3T, all ears were scored as *demonstrated, fair*, with only minor defects. Differentiation between NBs was not as clear at 3T, although all four nerves could be depicted separately.

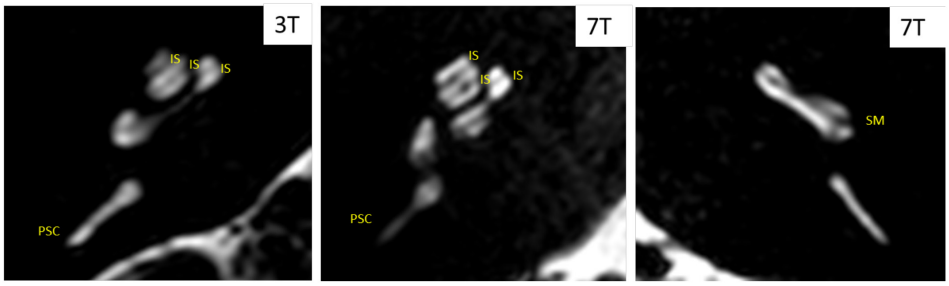

Figure 3: Axial view of interscalar septum (IS) of basal, mid, and apical cochlear turns and posterior semicircular canal (PSC). SM indicates scala media.

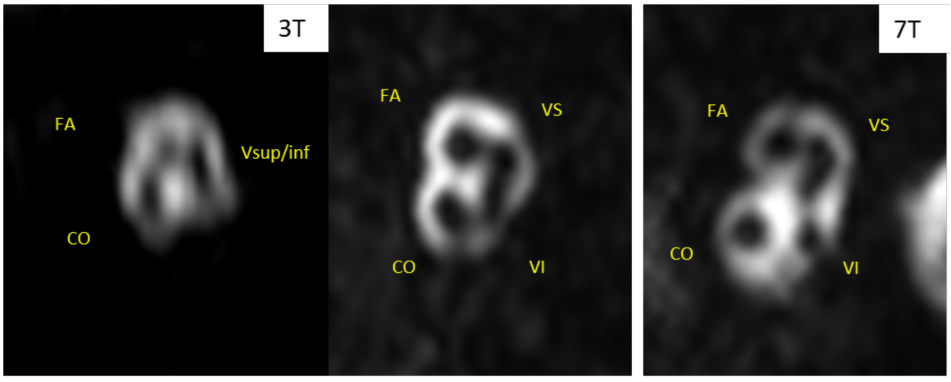

Figure 4: Sagittal-oblique (Stenvers) view, reconstructed perpendicular to the internal auditory canal (IAC). Comparison of nerve bundles in the IAC at 3T and 7T. CO indicates cochlear nerve; VI, inferior vestibular nerve; VS, superior vestibular nerve; FA, facial nerve.

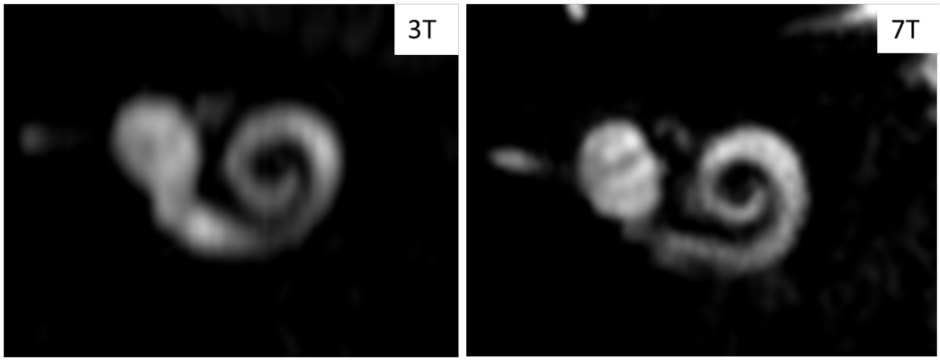

Figure 5: Coronal oblique image through the cochlea.

The endolymphatic duct and sac (VA) could not be demonstrated in all ears, except for one ear at 7T, which was scored by both readers as *demonstrated but unclear*. The cochlea was well visualized at both 3T and 7T (Figure 5), although inhomogeneities increased at 7T because of an increase in SNR. The Cohen's J for interrater agreement was 0.76 for a total evaluated number of 120 anatomic structures.

DISCUSSION

We performed a literature search using four different search engines (Pubmed, Embase/Medline, Cochrane, and Scopus). Results are summarized in a flowchart (Figure 6). When we filtered our search on 7T and the inner ear, we found three recent articles [8,9,10]. Brink et al. designed two dielectric pads that lead to an increase in the transmission efficiency and uniformity at the inner ear, resulting in an increased contrast homogeneity and increased diagnostic value[8]. Sato and Kawagishi performed 7T MRI in 18 patients with idiopathic sensorineural hearing loss and in 32 normal-hearing controls to compare the detection rates of the labyrinthine artery [9]. In all patients and in all but one healthy volunteer, the labyrinthine artery could be depicted. Ward et al. found support for the Lorentz force, a magneto-hydrodynamic force derived from ionic currents in the endolymph, pushing on the cupula [10]. This mechanism would cause a nystagmus in all normal humans when exposed to magnetic fields from high-strength MRI machines. Patients with unilateral deficits in labyrinthine function showed a nystagmus corresponding to their vestibular hypofunction.

In this study, we compared image quality in the depiction of the inner ear structures between 3T and 7T imaging in vivo. The FSE technique, already successful at 1.5T and 3T imaging [11], also proved to be successful in 7T.

At 7T, settings applied in 1.5T and 3T have to be strongly adjusted to optimize image quality. The increased SNR at 7T offers a great opportunity for the depiction of detailed structures of the inner ear. However, its unique anatomic location with surrounding bone, air-filled spaces, and the inner ear fluids causes differences in susceptibility, resulting in strong inhomogeneities in both static (B0) and transmit RF (B1) fields.

Although not as pronounced as on 7T, banding is more problematic on 3T than on 1.5T. With the arrival of 3T, the longer T1 time of cerebrospinal fluid necessitated a longer TR, resulting in prolonged acquisition times. With fast recovery FSE sequence, TR could be reduced while maintaining T2 contrast. Naganawa et al. optimized sequence parameters with an acquisition time of 13 minutes [11].

In our study, the labyrinth was clearly demonstrated at 3T. The four NBs and IS were scored as fair or demonstrated, referring to incomplete visualization with only minor

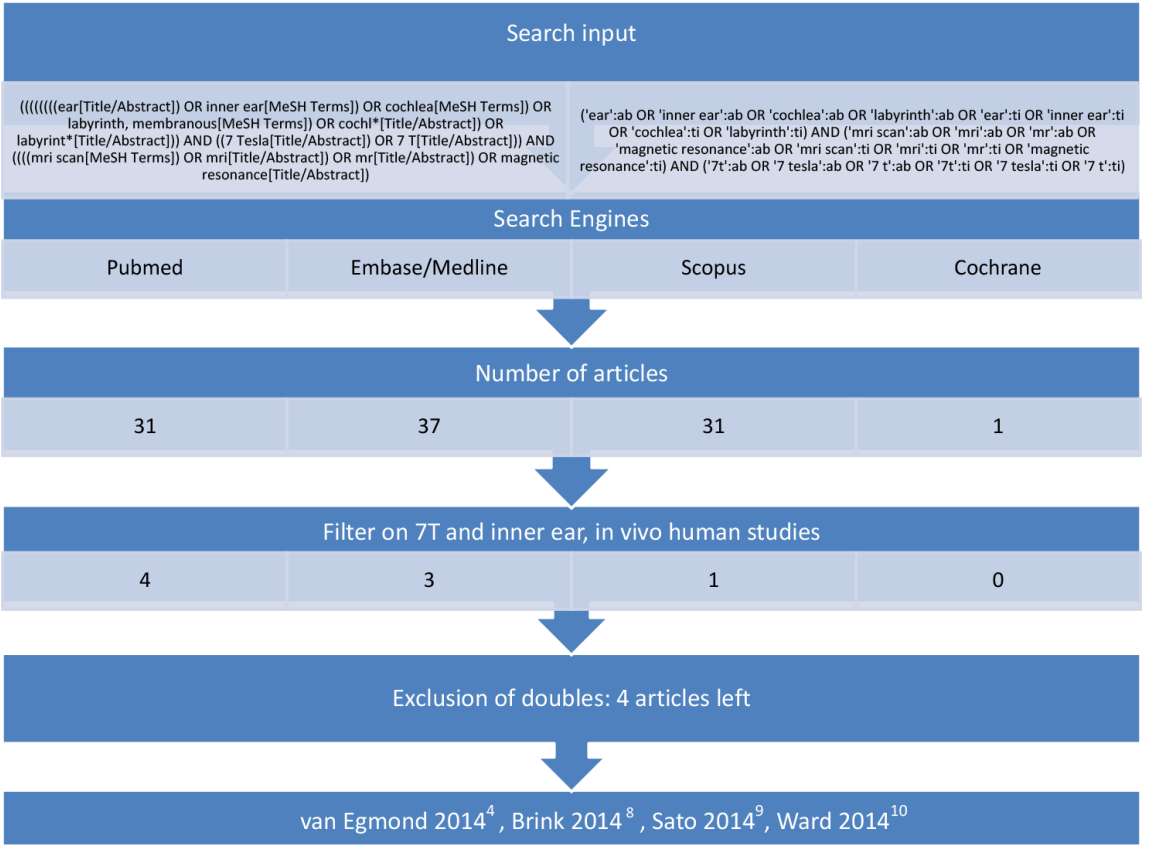

Figure 6: Flowchart literature search.

defects. The IS could be visualized clearly at the basal turn of the cochlea but had minor defects at the mid and apical turns.
Lane et al. evaluated 3D fast recovery FSE and 3D constructive interference in the steady state at 3T MRI [12]. The same anatomic structures scored by us were scored by two neuroradiologists using a two-point scale: adequately visualized or absent. Semicircular canals, endolymphatic duct, and facial nerve canal were not always visualized on 3D fast recovery FSE sequence. All anatomic structures were visualized on 3D constructive interference in the steady state sequence.
Byun et al. compared 3D driven equilibrium (DRIVE) imaging with 3D balanced fast field echo imaging at 3T [7]. Scoring was done using a two- or three-point scale. All anatomic structures on DRIVE sequence were rated as good image quality, except for the IS. The V and semicircular canals were apparently better visualized with DRIVE sequence, but this was not statistically significant. In accordance with our findings, the IS was scored as fair.

Other literature reports on 3T of the inner ear only include quantitative SNR and contrast-to-noise ratio measurements in their analyses.

With the aim to focus on the small structures of the membranous labyrinth, Lane et al. tried to reduce both susceptibility artifact and image blurring with a 3D Variable Flip Angle FSE sequence technique at 3T [1]. Image quality was not qualitatively scored, so a comparison with our 3T images is difficult. Lane's 3T images demonstrated a low signal intensity focus, corresponding to the UM. These findings are consistent with our image evaluation. Images could not differentiate the saccular macula from the medial wall of the V. The cochlear duct could not be depicted.

At 7T, wavelength shortens, decreasing from 52 cm at 1.5T to 12 cm at 7T, which is smaller than the diameter of the human head. This causes constructive interference in RF, an intrinsic problem at 7T. Without adjustments, signal intensity concentrates in the center of the head, resulting in diminished visualization of the more laterally situated inner ears. Therefore, the whole field of interest, including both inner ears, could not be depicted on 7T, without heavy adjustments, including B1 shimming, as described by Brink et al., using two dielectric pads. With the use of a unilateral dielectric pad, we optimized the signal intensity laterally, with optimization of image quality of the unilateral inner ear [8]. As a consequence, scan duration doubled, with a total scan time of 15 minutes. In the study of Brink et al., asymmetrically sized pads were required to compensate for the intrinsic asymmetry at B1, which is known to increase with field strength. With the use of a unilateral dielectric pad, we did not have to correct for this

problem [8]. We used a 32-channel receive coil. Brink et al. described an improvement in contrast homogeneity at 7T, especially at the IAC, when using a 32-channel receive array instead of a single surface coil [8].

All structures visualized on 3T imaging, including semicircular canals, V, four NBs, CM, and IS, could also be demonstrated on 7T.
The four NBs were visualized more clearly on 7T imaging. This is concordant with the literature [13]. Increasing MRI field strength has already made it possible to image the microstructure of the deep cerebellar nuclei in greater detail. Situated more centrally, substantial signal loss at the interface between the inner ear and its surroundings is of less importance in this area. Brink et al. also demonstrated a clear depiction of the four NBs [8]. In the left ear, the ear of their focus, the additional use of dielectric pads barely improved image quality.
The IS was clearly demonstrated in all cochlear turns, including mid and apical turns, in contrast to 3T. As mentioned earlier, Reissner's membrane could be depicted in some inner ears at the basal turn of the cochlea at both 3T and 7T. However, interrater agreement was 100% for this anatomic structure at 7T but 0% at 3T.
The endolymphatic duct and sac (VA) could not be demonstrated in all ears, except for one ear at 7T, which was scored by both readers as demonstrated but unclear. This is concurrent with previous findings in the literature. Depiction of these structures is only described in the large VA syndrome [14].

As mentioned earlier, literature regarding the depiction of the inner ear at 7T is very sparse. Brink et al. only assessed the semicircular canals (together as one entity), the cochlea, and the IAC . These were all nearly rated as good depiction, high diagnostic value with dielectric pads. Without pads, the left ear scored an average of poor visibility, inadequate diagnostic value, and the right ear scored an average of acceptable visibility, adequate diagnostic value. Nothing is mentioned concerning smaller and membranous structures of the ear including the modiolus, maculae, IS, or Reissner's membrane [8]. Sato and Kawagishi did not evaluate visibility of any inner ear structure besides the labyrinthine artery [9].

Interrater agreement was 0.76 for a total evaluated number of 120 anatomic structures. Brink et al. reported a κ value between 0.61 and 0.75, which is slightly lower, but still reflects an adequate agreement [8].

A drawback in our study was the doubling of scan duration at 7T, resulting from the need to use a unilateral dielectric pad, optimizing signal intensity at one inner ear at

the time. Total scan duration was therefore longer at 7T. One sequence at 3T takes only 4 minutes 32 seconds, but two sequences for oblique and transverse source data are necessary for reconstruction because of non-isotropic pixel size. Isotropic scanning of one ear at 7T could be accomplished in 7 minutes 31 seconds. Both inner ears could be scanned in 15 minutes (with a surplus of 2-3 min adjusting the dielectric pad to the contralateral ear). Brink et al. had an acquisition time of approximately 10 minutes [8]. A limitation of our study is the lack of blinding. The two readers could not be blinded for image modality because 7T scans only displayed one inner ear, whereas 3T scans visualized both inner ears. Although the readers independently evaluated all anatomic structures and images were presented in random sequence, this could have resulted in an observer bias and an overestimation of image accuracy on 7T.

Considering clinical application in preoperative and perioperative scanning for cochlear implantation, improved visualization of membranous structures including the IS at 7T could be of importance. At 7T, image quality of the IS was considered superior, although, at 3T, it was also demonstrated.

Further improvement of image quality could be achieved by developing dedicated surface coils for 7T scanning. Moreover, technical advancement in B1 shimming and dedicated RF pulses are expected to further improve quality, increasing its ability for clinical application in cochlear implantation. Third, fusion of MR and other imaging modalities, such as computed tomography and 3D rotational x-ray imaging, could further improve its impact on daily practice.

CONCLUSION

To our knowledge, this is the first comparison of 3T and 7T imaging of the inner ear in vivo. Most parts of the inner ear could be visualized well on both field strengths, although challenges, especially artifact reduction, remain at 7T. In this study, we were not able to visualize more anatomic details in the cochlea itself than those that have been demonstrated earlier in 1.5T and 3T
MR scanning.

REFERENCES

1. Lane JI, Witte RJ, Bolster B, et al. Imaging microscopy of the middle and inner ear. Part II: MR microscopy. State of the art: 3T imaging of the membranous labyrinth. *Clin Anat* 2005;18:409-15.

2. Kraff O, Fischer A, Nagel AM, Monninghoff C, Ladd ME. MRI at 7 tesla and above: demonstrated and potential capabilities. *J Magn Reson Imaging* 2015;41:13-33.

3. Umutlu L, Ladd ME, Forsting M, Lauenstein T. 7 Tesla MR imaging: opportunities and challenges. *Rofo* 2014;186:121-9.

4. Van Egmond SL, Visser F, Pameijer FA, Grolman W. Ex vivo and in vivo imaging of the inner ear at 7 Tesla MRI. *Otol Neurotol* 2014;35:725-9.

5. International Electrotechnical Commission. International Standard. Medical Electrical Equipment. Part 2-33: Particular Requirements for the Safety of Magnetic Resonance Equipment for Medical Diagnosis. 2008:33-5.

6. Dahmani-Causse M, Marx M, Deguine O, Fraysse B, Lepage B, Escude´ B. Morphologic examination of the temporal bone by cone beam computed tomography: comparison with multislice helical computed tomography. *Eur Ann Otorhinolaryngol Head Neck Dis* 2011;128:230-5.

7. Byun JS, Kim HJ, Yim YJ, et al. MR imaging of the internal auditory canal and inner ear at 3 T: comparison between 3D driven equilibrium and 3-D balanced fast field echo sequences. *Korean J Radiol* 2008;9:212-8.

8. Brink WM, van der Jagt AM, Versluis MJ, Verbist BM, Webb AG. High permittivity dielectric pads improve high spatial resolution magnetic resonance imaging of the inner ear at 7T. *Invest Radiol* 2014;49:271-7.

9. Sato H, Kawagishi K. Labyrinthine artery detection in patients with idiopathic sudden sensorineural hearing loss by 7T MRI. *Otolaryngol Head Neck Surg* 2014;150:455-9.

10. Ward BK, Roberts DC, Della Santina CC, et al. Magnetic vestibular stimulation in subject with unilateral labyrinthine disorders. *Front Neurol* 2014;5:28.

11. Naganawa S, Koshikawa T, Fukatsu H, Ishigaki T, Aoki I, Ninomiya A. Fast recovery 3D fast spin-echo MR imaging of the inner ear at 3 T. *AJNR Am J Neuroradiol* 2002;23:299-302.

12. Lane JI, Ward H, Witte RJ, Bernstein MA, Driscoll LW. 3T imaging of the cochlear nerve and labyrinth in cochlear-implant candidates: 3D fast recovery fast spin-echo versus 3D constructive interference in the steady state techniques. *Am J Neuroradiol* 2004;25:618-22.

13. Kuper M, Thurling M, Maderwald S, Ladd ME, Timmann D. Structural and functional magnetic resonance imaging of the human cerebellar nuclei. *Cerebellum* 2012;11:314-24.

14. Casselman JW, Offeciers EF, De Foer B, et al. CT and MR imaging of congenital abnormalities of the inner ear and internal auditory canal. *Eur J Radiol* 2001;40:94-104.

SECTION TWO

Malignant otolaryngology disease: larynx and neck

CHAPTER 5

Systematic review of the diagnostic value of Magnetic Resonance Imaging for early glottic carcinoma

Laryngoscope Investigative Otolaryngology. 2018;3(1):49-55.

Sylvia L. van Egmond
Inge Stegeman
Frank A. Pameijer
Johanna J. Bluemink
Chris H. Terhaard
Luuk M. Janssen

ABSTRACT

Objective

In early glottic cancer, accurate assessment of tumor extension, including depth infiltration, is of great importance for both staging, therapeutic approach and systematic comparison of data. Our goal was to assess the diagnostic value of MRI in pre-therapeutic staging of primary early stage (T1 and T2) glottic carcinoma.

Study design

Systematic review of literature.

Methods

We conducted a systematic search in Pubmed, Embase and Scopus up to September 23rd, 2016. Included studies were selected and critically appraised for relevance and validity.

Results

7 out of 938 unique articles were selected, including 64 cases. MRI overstaged 6% and understaged 13% of cT1 and cT2 tumors. However, available data is heterogeneous, very limited and mainly based on subanalysis of a small amount of patients. Reported MRI protocols appear to be suboptimal for small laryngeal lesions. Diagnostic value of MRI for subtle depth infiltration or laryngeal anatomical subsites (e.g. laryngeal ventricle, vocal cord etc.) could not be assessed.

Conclusions

More studies are needed to assess the diagnostic value of MRI for small glottic tumors.

INTRODUCTION

Laryngeal squamous cell carcinoma (SCC) is one of the most common head and neck cancers, arising from the mucosal surface of the larynx. Early stage squamous cell carcinomas of the larynx, especially in the glottic area, have high local control rates (76.8%-88.9%) [1,2,3]. The aim of treatment is to ensure oncological cure with preservation of function. The most important factor in treatment planning is the accuracy of pre-therapeutic staging with detailed assessment of neoplastic extension.
For superficial midcord T1a glottic tumors, comparable local control rates for both endoscopic laser surgery and radiotherapy are described. However, for more extended lesions, including the anterior commissure, contralateral vocal cord (T1b) or T2 lesions, there still is no consensus on treatment strategy with optimal outcome [2]. The main factor that prohibits the systematic evaluation and pooling is data is the uncertainty of tumor comparability, due to an absence of a standardized method that accurately measures tumor extent and depth. Furthermore, papers focusing on laser surgery do not uniformly categorize resection types. For endoscopic laser resections, tumor depth directly influences the type of European Laryngological Society (ELS) resection. With lesser resections, including subepithelial (type I) and subligamental (type II) and greater resections extending into the vocal muscle (type III), anterior commissure (type IV) or for example into the contralateral vocal cord (Va).

Detailed assessment of neoplastic invasion can be achieved with different modalities. Direct visualization of the tumor by indirect or direct laryngoscopy is the first step in diagnosis and evaluation of tumor extension. Although this can detect superficial tumor growth, subtle depth infiltration can only be estimated by palpation, and paraglottic invasion as well as deep tumor spread into the conus elasticus may be entirely occult. Also, endoscopic exposure of the AC area can be problematic. Reported rates of correct staging of AC invasion by direct laryngoscopy vary beteen 40-72% [4,5]. False-negative results are likely to result in insufficient treatment and recurrence, while false-positive evaluation results in overtreatment, unnecessary morbidity and patient burden.

Detailed, high resolution imaging of the larynx can give additional information about tumor infiltration, not visible with laryngoscopy. Cross-sectional imaging of the larynx can be performed with Computed Tomography (CT) or Magnetic Resonance Imaging (MRI). Although CT and MRI are routinely used to differentiate between limited or gross cartilage invasion and to evaluate deep soft-tissue extension, their role in early stage glottic carcinoma remains limited.

MRI had several advantages over CT. It does not require exposure to ionizing radiation and it provides superior soft tissue contrast compared to CT. Furthermore, MRI is considered to be superior for detection of cartilage invasion [6]. Also, MRI allows a multiparameter analysis (T1 weighted, T2 weighted, DWI and post-contrast acquisition). This amplifies the contrast resolution. MRI images are, however, more likely to be degraded by motion caused by swallowing and breathing. Also, MRI cannot be performed in patients with metallic foreign bodies, such as cochlear implants, and certain implant devices [7]. The detection of subtle tumor spread by imaging can be difficult. However, detailed evaluation of submucosal areas can both change the disease stage, and reassess the therapeutic approach. Therefore, our goal is to assess the diagnostic value of MRI in pre-therapeutic staging of primary early stage (T1 and T2) glottic carcinoma.

METHODS

Search strategy

We conducted a systematic search in Pubmed, Embase, Scopus and Cochrane up to September 23, 2016. A search syntax was developed by using synonyms for MRI (determinant) and laryngeal carcinoma (outcome) [figure 1]. Reporting of our data is done according to the PRISMA statement [8].

Study selection

Screening of publications was performed by two authors independently (SE, IS). Any difference in opinion was resolved by consensus. From the retrieved articles duplicates were removed. Title and abstract, and ultimately the full-text of potentially eligible articles were screened using criteria shown in Figure 2. A thorough analysis of selected articles was made, and their bibliographies were analyzed to identify any additional articles that could be relevant for this review. Histopathology was the reference standard in our study. Inclusion criteria were clinical T1 and T2 glottic squamous cell carcinomas. MRI had to be performed in all patients.

Critical appraisal of included studies

Using predefined criteria, articles were critically appraised for relevance and validity. Data collected included number of patients with T1 and T2 disease, MRI strength, standardized MRI protocol, reference standard, blinding, missing data and selection bias [Table 1].

A: PubMed
Search ((((((((((cancer*[Title/Abstract]) OR tumor*[Title/Abstract]) OR tumour*[Title/Abstract]) OR carcinoma[Title/Abstract]) OR malignan*[Title/Abstract])) AND ((laryngeal*[Title/Abstract]) OR glottic[Title/Abstract]))) OR (((cancer, laryngeal[MeSH Terms]) OR cancer of the larynx[MeSH Terms]) OR cancers, laryngeal[MeSH Terms]))) AND ((((mri scan[MeSH Terms]) AND mri scans[MeSH Terms])) OR ((((mri[Title/Abstract]) OR mr[Title/Abstract]) OR magnetic resonance[Title/Abstract]) OR mri-scan[Title/Abstract]))

B: Embase
('cancer':ti OR 'tumor':ti OR 'tumour':ti OR 'carcinoma':ti OR malignanc*:ti OR 'cancer':ab OR 'tumor':ab OR 'tumour':ab OR 'carcinoma':ab OR malignanc*:ab) AND ('larynx':ab,ti OR 'glottis':ab,ti OR 'glottic':ab,ti OR 'laryngeal':ab,ti OR 'larynge':ab,ti OR 'laryngo':ab,ti) OR ('laryngeal cancer':ab,ti OR 'glottic carcinoma':ab,ti) AND ('mri':ab,ti OR 'mr':ab,ti OR 'magnetic resonance':ab,ti OR 'mri scan':ab,ti)

C: Scopus
(TITLE-ABS(cancer * OR tumor* OR tumour* OR carcinoma* OR malignan*) AND (laryn* OR glottic) AND (mri* OR magnetic resonan* OR mri-scan* OR mr))

Figure 1: Search Syntax

Data Extraction and Statistics

To compare the diagnostic value of MRI, positive predictive value (PPV), negative predictive value (NPV), sensitivity (SN) and specificity (SP) were extracted from eligible articles or, when not described, calculated (when possible) from the original data.

RESULTS

Search strategy and study selection

Our search strategy yielded 938 unique publications [Figure 2]. After title and abstract screening 80 articles were left for full-text assessment, of which 73 were excluded for various reasons. This resulted in a total of 7 eligible studies.

Critical appraisal

Appraisal of the 7 eligible studies is presented in table 1. All 7 studies were prospective. Only 2 articles only included glottic laryngeal carcinoma and were therefore considered

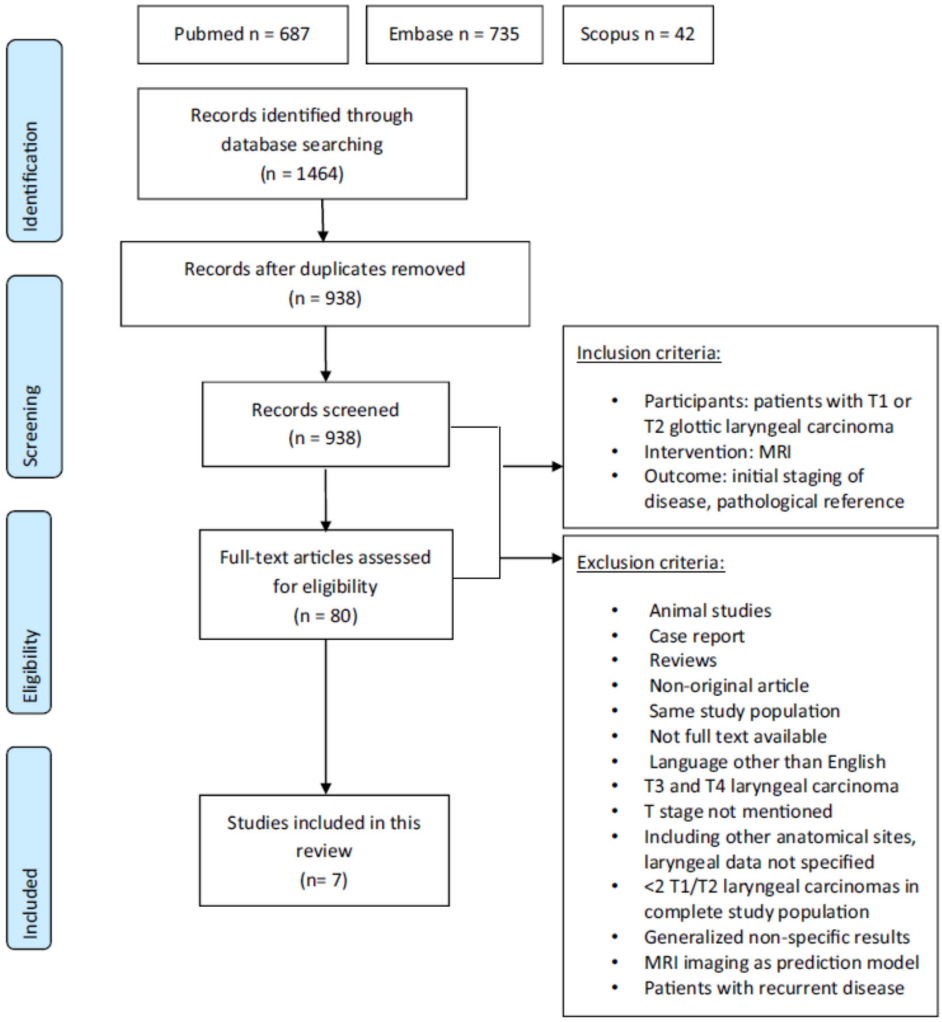

Figure 2: flow diagram

most relevant [10,13]. Two articles included supraglottic, glottic and subglottic carcinomas [12,15]. Banko et al included supraglottic and glottic tumors and Carriero and Wu evaluated 'laryngeal tumors' in which laryngeal level is not further specified, although Wu only included patients with involvement of the anterior vocal commissure. No subanalysis was done for glottic tumors only [9,14].

Furthermore, 5 articles included T1-T4 tumors, 1 article included T2-T4 tumors and 1 article included T1-T3 tumors [10]. MRI evaluation was done by 1 to 3 observers. Standardized MRI protocol was reported in 6 studies. Kraft et al did not specify MRI

Table 1: Critical appraisal

										Index test: MRI		Reference Test	
Author	Publication year	PTS with primary T1/ T2 laryngeal ca	MRI	outcome	No. glottic carcinomas	No cT1 carcinomas (T1a-T1b)	No cT2 carcinomas	Selection Bias Patient Sampling	Missing data	standardized protocol	Blinding (no. observers)	Standardized protocol	Blinding (no. Observers)
Wu[9]	2016	●	●	○	?/26	0	10	●	0	●	●(2)	●	●(2)
Allegra[10]	2014	●	●	●	20	14(8-6)	2	●	6/26	●	●(2)	●	●(2)
Banko[11]	2014	●	●	○	28/40	0	14	●	?	●	?	N/A	N/A
Kraft[12]	2013	●	●	○	27/76	11	26	●	8/84	?	●(1)	●	●(1)
Hu[13]	2011	●	●	●	30	5	12	●	0	●	●(2)	●	●(2)
Carriero[14]	2000	●	●	○	?/25	9	8	●	12/37	●	●(2)	N/A	N/A
Zbaren[15]	1996	●	●	○	34/40	0	5	●	?	●	●(3)	●	●(3)

Categories: ● Accurate , ○ Not Accurate , ? Unknown N/A: not applicable
../. number of glottic laryngeal episodes versus number of total laryngeal episodes (including supra- and subglottis)

settings or field strength. Missing data were not reported in 2 articles [11,15]. No cases of selection bias were found, although only Zbaren et al. and Hu et al. specifically report the inclusion of consecutive patients. Allegra et al. and Kraft et al. and excluded respectively 6 and 8 patients receiving curative radiotherapy instead of surgery. Carriero et al. excluded 12 patients because they were considered inoperable.

Study characteristics

Study characteristics are shown in table 2. Studies were heterogeneous in study methods and outcomes. Five studies describe completely excised tumors [9,10,12,13,15]. Allegra et al performed 2 excision biopsies, 4 chordectomies and 10 supracricoid laryngectomies (CHEP), all for T1 and T2 glottic carcinomas. Hu et al performed an endoscopic laser resection in 5 cases of T1 glottic carcinoma and partial laryngectomy in 12 cases of T2 disease [13]. Both studies performed analysis of laryngeal subsites for the whole study population only, including T3 and T4 tumors. Histopathologic correlation method for T1 and T2 disease is not described. Wu et al performed complete (8) or partial (18) laryngectomies in all 26 patients, of which 10 patients had a T2 carcinoma, and specimens underwent serial section [9]. However, only radiological and pathological T stages were compared, with no specifications on

Table 2: Study characteristics

Author	study design	MRI strength (tesla)	other imaging reference	Direct laryngoscopy
Wu[9]	P	3.0	CT/DW MRI	No
Allegra[10]	P	1.5	CT	No
Banko[11]	P	1.5	-	No
Kraft[12]	P	?	CT/ Endosono	Yes
Hu[13]	P	1.5	Sono	No
Carriero[14]	P?	1.0	-	Yes
Zbaren[15]	P	1.5	CT	Yes

P = prospective. En graag CT/endosono vervangen door CT/endosonography. En sono vervangen door sonography

laryngeal subsites. Zbaren et al evaluated only 4 patients with (laryngeal) cT2 tumors of a total of 40 included patients [15]. After histopathological verification, 10 were finally staged as pT2. Four patients underwent voice preserving laryngectomy (supraglottic laryngectomy in 3 cases and partial laryngectomy in one case), all others underwent total laryngectomy. Whole organ slices were cut parallel to the plane of the axial MRI. Kraft et al included 76 patients of which 11 T1 and 26 T2 tumors, both glottic and subglottic [12]. T stage according to laryngeal level is not further specified. Only patients undergoing complete surgical excision were included (chordectomy, laser resection, partial laryngectomy or total laryngectomy). 10 criteria, e.g. infiltration of the vocal fold, paraglottic space, midline crossing and maximum tumor diameter were scored.

In both studies of Banko et al and Carriero et al, 'surgery' and 'histology' are mentioned but not further specified. It is therefore unclear if complete surgical excision was carried out [11,14]. MRI field strengths varied between 1 and 3 Tesla and was not reported in one study [12]. Imaging consisted mostly of T2 and T1W contrasts with scans in several directions. Contrast was not used routinely in the study by Hu et al [13]. Three studies used contrast before a second T1W scan was performed [10,11,14]. The in-plane resolution was not always clearly described and (when reported) varied between 0.5x.0.5 mm2 and 1x1 mm2. Slice thickness was 3-4 mm in all included studies.

Data extraction and Statistics

Concordance between MRI and Pathological TNM Staging

A total of 64 patients were radiologically staged as T1 or T2 carcinomas [Table 3] [9,10,13,14,15]. Kraft et al. only reported final tumor staging and no comparison could be made between radiological and histopathological staging. Banko did not specify

Table 3: Total comparison of tumor staging between histopathology and Magnetic Resonance Imaging of selected articles [9,10,13,14,15].

PA Stage	**Radiological stage (MRI)**			
	T0	T1a/b	T2	Total
T0	-	2/-	-	2
T1a/b	3	23	-	26
T2	1	1	31	33
T3	-	-	3	3
T4	-	-	-	-
Total	4	26	34	64

number of patients that were over- or understaged and numbers could therefore not be calculated. Using TNM classification, overall concordance between MRI and histopathology was 81% (52 out of 64 patients). 6% (4 out of 64) of tumors were overstaged, 13% (8 out of 64) were understaged.

Four undetected lesions by MRI were finally confirmed as 3 T1 tumors and 1 T2 tumor[13]. These undetected tumors were small and without deep extension. On the contrary, two lesions classified as cT1a were squamous cell papillomas at pathological examination (no tumor) [10]. Subanalysis of T1a and T1b staging only, done by Allegra et al., further shows overstaging of two lesions classified as cT1b by MR, which were pT1a on histopathological conformation. Wu reports on one patient staged with a T1 lesion, which pathologically appeared to be a T2 lesion [9]. Carriero reports correct staging of all 17 patients with T1 and T2 carcinomas [14].

Except for T staging of the initial tumor, no data concerning tumor infiltration depth or tumor volume could be evaluated in the included studies.

Diagnostic value of imaging according to anatomical subsites

The diagnostic accuracy of MRI to predict invasion of anatomical subsites, including the anterior commissure, paraglottic space and cartilages was reported in several selected articles (ranging from 3 to 6 articles, depending on the subsite). However, since sensitivity, specificity, positive predictive value and negative predictive value could only be calculated for the whole study population, including T1-T4 tumors, no subanalysis could be done for T1 and T2 tumors only.

DISCUSSION

This systematic review evaluates the diagnostic value of MRI for pre-therapeutic staging of early glottic cancer (T1-T2). A standardized method that accurately measures tumor extent and depth, especially in case of more extensive T1or T2 lesions, is needed to systematically compare endoscopic resections and radiotherapy with the best possible functional outcome. For example, invasion of the vocal muscle automatically leads to an ELS type III resection, whereas more superficial lesions can be resected with an ELS type I or II.

Using TNM classification, overall concordance calculated from 5 articles, between MRI and histopathology was 81% (52 out of 64 patients). In total, 6% (4 out of 64) of tumors were overstaged, 13% (8 out of 64) were understaged. According to these numbers, MRI more often underestimates than overestimates tumor extent in small laryngeal carcinomas. This is not in concordance with the idea that peritumoral inflammation on MRI, which amplifies the boundaries of abnormal tissues, can lead to overestimation. However, these numbers must be seen in perspective.

First, all overstaged tumors calculated in this review were described by Allegra et al, which was considered the most relevant study population. All understaged tumors were scored by other articles of which only a small part of the study population consisted of T1 and T2 laryngeal tumors. Second, we screened all full text articles on clinical T1 and T2 carcinomas. As a result, all understaged and correctly staged tumors were included in this review. However, patients with cT3 and cT4 carcinomas, which were eventually downstaged to pT1 or pT2 on pathological examination could be left out. The number of overstaged tumors according to MRI can therefore be higher than calculated here. Patients with cT3 and cT4 of the included articles in this review were also not included, since our search did not screen on this population and numbers are not reliable. We conducted a broad search in literature and included all laryngeal carcinomas and MRI as diagnostic imaging modality. We detected a high level of bias in reported articles. Also our review showed that there is a very limited amount of studies in this field. Only two articles included glottic laryngeal carcinomas [10,13]. Second, none of the articles included T1 and T2 stages only, and no subanalysis was done for different T-stages. Third, studies are very heterogeneous. Only four studies describe completely excised tumors, of which histopathologic correlation for T1 and T2 stages is unclear in one of these studies [13]. Fourth, invasion of glottic subsites (eg anterior commissure or sinus of Morgagni) that can be relevant for therapeutic approach and functional outcome of early glottic carcinomas were only scored in two articles and

since numbers were not specified according to T stage, no subanalysis could be performed. Fifth, scanning protocols varied widely or were not described at all [12]. Field strengths varied between 1 and 3 Tesla and was not reported in one study [12]. Imaging consisted mostly of T2 and T1W contrasts with scans in several directions. Contrast was not used routinely in the study by Hu et al [13]. Three studies used contrast before a second T1W scan was performed [10,11,14]. The in-plane resolution was not always clearly described and (when reported) varied between 0.5x.0.5 mm2 and 1x1 mm2. Slice thickness was 3-4 mm in all included studies. For the depiction of anatomical (laryngeal) structures, a larger slice thickness has the benefit of strong signal to noise ratio (SNR). However, a slice thickness of 3-4 mm could give rise to large partial volume effects in case of smaller lesions. These partial volume effects may have been partly mitigated by scanning in axial, coronal and sagittal direction. But for small laryngeal lesions, with a possible cranio-caudal diameter of 1-2 mm, a slice thickness of 3 mm or more may greatly reduce visibility of the tumor. Furthermore, the use of neck receive coils was not reported in some studies. Two articles report the use of an anterior neck coil [10,15]. One article describes the use of a dedicated neck coil [14]. In general, higher field strength and receive coils located close to the larynx, in combination with sufficiently high resolution results in a better depiction of smaller lesions.

Another remark is the adjustment of the TNM staging in 2002. Imaging studies of glottic carcinoma before 2002 suggested that a tumor adjacent to the thyroid cartilage (adjacent sign) had an increased risk of local failure after definitive RT. In the sixth edition of the TNM staging system, proposed in 2002, paraglottic space invasion or minor thyroid cartilage erosion was upstaged to a T3, in addition to the vocal cord fixation in the fifth edition. As both studies of Zbaren and Carriero were published before 2002, this could have influenced their diagnostic T staging as presented in table 1.

MRI is generally used to supplement microlaryngoscopy under general anesthesia in the staging of glottic cancer. Ideally, additional imaging would detect exact tumor size and extension, submucosal spread, invasion of the vocal muscle or paraglottic space, possible spread to the anterior commissure or crossing of the midline (with the risk of tumor spread to the thyroid and subglottic area).
Although MRI evaluation does appear to be a helpful diagnostic method in the scarce literature that can be found, combined accuracy of MRI and clinical staging remains higher than MRI staging alone. According to Zbaren et al, the accuracy of clinical/endoscopic staging was 55% [15]. The accuracy of combined clinical and MR imaging staging was 87.5%. However, it must be taken into account that in this study, all T stages were included.

Champsaur et al studied the MRI radio-anatomy of the larynx based on correlations between MRI and histologic sections on non-oncologic cadaver specimens in vitro [16]. They identified the conus elasticus, paraglottic space, and the vocal processes of the arytenoid cartilages. It was impossible to delineate the thyroarytenoid muscle or the vocal muscle on MRI. The two muscles seem continuous. They emphasize that hyaline cartilages (cricoid, thyroid, arytenoids) are the site of endochondral ossification, which is very variable. Cartilaginous ossification, resulting from cartilaginous angiogenesis, may be misinterpreted as a tumoral invasion. The fibrocartilages (epiglottis, vocal process of the arytenoid) ossify only very rarely. Their signal intensity therefore remains constant irrespective of age. Both fibrocartilages displayed a low signal intensity, in the sagittal plane. Identification of the vocal process may allow a more precise assessment of cancers of the glottic plane.

Besides MRI, the introduction of new endoscopic devices have proven to be of additional value for defining tumor extension and delineating its resection margins. Especially narrow band imaging (NBI) is a promising tool. Filtered wavelengths enhance the microvascular abnormalities associated with preneoplastic changes of the mucosal lining. Routine intra-operative use would decrease the rate of positive superficial margins from 23.7% to 3.6% during transoral laser microsurgery for early glottic cancer [17]. Although NBI can detect subtle mucosal extension, the filtered wavelengths only penetrate the superficial layers of mucosa, enhancing the mucosal and submucosal microvascular networks only. And it has therefore no role in the evaluation of deep extension of neoplastic lesions and does not affect the incidence of deep positive margins.

With technological advancement, image quality of MRI is still increasing. The integration of DWI into the magnetic resonance protocol has the potential to increase the specificity [18]. Furthermore, developments in higher field strength are of potential benefit. Of the studies reviewed here, only two used a 3 Tesla MRI unit. All other patients were scanned at 1.5 Tesla. Nowadays, 3 Tesla units are more readily available and even 7 Tesla scanners can be used for clinical scanning. The implementation of 7 Tesla MRI for human use has the potential to further advance spatial resolution beyond that of 1.5T and 3T. 7 Tesla has already been used to produce high-definition images of various anatomical areas, including the brain and inner ear [19,20]. Challenges encountered are that higher field strengths are more prone to image artifacts and longer acquisition times. Hopefully, future studies can further address these developments.

CONCLUSION

This systematic review evaluates the diagnostic value of MRI for pre-therapeutic staging of early glottic cancer (T1-T2). A standardized method that accurately measures tumor extent and depth, especially in case of more extensive T1or T2 lesions, is needed to systematically compare endoscopic resections and radiotherapy with the best possible functional outcome. Overall concordance between MRI and histopathology was 81% (52 out of 64 patients). In total, 6% (4 out of 64) of tumors were overstaged, 13% (8 out of 64) were understaged. However, available data for MRI and T1 and T2 glottic carcinomas are very limited and numbers can be influenced by the necessity of subanalysis-based numbers based on a small amount of patients. Since no articles solely include the defined subgroup (cT1 and cT2 glottic carcinomas), no diagnostic values (sensitivity, specificity, PPV and NPV) could be calculated. Furthermore, neoplastic invasion of glottic subsites in cT1 and cT2 carcinomas cannot be reliably assessed. MRI protocols were heterogenous and included slice thickness of 3-4 mm, which may be suboptimal for small glottic lesions. More studies are needed to evaluate the additional diagnostic value of MRI compared to clinical evaluation alone. Moreover, with technological advancement, image quality of MRI is still increasing, with the potential of more detailed cross sectional imaging. Detection of subtle in-depth infiltration may be a step forward in treatment planning and patient counseling in the pre-operative stage.

REFERENCES

1. O'Hara J, Markey A, Homer JJ. Transoral laser surgery versus radiotherapy for the tumour stage 1a or 1b glottic squamous cell carcinoma: systematic review of local control outcomes. *J Laryngol Otol*. 2013;127(8):732-8.

2. Van Loon Y, Sjogren E, Langeveld T et al. Functional outcomes after radiotherapy or laser surgery in early glottic carcinoma: A systematic review. *Head Neck*. 2012;34(8):1179-89.

3. Abdurehim Y, Hua Z, Yasin Y, Xukurhan A, Imam I, Yuqin F. Transoral laser surgery versus radiotherapy: systematic review and meta-analysis for treatment options of T1a glottic cancer. *Head Neck*. 2012;34(1):23-33.

4. Barbosa MM, Araújo VJ Jr, Boasquevisque E et al. Anterior vocal commissure invasion in laryngeal carcinoma diagnosis. *Laryngoscope*. 2005;115:724–730.

5. Naiboglu B, Kinis V, Toros SZ et al. Diagnosis of anterior commissure invasion in laryngeal cancer. *Eur Arch Otorhinolaryngol*. 2010;267(4):551-5.

6. Becker M, Zbaren P, Laeng H, Stoupis C, Porcellini B, Vonck P. Neoplastic invasion of the laryngeal cartilage: comparison of MR imaging and CT with histopathologic correlation. *Radiology*. 1995:194(3):661-9.

7. Huang BY, Solle M, Weissler MC. Larynx: anatomic imaging for diagnosis and management. *Otolaryngol Clin North Am.* 2012;45(6):1325-61.

8. Moher D, Liberati A, Tetzlaff J, Altman DG, The PRISMA Group. Preferred Reporting Items for Systematic Reviews and Meta-Analyses: The PRISMA Statement. *PLoS Med*. 2009;6(6):e1000097.

9. Wu JH, Zhao J, Li ZH et al. Comparison of CT and MRI in diagnosis of laryngeal carcinoma with anterior vocal commissure involvement. *Sci Rep*. 2016;6:30353.

10. Allegra E, Ferrise P, Trapasso S et al. Early glottic cancer: role of MRI in the preoperative staging. *Biomed Res Int.* 2014;2014:890385.

11. Banko B, Djuvic V, Milovanovic J, Kovac J, Novakovic Z, Mksimovic R. MRI in evaluation of neoplastic invasion into preepiglottic and paraglottic space. *Auris Nasus Larynx.* 2014;41(5):471-4.

12. Kraft M, Bruns N, Hugens-Penzel M, Arens C. Clinical value of endosonography in the assessment of laryngeal cancer. *Head Neck.* 2013;35(2):195-200.

13. Hu Q, Zhu SY, Zhang Z, Luo F, Mao YP, Guan XH. Assessment of glottic squamous cell carcinoma: comparison of sonography and non-contrast enhanced magnetic resonance imaging. *J Ultrasound Med*. 2011;30(11):1467-74.

14. Carriero A, Scarabino T, Vallone A, Cammisa M, Salvolini U, Bonomo L. MRI T-staging of laryngeal tumours: role of contrast medium. *Neuroradiology*. 2000;42(1):66-71.

15. Zbaren P, Becker M, Läng H. Pretherapeutic staging of laryngeal carcinoma; clinical findings, computed tomography, and magnetic resonance imaging compares with histopathology. *Cancer.* 1996;77(7):1263-73.

16. Champsaur P, Parlier-Cuau C, Brunet C et al. Serial anatomy of the larynx in MRI: MRI-histologic correlations. *Surg Radiol Anat*. 2000;22(1):5-11.

17. Garofolo S, Piazza C, Del Bon F et al. Intraoperative narrow band imaging better delineates superficial resection margins during transoral laser microsurgery for early glottic cancer. *Ann Otol Rhinol Laryngol*. 2015;12(4):294-8.

18. Becker M, Zbaren P, Casselman JW, Kohler R, Dulguerov P, Becker CD. Neoplastic invasion of the laryngeal cartilage: reassessment of criteria for diagnosis at MR imaging. *Radiology.* 2008;249(2):551-9.

19. Zwanenburg JJ, Hendrikse J, Visser F, Takahara T, Luijten PR. Fluid attenuated inversion recovery (FLAIR) MRI at 7.0 Tesla: comparison with 1.5 and 3.0 Tesla. *Eur Radiol.* 2010;20(4):915-22.

20. Van Egmond SL, Visser F, Pameijer FA, Grolman W. Ex vivo and in vivo imaging of the inner ear at 7 Tesla MRI. *Otol Neurotol.* 2014;35(4):725-29.

CHAPTER 6

Clinical value of (dedicated) 3 Tesla and 7 Tesla MRI for cT1 Glottic Carcinoma: A feasibility study

Laryngoscope Investigative Otolaryngology. 2019;4(1): 95-101

Sylvia L. van Egmond
Bernard M. Vonck
Johanna J. Bluemink
Frank A. Pameijer
Jan Willem Dankbaar
Inge Stegeman
Marielle E.P. Philippens
Cornelis A.T. van den Berg
Luuk M. Janssen
Chris H. Terhaard

ABSTRACT

Objective

To assess the feasibility of the clinical use of 3 Tesla and 7 Tesla Magnetic Resonance Imaging for early (cT1) glottic carcinoma, including structural assessment of technical image quality and visibility of the tumor; and if feasible, to correlate MRI findings to routine diagnostics.

Methods

Prospective feasibility study. Twenty patients with primary clinical T1 glottic carcinoma underwent both routine clinical staging and CT. In addition, a 3T and 7T MRI protocol, developed for small laryngeal lesions, was performed in a 4-point immobilization mask, using dedicated surface coils. Afterwards, routine endoscopic direct suspension laryngoscopy under general anaesthesia was performed.

Results

Only 2/7 (29%) of 7T MRI scans were rated as moderate to good technical image quality. After exclusion of three patients with only mild to moderate dysplasia at the time of MRI, 13/17 (76%) of 3T MRI's were of adequate technical image quality. Tumor visualization was adequate in 8/13 (62%) of patients with invasive squamous cell carcinomas. With exclusion of the 4 MRI's with motion artefacts, the tumor and its boundaries could be adequately seen in 8/9 (89%) patients with squamous cell carcinoma versus only ¼ (25%) of patients with carcinoma in situ lesions.

Conclusions

7 Tesla MRI was considered not feasible. 3 Tesla MRI, with adequate patient selection, namely clinical exclusion of patients with a history of claustrophobia and inclusion of only histologically proven invasive squamous cell carcinoma, can be feasible. Especially with further improvement of MR image quality.

INTRODUCTION

Early stage squamous cell carcinoma (scc) of the glottic larynx, treated by radiotherapy or endoscopic laser surgery, is characterized by a low tumor volume and rare incidence of regional or distant metastatic spread [1,2]. Reported local control rates for both treatment modalities are equally high (71%-95%), depending on invasion of the anterior commissure (AC) [3]. Therefore, the aim of treatment is to achieve local control with the best possible functional outcome. Topic of controversy remains which treatment modality results in tumor eradication with preservation of functions, especially when the cancer involves the AC, involves the vocal muscle, or extends laterally in the laryngeal ventricle. The main factor that prohibits the systematic evaluation and pooling of data is the uncertainty of tumor comparability, due to an absence of a standardized method that accurately measures tumor extent and depth.

Both flexible laryngoscopy, videolaryngostroboscopy (VLS) and direct suspension laryngoscopy with an operating microscope can evaluate AC invasion, but no claims can be made about the extent of the tumor in depth, as well as submucosal intralaryngeal growth. Rates reported of correct staging of AC invasion vary beteen 40-72% [4,5]. Visualization of early glottic tumors by computed tomography (CT) imaging can also be difficult due to small tumor size and volume and the poor soft tissue detail. Invasion of the AC is more difficult to detect. Diagnostic value of CT varies widely in literature with a reported accuracy of 83-86% [6,7], a sensitivity of 43% and a specificity of 83% when compared to histopathological results[5]. However, these number encount for all T1-T4 laryngeal tumors. No subanalysis was done for cT1 tumors only. False-positive results may be caused by difficulty to discriminate reactive inflammation and edema from tumor [8].

A recent systematic review evaluating the diagnostic value of MRI for pre-therapeutic staging of early glottic cancer, showed that MRI data of T1 and T2 glottic carcinoma is limited, heterogenous and based on sub analysis[9]. Both slice thickness and the use of neck receive coils varied and was suboptimal for small laryngeal lesions.
7T ultra-high field MRI has the potential to depict smaller lesions [10,11]. In the head and neck region, the inner ear and the parotid gland and duct have been visualized with varying results [12,13]. Up to now, no studies have been performed to assess the diagnostic value of 7T for glottic carcinomas.

The primary goal of this study was to assess the feasibility of the clinical use of both an dedicated 3T MR protocol for small laryngeal lesions, and 7T MR imaging of clinical

T1 glottic carcinoma; Both (technical) image quality and tumor visibility were evaluated. Secondary goals were comparison of MRI data to routine diagnostics, including suspension laryngoscopy and computed tomography. And, in case of laser excision, verification of MRI with histopathological data.

MATERIALS AND METHODS

Ethical considerations

This prospective feasibility study was approved by the local ethics committee and written informed consent was obtained from all patients included in the study.

Methods

Following flexible laryngoscopy and videolaryngostroboscopy at the Out Patients Department, patients were staged by two independent head and neck surgeons according to the International TNM classification for malignant glottic tumors [14]. All patients with clinically staged T1 glottic carcinomas, referred to a tertiary referral center (Utrecht University Medical Center) between December 2014 and March 2017, were considered for this study. All patients had a histologically proven carcinoma in situ or invasive scc of the vocal cord(s). We excluded patients with a history of previous glottic surgery, patients with previous radiation therapy for a head and neck carcinoma, patients with recurrence of glottic disease, patients with legal incapability or insufficient command of the Dutch language, or patients who did not pass MRI screening criteria. Videolaryngoscopy was recorded and saved and glottal closure, regularity, mucosal wave and symmetry were scored using a four-point (0-3) grading scale by two ENT surgeons, specialized in head and neck oncology. Patients subsequently underwent CT, 3 Tesla MRI and 7 Tesla MRI.

CT imaging protocol

All contrast enhanced CT studies were performed on a 128 detector-row scanner (Philips iCT, Cleveland OH, USA). For the acquisition, first an injection of 90 ml of nonionic contrast material (Ultravist (Iopromide) 300 mg/ml, Bayer Healthcare Whippany NJ), at a rate of 4 ml/s followed by a 40 ml saline flush was given. Forty seconds after the first injection a second injection of 30 ml of contrast material and a 30 ml saline flush at a rate of 4 ml/s was given. A bolus triggered scan was started simultaneous with the second bolus with a locator in the descending aorta at a Hounsfield Units (HU) threshold of 170 with no scan delay. Acquisition was performed in axial plane during quiet breathing. Scanning parameters were: 128x0.625 mm

collimation, 120 kVp, 143 mAs, a rotation time of 0.4s, pitch of 0.914, 250 mm Field of View (FOV), and 512x512 matrix. 3mm axial, coronal and sagital sections were reconstructed. The axial images were reconstructed parallel to the plane of the true vocal cords.

MR Imaging protocol

To minimize movements of the head and neck region, 3 Tesla and 7 Tesla MRI were both performed using a four-point immobilisation mask for the head and neck region with individual head support, made prior to scanning at the Department of Radiotherapy. This mask is an adaption of the five-point immobillization mask used for head and neck radiotherapy, covering the region form the chin to the shoulders. Its use is standard practice for MRI performed for patients who are scheduled for radiotherapy of the head and neck region at our center[15]. Both MRI exams were performed with administration of 0.1 ml/kg single dose intravenous contrast agent gadolinium (Gadovist®) and 30cc saline flush. Scans were angulated along the C3-C4 or C4-C5 disk space (i.e. parallel to the plane of the true vocal cords).
The 3T and 7T protocol, optimized after a pilot study with healthy volunteers, consisted of planning scans, preparation scans to optimize the RF transmit field and for 7T the magnetic field homogeneity in the region of interest and T1 and T2 weighted scans optimized in volunteers.

The 3T and 7T sequences (following the scans for planning and optimization of the RF and magnetic field homogeneity) are listed in table 1. For the 7 Tesla MRI exam, a dedicated transmit neck coil was used in the form of a dielectric waveguide[16]. The weight of the dielectric bag filled with deuterated water was not sensed by the patient due to the stiffness of the mask material. Local receive coils were used to maximize the signal intensity obtained from the glottic area [17]. The receive coils were placed on the mask, covering the region of the larynx. Prior to the study, a risk analysis was performed in cooperation with the department of Medical Technology.

Diagnostic evaluation

CT, 3T MRI and 7T MRI scans were individually assessed for technical image quality and visibility of the tumor, scored with a four-point Likert scale, by three independent researchers (two experienced head and neck radiologists and one experienced head and neck radiation oncologist), blinded for patient data. In a second joint meeting, in case of visible tumor, the tumor was delineated and location, tumor size, tumor volume and depth were assessed.

Table 1: 3T and 7T scan protocol sequences

	3 Tesla MRI				**7 Tesla MRI**		
Subsequent scan protocols	1	2	3	4	1	2	3
Sequence	3D T2W SE	3D T2W SE	MS T1W SE + and - Gado	3D T1W SE Gado	MS T2W SE	MS T1W SE + and – Gado	MS T1W SE + Gado
Orientation	Transverse	Transverse	Transverse	Sagittal	Transverse	Transverse	Sagittal
TE/TR (ms)	157/2225	235/2100	20/500	25/400	68/3500	37/800	37/700
TSE factor	80	145	3	20	11	8	8
Flip angle (degrees)	90	90	90	90	90	100	100
Refocusing angle (degrees)	40-120	25-120	†	40	80	90	90
Field of view (mm3)	160x160x34	160x160x39	160x160x44	160x160x44	140x140x35	140x140x35	140x140x50
No transverse slices	34	39	20	88	32	16	65 - C
Acquisition pixel size (m3)	0.5x0.5x1	1x1x1	0.6x0.6	1x1x0.5	0.5x0.5x1	0.4x0.4x2	0.7x0.7x0.7
Imaging matrix	320x318	160x158	272x270	160x160	280x275	348x346	200x200
No of signal averages (NSA)	2	2	2	2	2	2	2
Sense factor	1.9	1.9	2	2	1	2	2
Scan duration (minutes)	6	2	4	3	6	2.5	4

MS= multislice, † No refocusing control, C=coronal

Following imaging, as part of standard clinical procedure, direct suspension laryngoscopy with a rigid endoscope was performed under general anaesthesia. Extent of the tumor was evaluated by visual examination through an operating microsope with a standard eye-to-object-distance of 400 mm and by palpation with microforceps. Images were recorded using a measuring tape (figure 1). Lesions were staged according to the international TNM Classification of Malignant Tumors in T1a, T1b or T2. Furthermore, appearance, length, expected depth invasion of the tumor and possible paraglottic or subglottic extension as well as involvement of the anterior comissure were reported. The decision for direct endoscopic excision with CO2 laser or radiotherapy was made during direct suspension laryngoscopy by the head and neck surgeon, independent of MRI results. In general, lesions with involvement of the anterior commissure, lesions with paraglottic extension or patients in which tumor visualization was inadequate, were not considered suitable for laser resection. When endoscopic laser resection was performed, pathologic specimens were fixed with needles onto a standardized full-scale image of the larynx, to enable optimal structured histopathological evaluation of tumor margins. When considered unsuitable for endoscopic excision, Intensity Modulated Radiotherapy (IMRT) was commenced with a daily fraction of 2.4 Gy, 5 days/week, for 25 days, resulting in a total irradiation fraction dose of 60 Gy in 5 weeks.

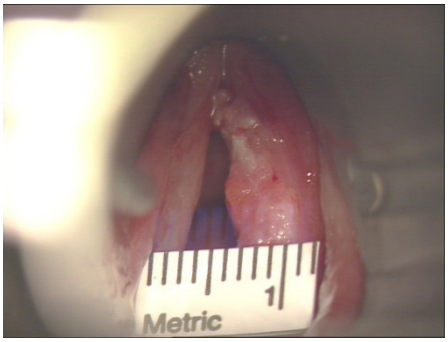

Figure 1: Tumor was measured with a measuring tape during direct laryngoscopy

Statistics

Since direct laryngoscopy cannot be used as a reference standard and a pathology specimen was not available in each patient, no diagnostic accuracy measures could be calculated. Results will be descriptive.

RESULTS

Number of scans

A flow diagram of all included patients and performed scans is shown in figure 2. After 10 patients, we evaluated the scan quality of both 3T and 7T MRI and considered the 7T MRI not feasible. Therefore, the last 10 patients did not undergo 7T scanning. In retrospect, two carcinoma in situ lesions and one scc were excised during an initial biopsy at the referral hospital. These three patients only had mild to moderate dysplasia during time of scanning and were excluded for evaluation. Therefore, 17 3T MRI's and 7 7T MRI's were included in our analysis.

Inter observer agreement

Assessment of MRI data by two radiologists and one radiation oncologist appeared to be heterogeneous. Intra class correlation coefficient for image quality and tumor visibility for CT and 3T MRI was 0.76, 0.80, 0.86, 0.91, respectively. When classified as 'acceptable' (moderate or good) or 'unacceptable' (bad or poor), a higher degree of inter observer agreement was reached.

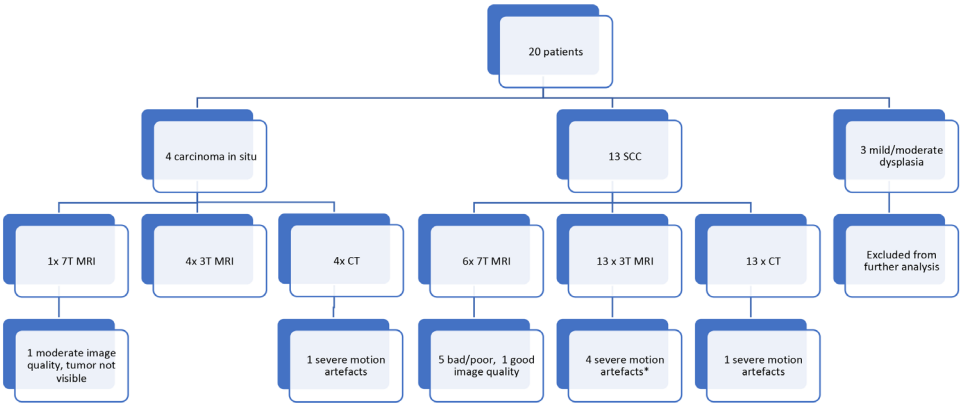

Tumor visibility / Image quality	Tumor not visible	Tumor visible, but no boundaries	Boundaries visible but not clear	Tumor and boundaries clearly visible
Bad	0	0	0	0
Poor	0	0	0	0
Moderate	0	1	0	0
Good	2	0	1	0

Tumor visibilty and image quality of carcinoma in situ lesions on 3 Tesla MRI

Tumor visibility / Image quality	Tumor not visible	Tumor visible, but no boundaries	Boundaries visible but not clear	Tumor and boundaries clearly visible
Bad	3*	0	0	0
Poor	0	1*	0	0
Moderate	0	0	4	0
Good	0	1	1	3

Tumor visibilty and image quality of invasive squamous cell carcinomas on 3 Tesla MRI

Figure 2: Flow diagram of included patients, number of scans, scan quality and tumor visibility

Table 2: Assessment of image quality by three independent observers, blinded for clinical data

Image quality	CT			3 Tesla MRI			7 Tesla MRI		
	R1	R2	R3	R1	R2	R3	R1	R2	R3
Bad	1 (6%)	0	0	3 (18%)	1(6%)	1 (6%)	3 (43%)	1 (14%)	4 (57%)
Poor	0	0	1 (6%)	1 (6%)	3 (18%)	3 (18%)	2 (29%)	4 (57%)	2 (29%)
Moderate	0	2 (12%)	10 (59%)	5 (29%)	8 (47%)	3 (18%)	1 (14%)	1 (14%)	0
Good	16 (94%)	15 (88%)	6 (35%)	8 (47%)	5 (29%)	10 (59%)	1 (14%)	1 (14%)	1 (14%)
Total	17	17	17	17	17	17	7	7	7

R1=radiologist 1 (FP), R2=radiologist 2 (JD), R3=radiation oncologist (CT)

Histopathological results

Five out of 17 tumors were considered suitable for endoscopic laser resection. Four tumors were excised, one was evaporated. Tumor diameters could only be assessed in the four excision histopathological specimens. A total of 12 patients received radiotherapy.

Technical image quality of CT and MRI

Data following exclusion of 3 patients with only mild/moderate dysplasia are presented in table 2. 94-100%, 76% and 14-29% of CT, 3T MRI and 7T MRI scans were rated as moderate to good technical image quality, respectively.

Tumor visibility of CT and MRI

Data are presented in table 3. In 30-59%, 47-53% and 14-29% of CT, 3T MRI and 7T MRI, respectively, the tumor and boundaries could be identified.

One of the patients with the best quality on 3T MRI and 7T MRI is shown in figure 3. CT and a clinical image during suspension laryngoscopy shows a comparable lesion of the left anterior vocal cord. This tumor was clinically scored as a T1b tumor, with involvement of the anterior commissure. In this case, radiotherapy was performed. Findings could therefore not be related to histopathological results.

Relation between image quality, tumor visibility and tumor dimensions in subgroups of patients on 3T MRI and CT

Patients with carcinoma in situ lesions

Four out of 17 patients had carcinoma in situ lesions. Although all 3T MRI scans were of moderate to good ('acceptable') image quality, in only one patient (25%), tumor boundaries could be visualized, although not clear. Concerning CT, the technical quality of all scans were good, but the tumor seen on MRI was not visible on CT. In another patient with Cis, visibility of tumor boundaries was slightly better on CT than on MR, leading to an 'acceptable' tumor visibility on CT.

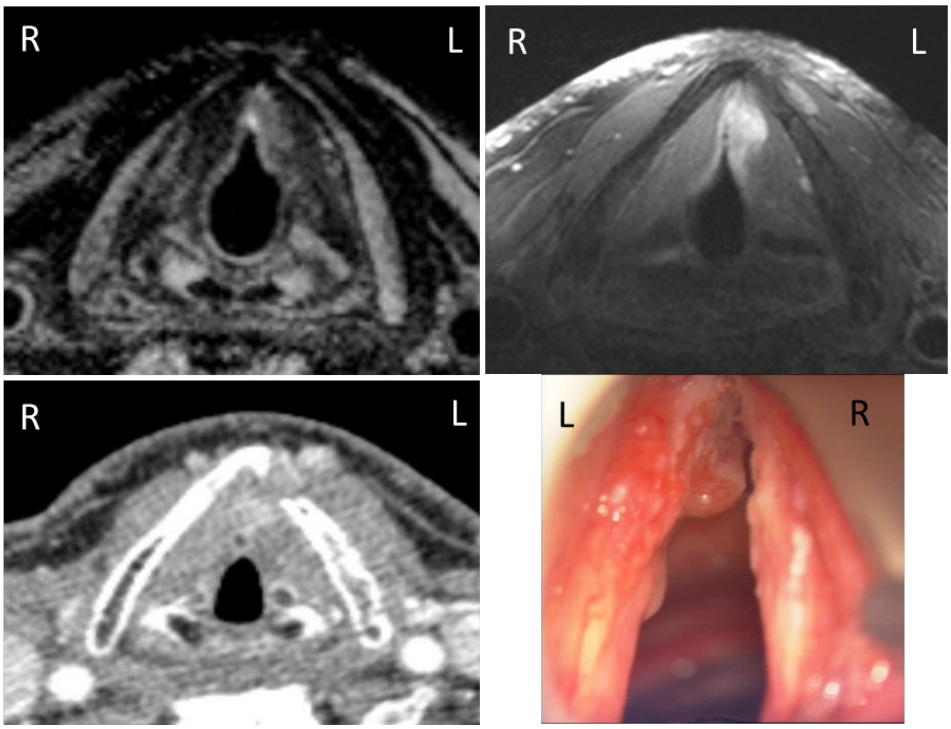

Figure 3: Axial images at the mid glottic level showing a lesion on the anterior half of the left true vocal cord with extension to the anterior commissure (arrows). On CT the lesion is isointense to the vocal cord and therefore difficult to see. 3T MRI (a), 7T MRI (b), contrast enhanced CT (c) and clinical photo during suspension laryngoscopy (d) of the same study patient.

Patients with invasive squamous cell carcinoma

Thirteen out of 17 patients had an invasive scc on histopathological report. Four MRI scans were of bad image quality, due to severe motion artefacts. One of these patients suffered from claustrophobia. The remaining nine scans were of moderate to good ('acceptable') image quality. In eight patients, the tumor and its boundaries could be adequately visualized. On CT, image quality was good patients, except for the one with claustrophobia. Tumor visibility was adequate in nine patients.

Comparison of tumor dimensions on CT, 3T, 7T and direct laryngoscopy

In eight patients with invasive scc, the tumor and its boundaries could be adequately visualized on 3T MRI and tumor dimensions could be measured (table 3). In a consensus meeting, tumors were delineated on 3 Tesla MRI and CT. Volumes variated from 0.036 to 2.38 cc and were slightly larger on MRI than on CT for all tumors. Tumor volume was

Table 3: assessment of image quality by three independent observers, blinded for clinical data.

Tumor visibility	CT			3 Tesla MRI			7 Tesla MRI		
	R1	R2	R3	R1	R2	R3	R1	R2	R3
Tumor not visible	4 (24%)	4 (24%)	7 (41%)	5 (29%)	5 (29%)	5 (29%)	5 (72%)	2 (29%)	5 (72%)
Tumor visible, but not the tumor boundaries	3 (18%)	3 (18%)	5 (29%)	3 (18%)	4 (24%)	4 (24%)	1 (14%)	3 (43%)	1 (14%)
Tumor boundaries visible, but not clear	6 (35%)	2 (12%)	2 (12%)	6 (35%)	5 (29%)	3 (18%)	0	1 (14%)	0
Both tumor and boundaries clearly visible	4 (24%)	8 (47%)	3 (18%)	3 (18%)	3 (18%)	5 (29%)	1 (14%)	1 (14%)	1 (14%)
Total	17	17	17	17	17	17	7	7	7

R1=radiologist 1 (FP), R2=radiologist 2 (JD), R3=radiation oncologist (CT)

not related to visibility of the tumor. In only one of these eight patients, laser excision was performed. Correlation of tumor diameters to pathological specimens was therefore not contributive.

Assessment of anatomical/glottic subsites

Presence or absence of tumor involvement of anatomical subsites was scored on both imaging and during suspension laryngoscopy. For the anterior commissure, concordance between CT, 3T MRI and laryngoscopy was low for the whole study population (including both superficial carcinoma in situ lesions and invasive bulky disease). For the eight patients with invasive scc with adequate tumor visualization, shown in table 4, concordance was higher. For these patients, a consensus was reached by the observers, blinded for clinical data. Two out of eight CT's and 3T MRI's (of the same patients) were false negative for tumor invasion of the AC, which was visible during direct laryngoscopy. This was due to superficial tumor extension of a more bulky midcord lesion into the AC. Four out of eight CT's and MRI's (of the same patients) were true positive. Two CT and MRI's were true negative.

The vocal muscle was scored as involved in 5 patients on both CT and MRI, it was scored as not involved in two patients and was scored as involved on MRI but not-involved on CT in the same patient. No verification with histopathology could be done. Other subsites were not, or rarely, involved.

Table 4: tumor dimensions measured on imaging and direct laryngoscopy

	Anterior-posterior dimeter (mm)			Lateral diameter (mm)		
In mm	**CT**	**3T MRI**	**Laryngoscopy**	**CT**	**3T MRI**	**Laryngoscopy**
Pt 2	8.6	14.2	17	3.7	8.9	5
Pt 3	8.6	9	10	4.5	4.2	5
Pt 4	20	27	15	8.5	10	10
Pt 9	5	11	7	5	5	3
Pt 12	10	10	12	3.4	3.4	3.5
Pt 14	11.8	26.0	15	5.0	9.0	8
Pt 16	5.2	6.4	7	3.8	3.5	5
Pt 20	4	5.8	9	1.4	2.3	1

DISCUSSION

Feasibility; primary endpoint

Twenty percent of patients refused 7T scanning because of claustrophobia. In contrast to our expectations, based on pilot data with detailed laryngeal visualization in healthy subjects, in only one out of 7 7T scans, the tumor and its boundaries could be clearly seen. We therefore considered 7T MRI not feasible.

Although the vast majority of 3T scans was of moderate to good technical quality, this only resulted in adequate tumor visibility on 3T MRI in nine out of the total group of 17 patients (53%) versus 10 out of 17 patients (59%) on CT. The tumor visibility was adequate in nine out of 13 (69%) 3T MRI's with moderate to good image quality, versus 10 out of 16 patients (63%) with good CT image quality. This was probably due to inadequate visibility of superficial (carcinoma in situ) lesions. When subgroup analysis was done, tumor visualization was adequate in 62% (or even 89% after exclusion of 4 MRI's with bad technical quality) with ssc versus only 25% of patients with carcinoma in situ lesions. On CT, tumor visibility was adequate in 25% of Cis lesions and in 69% of scc lesions (or 75% after exclusion of one CT with bad technical quality).

Study limitations

This study has several limitations. First, histopathology could not be used as a reference standard to validate the diagnostic value of the scans. Random biopsy of anatomic subsites, only for study purposes, was considered unethical and harmful for the study patients. Second, data were very heterogeneous. The low concordance between laryngoscopy and CT does not allow for a combined reference standard to validate MRI findings [18]. Third, the moderate intraclass correlation coefficient on a four-point

scale between two experienced head and neck radiologists and the radiation oncologist reflects the difficulty of image interpretation. When scored as 'adequate/acceptable' or 'inadequate/unacceptable', agreement was high. The intra-observer and inter-observer reproducibility in the delineation of head and neck tumors have a wide range, with a reported percentage measurement error for primary tumors of 0–53% [2119,20,21]. Between observers, the size of the largest Gross Tumor Volume (GTV) can be more than eight times the size of the smallest volume.

Comparison of MRI data to routine diagnostics; secondary endpoint

Anterior-posterior diameters measured during laryngoscopy compared to MRI and CT were comparable. However, clinical measurements can be difficult due to both invasive and exophytic tumor components with varying shapes of the vocal cord. The superficial component results in larger tumor diameters measured during laryngoscopy, which was not detected on imaging. Because of the lack of histopathological data, unfortunately, no relation between tumor visibility and depth invasion of the tumor could be addressed.

Challenges of 3T and 7T MRI scanning for small laryngeal lesions

For optimal detection of small laryngeal lesions and to avoid partial volume effect of scanning small lesions, we used a slice thickness of 0.5 to 1 mm. However, small slice thickness results in a diminished Signal to Noise Ratio (SNR). To optimize the signal in the area of interest, we used neck receive coils close to the larynx. At the surface the subcutaneous fat is located. This fat can cause large artefacts when patients move (for example due to breathing). These artefacts are more pronounced in the 7T scans than in the 3T MR scans, due to the high sensitivity of the small surface coils in the 7T setup close to the surface.

To minimize motion artefacts, all patients were scanned in a 4-point immobilisation mask. A benefit of the stiff mask material was that the transmit neck coil used on 7T, consisting of a dielectric bag filled with deuterated water, which can be quite heavy on the neck, was not sensed by the patient. Although the immobilisation mask minimizes external movements of the head and neck, internal motion as a result of breathing and swallowing cannot be prevented. To diminish the susceptibility for motion artefacts, we performed 4 dynamic scans with one-fourth scan duration each, but this was not beneficial. A solution for this problem appears to be 'in-vivo respiratory triggering', a method in which data acquisition is only done during expiration, since internal breathing motion will reduce and swallowing cannot occur [22].

At 7T, the Signal to Noise Ratio (SNR) increases linearly with field strength. However, the image homogeneity is generally less due to the smaller RF wavelength causing RF

interferences[23,24]. For this reason, a body coil is very hard to manufacture at such high field strength. We used a dedicated neck transmit coil with 2 antenna's to homogenize the transmit field based on the principle of a dielectric waveguide [16]. Another challenge, especially at 7T, is the energy absorbed by the human body (Specific Absorption Ratio of SAR in W/kg), which scales quadratically with the field strength. The higher SAR at 7T has to be compensated by fewer RF pulses per time unit, resulting in a longer acquisition time. Also, the water-fat shift is increased at 7T compared to 3T. This can be compensated for by a higher read-out bandwidth, this however reduces the SNR. Further improvement of scan quality at 3T might be accomplished by a neck receive coil consisting of multiple elements. At 7T, we already used receive coils with multiple elements. At 3T, we used a receive coil with two elements. Adding receive coils can lead to a higher acceleration factor with a shorter scan duration. This will especially be of benefit when data acquisition is limited to the expiration phase of breathing. With multiple elements, the signal remains high enough for optimal tumor visibility.

CONCLUSION

We conducted a feasibility study for 3T and 7T MRI for clinically staged Tis, T1a and T1b glottic carcinoma. 7T MRI was considered not feasible. 3 Tesla MRI, with clinical exclusion of patients with a history of claustrophobia, and with histologically proven invasive squamous cell carcinoma, can be feasible. Especially with further improvement of MR image quality. However, its superiority to CT could not be confirmed in this study. Superficial tumor extension remains difficult to detect on imaging.

REFERENCES

1. Van Loon Y, Sjogren E, Langeveld T, Baatenburg de Jong R, Schoones J, van Rossum M. Functional outcomes after radiotherapy or laser surgery in early glottic carcinoma: A systematic review. *Head Neck.* 2012; 34(8):1179-89.

2. Abdurehim Y, Hua Z, Yasin Y, Xukurhan A, Imam I, Yuqin F. Transoral laser surgery versus radiotherapy: systematic review and meta-analysis for treatment options of T1a glottic cancer. *Head Neck.* 2012;01;34(1):23-33.

3. Hakeem AH, Tubachi J, Pradhan SA. Significance of anterior commissure involvement in early glottic squamous cell carcinoma treated with trans-oral CO2 laser microsurgery. *Laryngoscope*. 2013;123(8):1912-7.

4. Barbosa MM, Araújo VJ Jr, Boasquevisque E, Carvalho R, Romano S, Lima RA, Dias FL, Salviano SK (2005) Anterior vocal commissure invasion in laryngeal carcinoma diagnosis. *Laryngoscope*. 2005;115:724–730.

5. Naiboglu B, Kinis V, Toros SZ, Habesoglu TE, Deveci I, Surmeli M, Egeli E. Diagnosis of anterior commissure invasion in laryngeal cancer. *Eur Arch Otorhinolaryngol.* 2010;267(4):551-5.

6. Zbären P, Christe A, Caversaccio MD, Stauffer E, Thoeny HC. Pretherapeutic staging of laryngeal carcinoma; clinical findings, computed tomography, and Magnetic resonance imaging compared with histopathology. *Otolaryngol Head Neck Surg*. 2007;137(3):487-91.

7. Hu Q, Luo F, Zhu SY, Zhang Z, Mao YP, Hui Guan X. Staging of laryngeal carcinoma: comparison of high-frequency sonography and contrast-enhanced computed tomography. *Clin Radiol*. 2012;67(2):140-147.

8. Becker M, Burkhardt K, Dulguerov P, Allal A. Imaging of the larynx and hypopharynx. *Eur J Radiol*. 2008;66(3):460-79.

9. van Egmond SL, Stegeman I, Pameijer FA, Bluemink JJ, Terhaard CH, Janssen LM. Systematic review of the diagnostic value of Magnetic Resonance Imaging for early glottic carcinoma. *Laryng Investig Otolaryngol*. 2018;3(1):49-55.

10. Heverhagen JT, Bourekas E, Sammet S, et al. Time-of-flight magnetic resonance angiography at 7 Tesla. *Invest Radiol*. 2008;43:568–73.

11. Kollia K, Maderwald S, Putzki N, et al. First clinical study on ultra-high-field MR imaging in patients with multiple sclerosis: comparison of 1.5 T and 7 T. *AJNR*. 2009;30:699–702.

12. Van Egmond SL, Visser F, Pameijer FA, Grolman W. Ex vivo and in vivo imaging of the inner ear at 7 Tesla MRI. *Otol Neurotol*. 2014;35(4):725-29.

13. Kraff O, Theysohn JM, Maderwald S, et al. High-resolution MRI of the human parotid gland and duct at 7 Tesla. *Invest Radiol.* 2009;44(9):518-24.

14. National Comprehensive Cancer Network. NCCN Clinical Practice Guidelines in Oncology: Head and Neck Cancers. V 1.2015. Available at http://www.nccn.org/professionals/physician_gls/pdf/head-and-neck.pdf

15. Verduijn GM, Bartels LW, Raaijmakers CP, Terhaard CH, Pameijer FA, van den Berg CA. Magnetic resonance imaging protocol optimization for delineation of gross tumor volume in hypopharyngeal and laryngeal tumors. *Int J Radiat Oncol Biol Phys*. 2009;74(2):630-6.

16. Bluemink JJ, Raaijmakers AJE, Koning W, Andreychenko A, Rivera DS, Luijten PR, Klomp DWJ, van den Berg CAT. Dielectric waveguides for ultrahigh field magnetic resonance imaging. *Magn Reson Med*. 2016;76:1314–1324.

17. Koning W, Bluemink JJ, Langenhuizen EAJ, Raaijmakers AJ, Andreychenko A, Van den Berg CAT, Luijten PR, Zwanenburg JJM, Klomp DWJ. High-resolution MRI of the carotid arteries using a leaky waveguide transmitter and a high-density receive array at 7T. *Magn Reson Med*. 2013;69:1186–1193.

18. Naaktgeboren CA, de Groot JH, Rutjes AWS, Bossuyt PMM, Reitsma JB, Moons KGM. Anticipating missing reference standard data when planning diagnostic accuracy studies. *BMJ.* 2016 Feb 9;352:i402.

19. Weiss E, Hess CF. The impact of gross tumor volume (GTV) and clinical target volume (CTV) definition on the total accuracy in radiotherapy theoretical aspects and practical experiences. *Strahlenther Onkol.* 2003 Jan;179(1):21-30.

20. C. F. Njeh. Tumor delineation: The weakest link in the search for accuracy in radiotherapy. *J Med Phys*. 2008; 33(4): 136–140.

21. Andrew R. Gordon, Laurie A. Loevner, Amita Shukla-Dave, Regina O. Redfern, Adina I. Sonners, Alex M. Kilger, Mark A. Elliott, Mitchell Machtay, Randal S. Weber, Jerry D. Glickson and David I. Rosenthal. Intraobserver Variability in the MR Determination of Tumor Volume in Squamous Cell Carcinoma of the Pharynx. *Am J Neuroradiol*. 2004;25(6):1092-1098.

22. Ruytenberg T, Verbist BM, Vonk-van Oosten J, Astreinidou E, Sjögren EV, Webb AG. Improvements in High Resolution Laryngeal Magnetic Resonance Imaging for Preoperative Transoral Laser Microsurgery and Radiotherapy Considerations in Early Lesions. *Front Oncol*. 2018;8:216.

23. Vaughan JT, Garwood M, Collins CM, Liu W, DelaBarre L, Adriany G, Andersen P, Merkle H, Goebel R, Smith MB, Ugurbil K. 7T vs 4T: RF power, homogeneity, and signal-to-noise comparison in head images. *Magn Reson Med*. 2001;46(1):24-30.

24. Theysohn JM, Maderwald S, Kraff O, et al. Subjective acceptance of 7 Tesla MRI for human imaging. *Magma*. 2008;21:63–72.

CHAPTER 7

Influence of FDG-PET on primary nodal target volume definition for head and neck carcinomas

Acta oncologica. 2016;55(9-10):1099–1106.

Sylvia L. van Egmond
Vera Piscaer
Luuk M. Janssen
Inge Stegeman
Monique G. Hobbelink
Wilko Grolman
Chris H. Terhaard

ABSTRACT

Background

The role of 2-[18F]-fluoro-2-deoxy-D-glucose (FDG)-positron emission tomography (PET)/computed tomography (CT) in routine diagnostic staging remains controversial. In case of discordance between FDG-PET and CT, a compromise has to be made between the risk of false positive FDG-PET and the risk of delaying appropriate salvage intervention. Second, with intensity modulated radiation therapy (IMRT), smaller radiation fields allow tissue sparing, but could also lead to more marginal failures.

Methods

We retrospectively studied 283 patients with head and neck carcinoma scheduled for radiotherapy between 2002 and 2010. We analyzed the influence of FDG-PET/CT versus CT alone on defining nodal target volume definition and evaluated its long-term clinical results. Second, the location of nodal recurrences was related to the radiation regional dose distribution.

Results

In 92 patients, CT and FDG-PET, performed in mold, showed discordant results. In 33%, nodal staging was altered by FDG-PET. In 24%, FDG-PET also led to an alteration in nodal treatment, including a nodal upstage of 18% and downstage of 6%. In eight of these 92 patients, a regional recurrence occurred. Only two patients had a recurrence in the discordant node on FDG-PET and CT and both received a boost (high dose radiation).

Conclusion

These results support the complementary value of FDG-PET/CT compared to CT alone in defining nodal target volume definition for radiotherapy of head and neck cancer.

INRODUCTION

Lymph node involvement is the most important prognostic indicator for survival of patients with head and neck cancer (HNC). The detection of lymph node metastases with optimal imaging techniques is therefore a fundamental part of preoperative evaluation.
Progress in radiation therapy (RT) had been directed towards increased selectivity of irradiation field size. The introduction of intensity modulated radiation therapy (IMRT) allows the irradiation dose to be shaped around complex tumors and adjacent positive lymph nodes in three-dimensional (3D) spaces to achieve optimal tissue sparing with optimal preservation of function. The benefit of IMRT in the treatment of HNC has already been proven in numerous studies [1-3].
In IMRT planning, clear delineation of both targets and organs at risk is essential. The accuracy of IMRT with often steep dose gradients is therefore directly linked to the applied imaging techniques.

Routine staging protocols include clinical examination, chest X-ray and conventional computed tomography (CT) in their work up. Although CT can offer sufficient anatomical details, images lack metabolic information. Furthermore, diagnostic accuracy of the node negative neck is insufficient. Reported sensitivities in literature range from 14% to 80% for CT [4-6].
2-[18F]-fluoro-2-deoxy-D-glucose (FDG)-positron emission tomography (PET) has a high sensitivity in detecting unsuspected second primary tumors, distant metastases and locoregional disease, however, with significant loss of anatomic detail. Combined FDG-PET/CT, developed in 1998, allows for synchronous image acquisition and comparison of FDG-PET metabolic data with CT anatomical data. The superiority of integrated FDG-PET/CT over FDG-PET alone has been confirmed in literature and is now widely used in the oncological setting [7,8].

However, the role of FDG-PET/CT in routine diagnostic staging remains controversial. The National Comprehensive Cancer Network (NCCN) in the US, for example does not include this scanning modality as part of their routine staging protocols. Meta-analyses of FDG-PET/CT showed a pooled sensitivity and specificity on a per-neck-side analysis of both 83–84%, and on a per-nodal-level analysis of, respectively, 80–84% and 96% [9,10]. For the patients without neck metastases, as determined from physical examination (the clinically negative neck), FDG-PET/CT has a lower positive predicting value (PPV) of 58% and sensitivity of 50–71% [11,12-14]. For the node positive neck PPV reaches 80% and sensitivity 87% [11,12].

Several studies have reported how FDG-PET/CT led to a change in patient management in 6–57% of the cases [15-27]. This included upstaging, downstaging as well as diagnosing synchronic lesions and distant metastasis. It also led to additional imaging and histopathological studies. Furthermore, FDG-PET/CT is reported to have a beneficial effect for RT target definition in IMRT planning for primary disease, with a change in gross target volumes (primary and nodal GTV) in 57% [17].

In the clinical setting, the relevant question remains which treatment is justified in case of discordance between FDG-PET and CT results. Should pathologically suspect lymph nodes on either FDG-PET or CT be treated with high dose radiation (boost), as shown in Figure 1. A compromise has to be made between the risk of false positive FDG-PET and the risk of delaying appropriate salvage intervention. Second, smaller radiation fields using IMRT, allow tissue sparing, but could also lead to more marginal failures.

Therefore, the aims of this study were:

1. To analyze the influence of FDG-PET/CT versus CT alone on defining nodal target volume definition;
2. To analyze the long-term clinical results of [1];
3. In case of nodal recurrences, to relate the location of nodal recurrence to the radiation regional dose distribution and to determine if these recurrences are located in the high dose field, elective dose field or outside the radiation field.

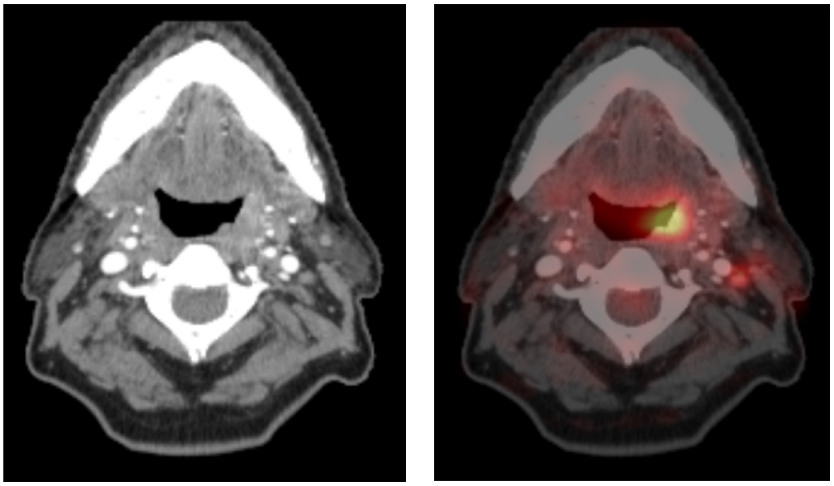

Figure 1: Patient with stage II oropharyngeal carcinoma with a focal uptake in a small lymph node on the left side (level II) on FDG-PET, not diagnosed on CT.

PATIENTS AND METHODS

This retrospective descriptive study included 327 patients with head and neck carcinoma scheduled for RT at University Medical Center, Utrecht, The Netherlands, between 2002 and 2010. All patients underwent CT and FDG-PET scanning in mold and had a minimum of two years follow-up. We excluded 44 patients: 31 patients received previous irradiation, 10 patients were treated for recurrent HNC, one patient died during irradiation, one patient refused radiation and one patient had a non-Hodgkin lymphoma with multiple lymph nodes in which case no difference could be made between lymphomas and pathological squamous cell carcinoma (SCC) nodes. A total of 283 patients were analyzed. There was no loss to follow-up. Baseline characteristics are summarized in Table 1.

Table 1: Patient characteristics

Characteristics	No.
Male/Female	187/96
Site of primary tumour:	
Oropharynx	151
Nasopharynx	34
Hypopharynx	30
Larynx	26
Oral cavity	19
Double primary tumor	14
Proximal esophagus	4
Unknown primary	3
Nasal Cavity	1
External ear canal	1
Primary radiotherapy	120
Chemoradiotherapy	122
Surgical resection and radiotherapy	38
Surgical resection and chemoradiotherapy	3

FDG-PET

All patients fasted for at least six hours before the intravenous administration of FDG, with a preferred serum glucose level of<10 mmol/l. FDG-PET imaging was performed with a standalone PET system, one hour after the intravenous administration of 3.7 MBq/kg. The first 131 patients were scanned with Philips C PET plus (with sodium iodide- NaI crystals). The subsequent 152 patients were scanned with a Philips Allegro PET scan (cerium-doped gadolinium oxyorthosilicate-GSO crystals) of FDG. In all

patients, positron emission and transmission scanning was performed from the head and neck area with additional recordings from the upper thighs to the neck. All patients were scanned in mold, so the exact same individual position was maintained during scanning. Tomographic images (with and without attenuation correction) were viewed by a radiation oncologist as well as an experienced nuclear medicine physician. Images were interpreted by qualitative visual analysis; lesions were identified as areas of FDG uptake considered by the reader to be notably above surrounding or expected normal metabolic tissue activity. FDG accumulation was reported as mild, moderate, or intense and compared to background uptake. The presence or absence of abnormal FDG accumulation, especially focal accumulation, in combination with their size and intensity were evaluated. Both uncorrected and attenuation-corrected images were assessed in order to identify any artifacts. More objective methods to depict FDG hot spots equivalent to GTV are cutoff standardized uptake value (SUV) thresholds. We did not calculate the SUV routinely as there is no optimal SUVmax cut off value to differentiate between malignant and benign neck lesions in the literature [28-30]. The quantification of small lesions is particularly difficult, because the impact of partial volume effects and image noise increases.

CT scan

Standard clinical CT of the head and neck was performed with a Philips CT Aura, after the injection of non-ionic contrast material. Acquisition of 1.5 or 2mm slices were reformatted into 3-mm thick sections in transverse and coronal directions (exposureTime 1000, XRay Tube Current 120–140 mAs, Exposure 120–140 mAs).
Images were first viewed by the radiologist specialized in head and neck oncology, where after they were discussed for consensus in the multidisciplinary meeting with the experienced head and neck radiation oncologist.
Lymph nodes were diagnosed as pathological when the minimal (shortest) axial nodal diameter exceeded 10mm (with consideration of node level, i.e. 8mm retropharyngeal), when 'nodal grouping' occurred (three or more contiguous and confluent lymph nodes, each of which had a maximal diameter of 8–15 mm), or if loss of fatty hilum and/or central necrosis was present without any clinical signs of inflammation [6].

Treatment

All 283 patients included in this study received primary IMRT for head and neck carcinoma. In accordance with local treatment policy, 41 patients had selective or (modified) radical neck dissection before RT, generally for bulky neck disease (N2a or multiple adjacent lymph nodes) (Table 1). Surgery was otherwise reserved for treatment of recurrent disease. A total of 125 patients (44%) received concomitant chemotherapy,

three of them following surgical resection. Chemotherapy was given to patients with stage III–IV disease, who accepted this therapy and were fit enough to receive it (considering age ≥ 70 and comorbidities). A total of 120 patients received RT only.
In this study, clinical policy was not based on FDG-PET in case of very low uptake or when the neck level of clearly elevated FDG uptake did not correspond with the expected drainage area of the primary tumor.
For IMRT planning, FDG-PET images were fused with CT data. The GTV, clinical target volume (CTV) and critical structures were contoured by the radiation oncologists. The gross disease CTV included GTV plus 1 cm within the anatomic boundaries. For the planning target volume (PTV) a margin of 3–5mm was used. Nodal regions considered pathological on FDG-PET/CT received doses of 64–72 Gy at 2 Gy per fraction. For low-risk subclinical nodal regions (elective dose area) 45–50 Gy was prescribed. Postoperatively intermediate-risk nodal regions (positive nodes without extranodal disease) received 56–60 Gy. All patients completed their planned course of IMRT. Concurrent chemotherapy was mostly platinum-based (Cisplatin, 100 mg/m2, every 3 weeks).

Nodal stage grouping

As reported sensitivity for FDG-PET is much lower in patients with a clinically negative neck (i.e. patients without neck metastases, as determined from physical examination) compared to clinically positive neck, analysis was done in subgroups.
A total of four subgroups were analyzed:

1. Patients with a clinically negative neck and CT showing pathological lymph nodes, not seen on FDG-PET.
2. Patients with a clinically negative neck and focal uptake on FDG-PET, without signs of lymphadenopathy on CT.
3. Patients with a clinically positive neck and CT showing more pathological nodes than FDG-PET.
4. Patients with a clinically positive neck and FDG-PET showing more pathological nodes than CT.

Data collection

Data on each patient was recorded in a computerized database (SPSS 20.0). Analysis was performed with the SPSS 20.0 statistical package for Windows.
TNM stage previously evaluated on CT scans by a head and neck radiologist was registered, as well as TNM stage recorded by consensus of the nuclear medicine physician and radiation oncologist after fusion of CT and FDG-PET. Irradiation dates and schedule was recorded as well as mean irradiation dose for each pathological

lymph node. In case of locoregional or regional recurrence, determined by histology and/or imaging, date of recurrence was noted and regional recurrence-free survival was calculated.
In addition, the location of recurrences was scored according to the initial IMRT planning (Figure 2). Initial irradiation dose was evaluated and recurrences were classified as infield (originating within the GTV and CTV), elective field (originating in the elective dose field), or outfield (receiving no radiation dose) [31].

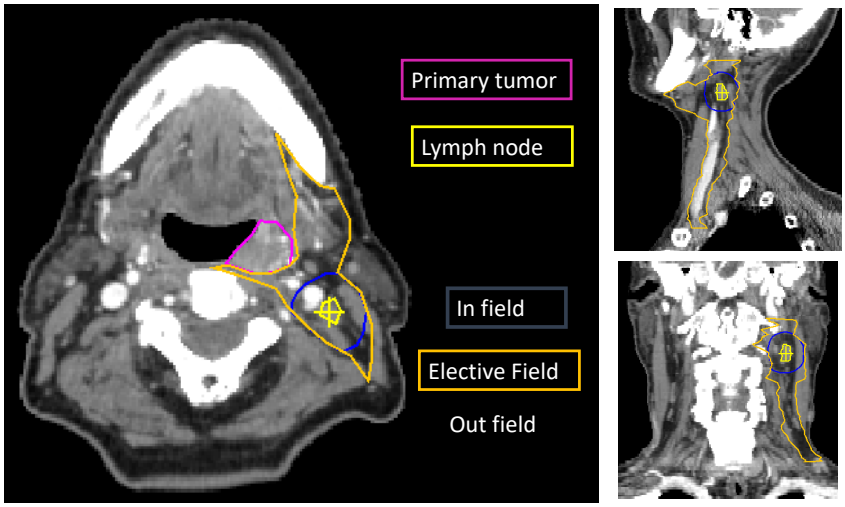

Figure 2: Recurrences were scored according to the initial IMRT planning as in field (high dose), elective field or out field (without irradiation) recurrences.

RESULTS

Influence of imaging on clinical policy

Overall
In 191 patients, CT and FDG-PET results for nodal stage (N stage) were equal (Table 2). In 92 patients, CT and FDGPET showed discordant results. In 31 patients, a total of 51 pathological nodes were seen on CT, without suspicious focal uptake on FDG-PET. In 61 patients, a total of 81 nodes had focal uptake on FDG-PET, but were not classified as pathological on CT.
A cross table (Table 3) shows the difference in N stage of different modalities. Most notable are 19 patients with N0 on CT versus N1 on FDG-PET. And 12 patients scored

with bilateral disease (N2c) on FDG-PET compared to unilateral disease (N2b) on CT. With the addition of FDG-PET to CT, nodal upstage was seen in 61 patients (22%) and nodal downstage was seen in 31 patients (11%). When considering chosen clinical policy, a total of 69 nodes in 52 patients, received a high radiation dose (boost) as a result of focal uptake on FDG-PET. Treatment-based nodal upstage was therefore 18% as a result of FDG-PET. A total of 27 nodes in 16 patients were not treated with high dose as a result of negative findings on FDG-PET, although these nodes were classified as pathological on CT. Treatment-based nodal downstage was therefore 6% as a result of FDG-PET.
In 24 of the 92 patients with discordant results, CT was the decisive factor for clinical policy. In 68 patients, clinical policy was based on the additional FDG-PET imaging.

Table 2: Overall concordance FDG PET and CT results.

	Number of patients	Number of discordant nodes
CT = PET	191	
CT +/ PET -	31	51
CT -/ PET +	61	81
Total	283	132

Results by grouping

Group 1 (Figure 3) includes 13 patients with a clinically negative neck (cN0) and CT showing pathological lymph nodes, not seen on FDG-PET. In six of them, clinical policy was based on CT and patients received high dose radiation (boost). In seven of them, clinical policy was based on FDG-PET and patients did not receive a boost on the discordant nodes.
Group 2 (Figure 4) includes 29 patients with a clinically negative neck and without signs of lymphadenopathy on CT, however, with focal uptake on FDG-PET. In 24 patients, FDGPET was the decisive factor for clinical policy and patients received a boost. In five patients, no boost was applied. In most of these cases, SUV was very low or focal uptake was seen on FDG-PET in an unlikely node level according to the primary tumor drainage area.
Group 3 (Figure 5) includes 18 patients with a clinically positive neck and CT showing more pathological nodes than FDG-PET. In 50% of these cases, clinical policy was based on CT. In the other 50%, clinical policy was based on FDG-PET.
Group 4 (Figure 6) includes 32 patients with a clinically positive neck and FDG-PET showing more pathological nodes than CT. In this case 28 patients (88%) received a boost following the results of FDG-PET, compared to only four patients without a boost.

Long-term clinical results

Minimum follow-up time was two years, maximum was 8.8 years. Average follow-up was 3.3 years in the whole study group and 4.6 years in patients who were not deceased during routine follow-up. Locoregional control was high for all groups. Figures 3–6 show the number of regional and locoregional recurrences in each subgroup of patients.

Recurrences

We found a total of 38 patients with regional recurrences (13.4%). In total 21 were regional recurrences only and 17 were locoregional recurrences. Eight of these patients had discordant results on FDG-PET and CT (Figures 3–6).

Regional control

Three-year actuarial regional control after primary RT or concurrent chemoradiotherapy correlated to N stage, respectively, N0 96% versus 94%, N1 86% versus 90%, N2a 50% versus 60%, N2b 83% versus 81%, N2c 78% versus 74% and N3 42% versus 42% for FDG-PET-based N stage versus CT based N stage, respectively. Results are shown in Table 4. In the concordant group of 191 patients, three-year regional control for CT and FDG-PET negative patients (60 patients) and for CT and FDG-PET positive patients (131 patients) was 95% and 73%, respectively.

Table 4: Three year actuarial regional control (%) according to N stage after primary radiotherapy or concurrent chemoradiotherapy.

	Lambrecht 2009	Rengan 2008	Porceddu 2008	Our study PET	Our study CT
N0	95			96	94
N1	84	86	88	86	90
N2a	83	85	81	50	60
N2b	70			83	81
N2c	70			78	74
N3		100 (0/4)	50	42	42

Nodal recurrences

Analysis of all included patients, showed 38 patients with a regional recurrence, in which a total of 76 recurrent nodes were found. Recurrences were identified by imaging [CT, magnetic resonance imaging (MRI) and/or PET] in 32 patients. Thirty-four patients underwent ultrasound-guided fine needle aspiration. Four recurrences were very suspicious on clinical evaluation with progression during follow-up. Recurrences were compared to their location on initial IMRT planning
(Figure 2).

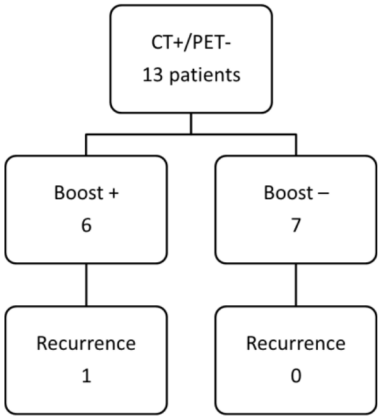

Figure 3: Flow chart of patients with clinically negative neck and CT showing pathologic nodes without suspicious focal uptake on FDG-PET (Group 1).

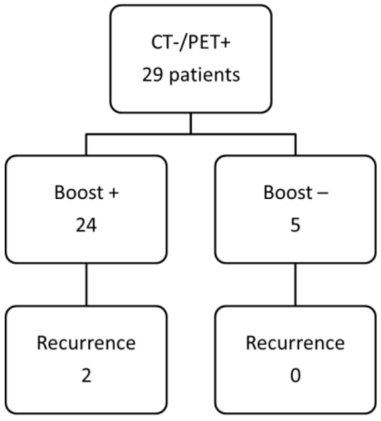

Figure 4: Flow chart of patients with clinically negative neck and no pathological nodes on CT, but with focal uptake in lymph nodes on FDG-PET (Group 2).

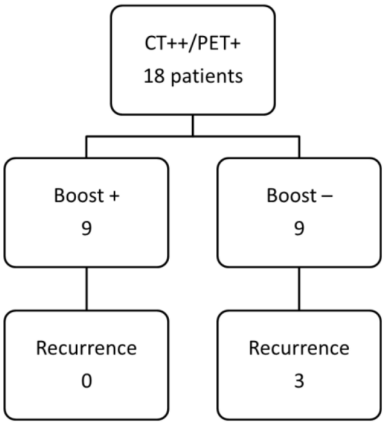

Figure 5: Flow chart of patients with a clinically positive neck and CT showing more pathological nodes than FDG-PET (Group 3).

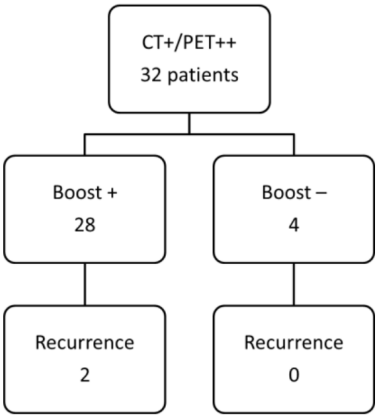

Figure 6: Flow chart of patients with a clinically positive neck and FDG-PET showing more pathological nodes than CT (Group 4).

Sub analysis of the discordant patient group of 92 patients, showed five patients with a locoregional and three patients with a regional recurrence (Figures 3–6). A total of 15 recurrent nodes where found in these eight patients.

In Group 1 (clinically negative neck and CT showing pathologic nodes), one patient had a regional recurrence, consisting of one node in the elective dose field. This was not the discordant node on imaging.

In Group 2 (clinically negative neck and FDG-PET showing pathologic nodes), two patients had a regional recurrence with a total of three recurrent infield nodes. All nodes were discordant nodes, with high uptake on FDG-PET, but not reported as pathological on CT. Both patients received a boost on the discordant nodes.

In Group 3 (more pathological nodes on CT than on FDGPET), three patients had a regional recurrence with six infield recurrent nodes and one outfield recurrent node. None of these were discordant nodes.

In Group 4 (more pathological nodes on FDG-PET than on CT), regional recurrence was seen in two patients. One node was infield, one was in the elective dose field and two were outfield nodal recurrences. None of these were discordant nodes.

DISCUSSION

To the authors' knowledge this is the largest study reporting the added value of the FDG-PET scan to CT alone in the clinical decision making in IMRT planning of lymph nodes in HNC.

Table 5: Studies addressing the role of FDG PET on the initial nodal staging of head and neck carcinomas.

Author	year	No. PETs		Other Imaging	PA	change N-stage
Smid	2003	48	P	CT	-	6% ↑
Koshy	2005	36	R	CT+/- MR	-	8% ↑, 11% ↓
Zanation	2005	15 (97)	R	CT	-	(22%)
Wang	2006	28	R	CT	-	21% ↑
Connell	2007	35 (76)	P	CT or MR	-	23% ↑, 6% ↓
Fleming	2007	123	R	CT	+/-	(31%)
Gordin	2007	21 (90)	P	CT and/or MR	+/-	14% ↑
Guido	2009	38	P	CT	-	13% ↑, 3% ↓
Delouya	2011	29	P	CT	+/-	0% (9% ↑, 5% ↓)
Abramyuk	2013	102	R	CT	-	8% ↑, 26% ↓
This study	2014	283	R	CT	-	18% ↑, 6% ↓
Arias	2015	72	R	CT	+/-	26% ↑, 3% ↓

P=prospective, R=retrospective, PA=histopathology as reference standard

Influence of imaging on clinical policy

Overall

In our study, FDG-PET led to an alteration in nodal treatment management in 24% of the cases, including a nodal upstage of 18% and a nodal downstage of 6%. This is in concordance with literature, reporting a PET/CT-based change in patient management in 6–31% (Table 5) [15-27].

Several studies have addressed the impact of FDG-PET on clinical practice in the initial (nodal) staging of head and neck carcinomas, most with retrospective design and most without histopathologic reference standard. Four studies attempted to verify imaging finding with pathological specimens [20-22,26]. Delouya performed 10 biopsies for lymph nodes that were discordant between modalities and all were of benign histology. Nodal target volume was therefore not adjusted. In the study done by Arias, histological confirmation was only made by fine needle aspiration (FNA) in patients in whom FDG-PET data raised doubt and assumed modification of the therapeutic approach. FNA results are unfortunately not specified. Fleming evaluated 123 patients with histopathology. However, only a subset of 67 patients underwent neck dissection. Furthermore, only general treatment alteration is mentioned, including detection of synchronous and distant metastases. Nodal treatment alteration is not specified. Gordin included 90 patients, but only 21 patients were treated for primary disease. In

a subset of 56 patients (of 92), biopsy, FNA or surgery was performed for histopathologic verification, in the other 28 patients, clinical and radiological follow-up were used as reference standard. In our study, reliable FNA could not be performed in a significant number of patients, as nodes with pathologic uptake on FDG-PET were not considered as pathologic on CT as well as on ultrasound. Furthermore, FNA can be inconclusive, especially in necrotic tissue. Therefore, FNA as verification method in these studies can be questionable.

Patient numbers in these studies vary between 15 and 123. In some studies, only a subset of patients is comparable to our study population. Zanation et al., for example retrospectively studied 97 patients [16]. Only 15 patients were staged for initial disease. In 22%, PET/CT results led to a major change in management including upstage or further major surgery. Data are not specified. Connell et al. prospectively evaluated the clinical value of PET/CT over conventional assessment in 76 patients [18]. Only 35 included initial staging. FDG-PET resulted in an alteration (enlargement and reduction) in RT planning in 10 of 35 patients (29%); eight patients (23%) had a treatment-based nodal upstage, two patients (6%) had a nodal downstage as a result of FDG-PET. As mentioned before, Gordin et al. assessed FDG-PET/CT in 90 patients [20]. However again, only 21 patients were treated for primary disease. FDG-PET/CT diagnosed three patients (14%) with have a positive lymph node, not seen on conventional imaging (CT or MRI). Final pathologic results following neck dissection confirmed the presence of malignancy. We included 283 patients. This is so far the largest cohort assessing the clinical value of FDG-PET on patients treated with RT for primary disease. All studies support the use of PET/CT in patients with newly diagnosed HNC, mainly because of its high PPV and superiority of detecting distant metastases and synchronous lesions.

In this study, both improvement of integrated PET-CT scanners as well as optimized head and neck reconstruction (OHR) adapted to low photon attenuation in the head and neck area, may have improved image quality and the diagnostic value of FDG-PET[32].

Results by grouping

In Group 1, including patients with a clinically negative neck and CT showing pathological nodes, not seen on FDG-PET, 46% of the patients received a boost. Regional control was 92% in case of boost and 100% without a boost. As regional control was so high in both groups, pathological nodes on CT could have been false positive. Sensitivity of CT in the clinically negative neck has been reported between 14% and 80%. However, FDG-PET may also be false negative, due to a low tumor load. An intermediate radiation dose might therefore be justified.

In Group 2, including patients with a clinically negative neck, with no pathological nodes on CT, but with suspicious focal uptake on FDG-PET, 83% received a boost. The decision not to boost was made in case of very low uptake on PET or in case of uptake in a very unlikely nodal region (concerning the drainage area of the primary tumor). Regional control was 93% in case of boost and 100% without boost. Although sensitivity of FDG-PET in the clinically negative neck is only 50%, there is still a 50% chance of pathology[11]. This probably resulted in some overtreatment. However, elective treatment is already considered to be justified in case of a 20% change for occult metastases. FDG-PET positivity will be seen in case of a higher tumor load: a high dose to the FDG positive nodes is advisable.
In Group 3, including patients with a clinically positive neck and CT showing more pathological nodes than FDG-PET, 50% received a boost. Locoregional control was 100% in case of boost and 67% without boost. As overall sensitivity of CT is 74% with range 61–83% (numbers extracted from 16 studies), and regional control is expected to be lower as a result of higher lymph node staging, a high dose radiation on these discordant nodes is advised [11].
In Group 4, including patients with a clinically positive neck and FDG-PET showing more pathological nodes than CT, most patients (88%) received a boost. Regional control was 94% (30/34) in case of boost and 100% (0/4) without boost. Concerning the fact that these patients had a clinically positive neck with higher nodal stages, (loco)regional control is considered high. In case of elective low dose treatment only on these nodes, a higher recurrence rate would be expected in this group. Furthermore, in most cases only a minimal adjustment in radiation field was necessary with a low risk of extra morbidity. High dose radiation on the FDG-PET positive nodes might therefore be justified.

Long-term clinical results

The most important factor that influences clinical outcome is the presence of metastatic cervical lymphadenopathy. Regardless to the site of the primary tumor, the presence of a single metastatic lymph node in each site of the neck reduces the survival rate to nearly 25% of that expected in patients without any cervical nodal metastases. The presence of extranodal spread can further reduce the survival rate by half [6]. The results of our database suggest N-staging by FDG-PET results in a somewhat better distinction in prognostic N-groups compared to N-staging based on CT only. In Table 4 our actuarial three-year regional control for N0 and N positive, depending on PET or CT, is comparable to published results in literature [33-35]. Lambrecht et al. published a nodal control for N0, N1, N2a, N2b, N2c disease of, respectively, 95%, 84%, 83%, 70% and 70% in a cohort of 368 patients.

Porceddu calculated the regional control in 117 patients following chemoradiation, based on N stage, using the major groupings N1, N2 and N3 and found 88%, 81% and 50%, respectively. Rengan et al. found a long-term neck control rate of at least 85% without neck dissection in 65 patients with node positive disease, who initially achieved clinical complete response after chemoradiation. Patients without clinically complete response were excluded from the analysis. Subsequent neck failure among patients with complete response according to initial nodal classification was: N1 14% (3 of 21), N2: 15% (6 of 40), N3: 0% (0 of 4). The median overall survival of these patients was: N1: 12.2 years; N2: 6.5 years; N3: 0.8 years. In other studies, regional control was calculated for a different period and/or N stage subgroups were not specified.

Nodal recurrences

The location of the recurrence in relation to the original treatment volume indicates the possible cause of treatment failure and can be used to guide treatment optimization. Steep dose gradients in IMRT are beneficial for sparing healthy tissue, but address less radiation at surrounding tissues. In the case of neck nodes metastases, nodal recurrences might suggest occult metastases that where undetected on imaging. This could be the case for three outfield and two elective dose nodal field recurrences found in three patients. All of these recurrences, however, occurred in concordant nodes and were not detected by both FDG-PET and CT.

Ten nodal field recurrences (in 92 patients) were infield recurrences and occurred despite of high dose radiation. Treatment could therefore not be optimized. Three of these nodes (in two patients) were discordant on FDG-PET and CT but did receive high dose radiation. In these two cases, FDG-PET showed nodal uptake, but the nodes were not enlarged on CT. In clinically negative necks, with uptake on FDG-PET, a boost dose could therefore be justified.

This study has several limitations. One limitation is the retrospective study design. A prospective trial, however, may not be ethically justified as patients with suspicious lymph nodes on FDG-PET may be excluded from irradiation on these nodes, which may lead to undertreatment, and therefore to a possible worse clinical outcome.
Another limitation is the lack of histopathology. Assessment of the accuracy of staging with addition of FDG-PET was not possible in our cohort as most patients received definitive RT or chemoradiation and histopathologic confirmation could not be obtained. Nakamura et al. investigated the sensitivity and specificity of FDG-PET compared to neck dissection resulting in a sensitivity of 83% and specificity of 86% [36]. Although it would have been ideal to have histopathologic findings of each node,

neck dissections add significant morbidity in patients with HNC [37]. As not all lymph nodes in this study were histopathologically evaluated, a gold standard reference is missing and lymph nodes could be false positive on imaging, resulting in a higher (unnecessary) local irradiation dose. In clinical practice, this remains a compromise between the risk of false positive FDG-PET with subsequent overtreatment and the risk of undertreatment.
The percentage of overtreatment is the result of the total number of nodes that received a high dose minus the true PET positive nodes. Not all PET positive nodes in our study received a high dose. Furthermore, when clinical decision was made to give a boost dose, only the node itself received a high IMRT dose, not the whole neck level in which the node was found. Subsequently, morbidity due to the boost dose was limited. Another concern is that under treatment can lead to a higher rate of regional recurrences with consequently poor prognosis.

Finally, we reached a high regional control. Only eight patients of 92 with discordant results on CT and FDG-PET had a regional recurrence. All other regional recurrences were found in 30 patients with concordant results on CT and FDGPET. Although this is satisfactory for daily clinical practice, it makes it more difficult to draw conclusions.

CONCLUSION

We included FDG-PET in a large cohort of patients, performed in a RT mold, in our decision to treat suspected lymph node regions with or without high radiation dose (boost), resulting in a high nodal control rate. In case of a clinically negative neck, a boost dose for FDG-PET negative nodes, although suspicious on CT, maybe be omitted, based on our 96% nodal control rate. Sensitivity of CT ranges between 14% and 80% in these cases. In case of a clinically negative neck with FDG-PET positive and CT negative nodes, recurrence rate was 7%. As these recurrences occurred even when high dose irradiation was prescribed, we would advise to treat patients based on FDG-PET.
In case of CT showing more pathological nodes than FDG-PET, regional control reached 100% in case of boost, but only 83% without boost. In case of FDG-PET showing suspicious nodes, not seen on CT, we reached a high regional control with 88% of these patients clinically treated with a boost dose. These results support the complementary value of FDGPET/CT compared to CT alone in defining nodal target volume definition for RT of HNC.

REFERENCES

1. Nutting CM, Morden JP, Harrington KJ, Urbano TG, Bhide SA, Clark C, et al. PARSPORT trial management group. Parotid-sparing intensity modulated versus conventional radiotherapy in head and neck cancer (PARSPORT): a phase 3 multicentre randomised controlled trial. *Lancet Oncol*. 2011;12:127–36.

2. Gupta T, Agarwal J, Jain S, Phurailatpam R, Kannan S Ghosh-Laskar S, et al. Three-dimensional conformal radiotherapy (3D-CRT) versus intensity modulated radiation therapy (IMRT) in squamous cell carcinoma of the head and neck: a randomized controlled trial. *Radiother Oncol*. 2012;104:343–8.

3. Braam PM, Terhaard CH, Roesink JM, Raaijmakers CP. Intensitymodulated radiotherapy significantly reduces xerostomia compared with conventional radiotherapy. *Int J Radiat Oncol Biol Phys.* 2006;66:975–80.

4. Castelijns JA, van den Brekel MW. Imaging of lymphadenopathy in the neck. *Eur Radiol.* 2002;12:727–38.

5. Curtin HD, Ishwaran H, Mancuso AA, Dalley RW, Caudry DJ, McNeil BJ. Comparison of CT and MR imaging in staging of neck metastases. *Radiology* 1998;207:123–30.

6. Som PM. Detection of metastasis in cervical lymph nodes: CT and MR criteria and differential diagnosis. *AJR Am J Roentgenol*. 1992;158:961–9.

7. Madani I, Duthoy W, Derie C, De Gersem W, Boterberg T, Saerens M, et al. Positron emission tomography-guided, focal-dose escalation using intensity-modulated radiotherapy for head and neck cancer. *Int J Radiat Oncol Biol Phys.* 2007;68:126–35.

8. Troost EG, Schinagl DA, Bussink J, Oyen WJ, Kaanders JH. Clinical evidence on PET-CT for radiation therapy planning in head and neck tumours. *Radiother Oncol*. 2010;96:328–34.

9. Yongkui L, Jian L, Wanghan Jingui L. 18FDG-PET/CT for the detection of regional nodal metastasis in patients with primary head and neck cancer before treatment: a meta-analysis. *Surg Oncol.* 2013;22:e11–16.

10. Sun R, Tang X, Yang Y, Zhang C. 18FDG-PET/CT for the detection of regional nodal metastasis in patients with head and neck cancer. A meta-analysis. *Oral Oncol.* 2015;51:314–20.

11. Kyzas PA, Evangelou E, Denaxa-Kyza D, Ioannidis JP. 18F-fluorodeoxyglucose positron emission tomography to evaluate cervical node metastases in patients with head and neck squamous cell carcinoma: a meta-analysis. *J Natl Cancer Inst*. 2008;100:712–20.

12. Ozer E, Naibo_glu B, Meacham R, Ryoo C, Agrawal A, Schuller DE. The value of PET/CT to assess clinically negative necks. *Eur Arch Otorhinolaryngol*. 2012;269:2411–14.

13. Roh J, Park JP, Kim JS, Lee JH, Cho KJ, Choi SH, et al. 18F Fluorodeoxyglucose PET/CT in head and neck squamous cell carcinoma with negative neck palpation findings: a prospective study. *Radiology* 2014;271:153–61.

14. Lee HJ, Kim J, Woo HY, Kang WJ, Lee JH, Koh YW. 18F-FDG PET-CT as a supplement to CT/MRI for detection of nodal metastasis in hypopharyngeal SCC with palpably negative neck. *Laryngoscope* 2015;125:1607–12.

15. Schmid DT, Stoeckli SJ, Bandhauer F, Huguenin P, Schmid S, von Schulthess GK, et al. Impact of positron emission tomography on the initial staging and therapy in locoregional advanced squamous cell carcinoma of the head and neck. *Laryngoscope* 2003;113:888–91.

16. Zanation AM, Sutton DK, Couch ME, Weissler MC, Shockley WW, Shores CG. Use, accuracy, and implications for patient management of [18F]-2-fluorodeoxyglucose-positron emission/- computerized tomography for head and neck tumors. *Laryngoscope* 2005;115:1186–90.

17. Wang D, Schultz CJ, Jursinic PA, Bialkowski M, Zhu XR, Brown WD, et al. Initial experience of FDG-PET/CT guided IMRT of head- and neck carcinoma*. Int J Radiat Oncol Biol Phys.* 2006;65:143–51.

18. Connell CA, Corry J, Milner AD, Hogg A, Hicks RJ, Rischin D, et al. Clinical impact of, and prognostic stratification by, F-18 FDG PET/ CT in head and neck mucosal squamous cell carcinoma. *Head Neck* 2007;29:979–85.

19. Schoder H, Carlson DL, Kraus DH, Stambuk HE, G€onen M, Erdi YE, et al. 18F-FDG PET/CT for detecting nodal metastases in patients with oral cancer staged N0 by clinical examination and CT/MRI*. J Nucl Med*. 2006;47:755–62.

20. Gordin A, Golz A, Keidar Z, Daitzchman M, Bar-Shalom R, Israel O. The role of FDG-PET/CT imaging in head and neck malignant conditions: impact on diagnostic accuracy and patient care. *Otolaryngol Head Neck Surg.* 2007;137:130–7.

21. Fleming AJ Jr., Smith SP Jr., Paul CM, Hall NC, Daly BT, Agrawal A, et al. Impact of [18F]-2 fluorodeoxyglucose-positron emission tomography/computed tomography on previously untreated head and neck cancer patients. *Laryngoscope* 2007;117:1173–9.

22. Arias F, Chicata V, Garc_ıa-Velloso MJ, Ass_ın G, Uzcanqua M, Eito C, et al. Impact of initial FDG PET/CT in the management plan of patients with locally advanced head and neck cancer*. Clin Transl Oncol.* 2015;17:139–44.

23. Schwartz DL, Ford E, Rajendran J, Yueh B, Coltrera MD, Virgin J, et al. FDG-PET/CT imaging for preradiotherapy staging of head- and neck squamous cell carcinoma. *Int J Radiat Oncol Biol Phys.* 2005;61:129–36.

24. Koshy M, Paulino AC, Howell R, Schuster D, Halkar R, Davis LW. F- 18 FDG PET-CT fusion in radiotherapy treatment planning for head and neck cancer. *Head Neck* 2005;27:494–502.

25. Guido A, Fuccio L, Rombi B, Castellucci P, Cecconi A, Bunkheila F, et al. Combined 18F-FDG-PET/CT imaging in radiotherapy target delineation for head-and-neck cancer. *Int J Radiat Oncol Biol Phys* 2009;73:759–63.

26. Delouya G, Igidbashian L, Houle A, B_elair M, Boucher L, Cohade C, et al. 18F-FDG-PET imaging in radiotherapy tumor volume delineation in treatment of head and neck cancer. *Radiother Oncol* . 2011;101:362–8.

27. Abramyuk A, Appold S, Z€ophel K, Baumann M, Abolmaali N. Modification of staging and treatment of head and neck cancer by FDG-PET/CT prior to radiotherapy. *Strahlenther Onkol.* 2013;189:197–201.

28. Payabvash S, Meric K, Cayci Z. Differentiation of benign from malignant cervical lymph nodes in patients with head and neck cancer using PET/CT imaging. *Clin Imaging* 2015;40:101–5.

29. Wong RJ, Lin DT, Schoder H, Patel SG, Gonen M, Wolden S, et al. Diagnostic and prognostic value of [(18)F]fluorodeoxyglucose positron emission tomography for recurrent head and neck squamous cell carcinoma. *J Clin Oncol*. 2002;20:4199–208.

30. Allal AS, Dulguerov P, Allaoua M, Haenggeli CA, El-Ghazi el A, Lehmann W, et al. Standardized uptake value of 2-[(18)F] fluoro-2- deoxy-D-glucose in predicting outcome in head and neck carcinomas treated by radiotherapy with or without chemotherapy. *J Clin Oncol.* 2002;20:1398–404.

31. Raktoe SA, Dehnad H, Raaijmakers CP, Braunius W, Terhaard CH. Origin of tumor recurrence after intensity modulated radiation therapy for oropharyngeal squamous cell carcinoma. *Int J Radiat Oncol Biol Phys.* 2013;85:136–41.

32. Vogel WV, Wensing BM, van Dalen JA, Krabbe PF, van den Hoogen FJ, Oyen WJ. Optimised PET reconstruction of the head and neck area: improved diagnostic accuracy*. Eur J Nucl Med Mol.* Imaging 2005;32:1276–82.

33. Lambrecht M, Dirix P, Van den Bogaert W, Nuyts S. Incidence of isolated regional recurrence after definitive (chemo-) radiotherapy for head and neck squamous cell carcinoma. *Radiother Oncol*. 2009;93:498–502.

34. Rengan R, Pfister DG, Lee NY, Kraus DH, Shah JP Shaha AR, et al. Long-term neck control rates after complete response to chemoradiation in patients with advanced head and neck cancer*. Am J Clin Oncol.* 2008;31:465–9.

35. Porceddu SV, Sidhom M, Foote M, Burmeister E, Stoneley A, El Hawwari B, et al. Predicting regional control based on pretreatment nodal size in squamous cell carcinoma of the head and neck treated with chemoradiotherapy: a clinician's guide*. J Med Imaging Radiat Oncol.* 2008;52:491–6.

36. Nakamura S, Okochi K, Kurabayashi T. Dual-time-point fluorodeoxyglucose positron emission tomography for diagnosis of cervical lymph node metastases in patients with head and neck squamous cell carcinoma. *J Comput Assist Tomogr.* 2011;35:303–7.

37. Machtay M, Moughan J, Trotti A, Garden AS, Weber RS, Cooper JS, et al. Factors associated with severe late toxicity after concurrent chemoradiation for locally advanced head and neck cancer: an RTOG analysis. *J Clin Oncol.* 2008;26:3582–9.

CHAPTER 8

Summary

Medical imaging began in 1895 with the discovery of the X-ray by German professor of physics Wilhelm Conrad Roentgen. He noticed that the invisible rays were able to penetrate tissues (like skin or muscle) better than others (like bone or metals). Nearly two weeks after his discovery, he took the very first picture of his wife's hand using X-rays. In the past (nearly) 125 years, technical development in medical imaging has been enormous. Today's multi-slice CT systems, using the same X-ray principle, can collect up to 4 slices of data in about 350 ms and reconstruct a 512 x 512-matrix image from millions of data points in less than a second.
Magnetic Resonance Imaging evolved during the 1970s. MRI makes use of the magnetic properties of hydrogen nuclei. These nuclei can be rotated ('spinned') using radio waves. They subsequently oscillate in the magnetic field while returning to equilibrium. Simultaneously they emit a radio signal. This is detected using antennas (coils), localizing the signal in space. By varying the parameters of the radiowave pulse sequence, different contrasts may be generated between tissues based on the relaxation properties of the hydrogen atoms in the tissues. The tissue that has the least hydrogen atoms (such as bones) turns out dark, while the tissue that has many hydrogen atoms (such as fatty tissue) looks much brighter. By advanced computer processing, it is possible to build up a three-dimensional image that reflects the chemical structure of the tissue, including differences in water content and in movements of the water molecules. This results in a very detailed image of the area of interest. The advantages of MRI over other imaging modalities include absence of ionizing radiation, superior soft tissue contrast resolution, high-resolution imaging, and multiplanar imaging capabilities. In head and neck oncology, the superior soft tissue contrast resolution of MRI compared to CT has its benefits for skin carcinoma's, salivary gland tumors and paraphayngeal space tumors. Also, discrimination of tumor from mucous retention in nasal cavity/sinus tumors, identification of perineural and intracranial tumor spread, altered bone marrow signal as a result of early bone invasion and superior tumor delineation in the soft tissues of the head and neck, including oral cavity carcinomas. Development in MRI techniques is evolving very fast. In 1980s and 1990s, superconducting magnets became common, initially at 1.5 Tesla (measure of magnetic field strength). Nowadays, MRI units as high as 7 Tesla are in clinical use. To put things in perspective, the earth's magnetic field is .00005 Tesla. Thus a 7 T magnet has a field strength 140.000 times stronger than that of the earth.

In daily otolaryngology practice, we encounter numerous clinical problems. First, accurate diagnosis and evaluation of the extent of the disease, is crucial for choosing a treatment strategy, together with the patient. A therapy, with the best curable intent, taking into account both physical comorbidities, morbidity of the treatment, expected treatment outcomes and patients preference.

For accurate diagnosis, both physical examination and diagnostic imaging can complement each other. This thesis focuses on diagnostic imaging, mainly MRI. We evaluate its accuracy for three anatomical regions; The first half of this thesis focuses on anatomy and benign disease of the middle - and inner ear. The second half on malignant disease of the larynx (small laryngeal carcinomas) and the neck (for primary staging of neck metastases in head and neck cancer).

Benign otolaryngology disease

One of the benign otolaryngology diseases is a cholesteatoma, a skin-lined cyst, consisting of keratin within a sac of squamous epithelium, potentially causing damage to the ossicles and/or other surrounding structures, indicating a need for surgical removal. Surgery can be classified into canal wall up (CWU) or canal wall down (CWD). Because of possible residual or recurrent disease, patients often undergo a second look procedure later on, with exploration of the mastoid and middle ear and, if necessary, hearing restoration. More recently a shift is seen towards a single stage procedure with cholesteatoma removal and obliteration of the mastoid cavity. A reliable imaging tool can avoid the necessity for a second look procedure and advocate a one stage procedure. **Chapter 2** describes a systematic literature search in PubMed, Embase, and Cochrane up to October 22, 2014 to evaluate the diagnostic value of non–echo planar (non-EPI) diffusion-weighted magnetic resonance imaging (DW MRI) for primary and recurrent/residual (postoperative) cholesteatoma in adults (>18 years) after canal wall up surgery. In total, 779 unique articles were identified, of which 23 articles were included for critical appraisal. Seven articles met our criteria for relevance and validity for postoperative cholesteatoma. Four studies were additionally included for subgroup analysis of primary cases only. Ranges of sensitivity, specificity, positive predictive value, and negative predictive value in the whole patient group yielded 43%-92%, 58%-100%, 50%-100% and 64%-100%, respectively. Results for primary subgroup analysis were 83%-100%, 50%-100%, 85%-100%, and 50%-100%, respectively. Results for subgroup analysis for only postoperative cases yielded 80%-82%, 90%-100%, 96%-100%, 64%-85%, respectively. Despite a higher prevalence of cholesteatoma in the primary cases, there was no clinical difference in added value of DW MRI between primary and postoperative cases. We found a high predictive value of non–echo planar DW MRI for the detection of primary and postoperative cholesteatoma. Given the moderate quality of evidence, we strongly recommend both the use of non-echo planar DW MRI scans for the follow-up after cholesteatoma surgery, and when the correct diagnosis is questioned in selected primary preoperative cases.

Pathology of the cochlea or the signaling pathway beyond the cochlea, along the 8th cranial nerve or other areas of the central auditory system can result in sensorineural hearing loss (SNHL). Depiction of the cochlea in more anatomical detail has its benefits for accurate diagnosis, localization of pathology and surgical planning. Obtaining normative measurements of normal and pathological variants of the cochlea can especially help in patients that suffer from severe SNHL and are eligible for cochlear implant surgery. Another application of MRI of the inner ear is the imaging of endolymphatic hydrops (EH). The implementation of 7.0 Tesla magnetic resonance imaging (MRI) for human use has the potential to further advance spatial resolution beyond that of 1.5T and 3T. This could result in potential advantages in the depiction of the membranous structures of the inner ear. The inner ear is particularly challenging to visualize at 7T. Where the signal-to-noise ratio will scale linear with the field strength, the proximity of the inner ear to the cerebrospinal fluid, nerves, and bone can lead to susceptibility banding artifacts and signal loss at the interface between the inner ear and its surroundings. In **chapter 3**, we scanned both a human head specimen, and 2 healthy volunteers at 7 Tesla MRI. First aim was to scan with ultrahigh resolution, independent of scan duration. Second aim was to reduce scan duration. The final step was to develop a scanning protocol suitable for clinical practice, based on previous information from ex vivo imaging. Both in and ex vivo, large objects like the cochlear basal turn, vestibule, and semicircular canals were visualized clearly. The nerves were depicted in more detail in vivo. The interscalar septum was visible in all images. A prolonged acquisition time ex vivo showed more detail of the scala tympani and vestibuli. However, the scala media was never visible, even with maximal resolution. Although inhomogeneities remain present, maximum resolution scanning ex vivo as well as scanning in vivo at 7T MRI resulted in clear depiction of the major membranous structures of the inner ear.

Following the development of a scanning protocol suitable for clinical practice on 7T MRI, in **chapter 4**, three healthy volunteers underwent magnetic resonance imaging at 3T and 7T scanner. At 7T, a unilateral dielectric pad was used for image optimization. Scan duration therefore doubled to a total of 15 minutes at 7T. The depiction of 10 anatomic parts of the inner ear was evaluated by two independent readers using a four-point grading scale. The interscalar septum, utricular macula, and the nerve bundles in the internal auditory canal were visualized more clearly at 7T. Although reduction of image artifacts remains challenging, especially at 7T, all structures depicted at 3T could be depicted at 7T. Image quality for some anatomic structures was superior at 7T. Further improvement of image quality could be achieved by developing dedicated surface coils and by technical advancement in B1 shimming and dedicated radiofrequency pulses.

Malignant otolaryngology disease

In the second half of this thesis, we focused on malignant otolaryngology disease. Laryngeal cancer (meaning cancer of the voice box) generally arises from the mucosal surface. It can therefore be easily detected by direct laryngoscopy (inspection of the larynx by flexible or rigid endoscope) and endoscopic biopsy (tissue sampling) to confirm the diagnosis. However, depth invasion of submucosal tissues cannot be reliably addressed. Accurate assessment of tumor extension, including depth infiltration, is of great importance for both staging, therapeutic approach and systematic comparison of data. In **chapter 5**, our goal was to assess the diagnostic value of MRI in pre-therapeutic staging of primary early stage (T1 and T2) glottic carcinoma. We conducted a systematic search in Pubmed, Embase and Scopus up to September 23rd, 2016. Included studies were selected and critically appraised for relevance and validity. 7 out of 938 unique articles were selected, including 64 cases. MRI overstaged 6% and understaged 13% of cT1 and cT2 tumors. However, available data is heterogeneous, very limited and mainly based on subanalysis of a small amount of patients. Reported MRI protocols appear to be suboptimal for small laryngeal lesions. Diagnostic value of MRI for subtle depth infiltration or laryngeal anatomical subsites (e.g. laryngeal ventricle, vocal cord etc.) could not be assessed. More studies are needed to assess the diagnostic value of MRI for small glottic tumors.

In **chapter 6**, we have tried to fill some of the gap of data found in chapter 5. In a clinical prospective study, we evaluated the feasibility of the clinical use of 3 Tesla and 7 Tesla Magnetic Resonance Imaging for early (cT1) glottic carcinoma, including structural assessment of technical image quality and visibility of the tumor. Twenty patients with primary clinical T1 glottic carcinoma underwent both routine clinical staging and CT. In addition, a 3T and 7T MRI protocol, developed for small laryngeal lesions, was performed in a 4-point immobilization mask, using dedicated surface coils. Afterwards, routine endoscopic direct suspension laryngoscopy under general anaesthesia was performed. Only 2/7 (29%) of 7T MRI scans were rated as moderate to good technical image quality. After exclusion of three patients with only mild to moderate dysplasia at the time of MRI, 13/17 (76%) of 3T MRI's were of adequate technical image quality. Tumor visualization was adequate in 8/13 (62%) of patients with invasive squamous cell carcinomas. With exclusion of the 4 MRI's with motion artefacts, the tumor and its boundaries could be adequately seen in 8/9 (89%) patients with squamous cell carcinoma versus only ¼ (25%) of patients with carcinoma in situ lesions. In conclusion, 7 Tesla MRI was considered not feasible. 3 Tesla MRI, with adequate patient selection, namely clinical exclusion of patients with a history of claustrophobia and inclusion of

only histologically proven invasive squamous cell carcinoma, can be feasible. Especially with further improvement of MR image quality. However, its superiority to CT could not be confirmed in this study. Superficial tumor extension remains difficult to detect on imaging.

In **chapter 7**, we focused on another imaging modality, namely 2-[18F]-fluoro-2-deoxy-D-glucose (FDG)-positron emission tomography (PET)/computed tomography (CT), which has various applications for malignant head and neck disease. The role of 18-FDG-PET/CT in routine diagnostic staging remains controversial. In case of discordance between FDG-PET and CT, a compromise has to be made between the risk of false positive FDG-PET and the risk of delaying appropriate salvage intervention. Second, with intensity modulated radiation therapy (IMRT), smaller radiation fields allow tissue sparing, but could also lead to more marginal failures. We retrospectively studied 283 patients with head and neck carcinoma scheduled for radiotherapy between 2002 and 2010. We analyzed the influence of FDG-PET/CT versus CT alone on defining nodal target volume definition and evaluated its long-term clinical results. Second, the location of nodal recurrences was related to the radiation regional dose distribution. In 92 patients, CT and FDG-PET, performed in mold, showed discordant results. In 33%, nodal staging was altered by FDG-PET. In 24%, FDG-PET also led to an alteration in nodal treatment, including a nodal upstage of 18% and downstage of 6%. In eight of these 92 patients, a regional recurrence occurred. Only two patients had a recurrence in the discordant node on FDG-PET and CT and both received a boost (high dose radiation).
These results support the complementary value of FDG-PET/CT compared to CT alone in defining nodal target volume definition for radiotherapy of head and neck cancer.

CHAPTER 9

Summary in Dutch
Nederlandse samenvatting

De mogelijkheid tot het afbeelden van het menselijk lichaam begon in 1895, met de uitvinding van röntgenstraling door de Duitse Fysica professor Wilhelm Conrad Roentgen. Het viel hem op dat de onzichtbare stralen gemakkelijker door bepaalde weefsels penetreerden (bijvoorbeeld huid of spier) dan door andere (bijvoorbeeld bot of metaal). Bijna twee weken na zijn eerste ontdekking maakte bij de eerste röntgenfoto van de hand van zijn vrouw. Sinds 1895 is er ontzettend veel veranderd. Vandaag de dag worden CT scanners gebruikt, die gebruik maken van dezelfde röntgenstraling, die 4 'doorsnedes' van het lichaam kunnen maken in 350 milliseconden en deze data kunnen reconstrueren in minder dan een seconde.

MRI (Magnetic Resonance Imaging) ontwikkelde zich in de 70-er jaren van de vorige eeuw. MRI maakt gebruik van de eigenschappen van waterstofkernen. Deze kernen kunnen, onder invloed van electromagnetische straling (radiogolven) omklappen, waarna de 'aangeslagen' kern na enige tijd weer terug valt in zijn grondtoestand. Tijdens dit proces komt een radiosignaal vrij. Dit wordt gemeten door antennes (coils). Door de parameters van de uitgezonden radiogolven te veranderen, kunnen verschillende contrasten tussen de weefsels ontstaan, gebaseerd op de relaxatie eigenschappen van de waterstofkernen in die weefsels. Weefsels met weinig waterstofatomen (bijvoorbeeld bot) worden donker, terwijl weefsels met veel waterstofatomen (bijvoorbeeld vetweefsel) veel lichter worden. Geavanceerde computersystemen verwerken deze data vervolgens tot een 3 dimensionaal beeld waarbij gedetailleerde beelden van het lichaam kunnen worden opgebouwd.

Voordelen van MRI ten opzichte van bijvoorbeeld CT zijn het ontbreken van ioniserende straling (met bijbehorende schadelijke effecten), betere contrastresolutie in 'weke delen' zoals huid-, vet- en spierweefsel en de mogelijkheid te scannen en reconstrueren in verschillende 'richtingen' (bijvoorbeeld van boven naar beneden, van links naar rechts etc). MRI technieken ontwikkelen zich erg snel. In de jaren 80 en 90 kwamen MRI scanners op de markt met een sterkte van 1.5 Tesla. Tegenwoordig zijn er MRI scanners met een sterkte van 7.0 Tesla beschikbaar voor zowel onderzoek als klinisch gebruik. Ter vergelijking, het magnetisch veld van de aarde is 0.00005 Tesla. Dus een 7 Tesla magneet heeft een veldsterkte die 140.000 keer groter is dan die van de aarde.
Binnen de KNO (keel, neus en oor) heelkunde praktijk ondervinden we dagelijks vele klinische problemen. Ten eerste is het stellen van de juiste diagnose en de mate van uitbreiding van de ziekte cruciaal. Pas dan kan, samen met de patiënt, gekozen worden voor de 'beste' behandeling, op grond van de effectiviteit van de behandeling, voorkeuren van de patiënt, leeftijd en bijkomende gezondheidsaspecten van de patiënt. Voor het stellen van de juiste diagnose vullen het lichamelijk onderzoek en aanvullende

beeldvorming elkaar vaak aan. Dit proefschrift richt zich op de klinische waarde van diagnostische beeldvorming, met name MRI voor het afbeelden van verschillende anatomische gebieden binnen de KNO. De eerste helft van dit proefschrift richt zich op de anatomie van het binnenoor en een goedaardige afwijking (cholesteatoom) van het middenoor. De tweede helft richt zich op kwaadaardige afwijkingen, namelijk kleine stembandtumoren en halskliermetastasen (uitzaaiingen in de hals) ten gevolge van hoofd hals kanker.

Benigne (goedaardige) KNO aandoeningen

Een van de goedaardige KNO aandoeningen is het cholesteatoom. Dit is een cyste bestaande uit huidcellen en keratine, die zich bevindt in het middenoor, de ruimte achter het trommelvlies waar oa de gehoorbeentjes zich bevinden. De cyste ontstaat meestal ten gevolge van een intrekking van het trommelvlies. Als een cholesteatoom niet tijdig chirurgisch verwijderd wordt kan deze schade aanrichten aan oa de gehoorbeenketen. Er bestaan verschillende chirurgische mogelijkheden om een cholesteatoom te opereren, de zogenaamde 'canal wall up' (CWU) procedure, waarbij de achterwand van de gehoorgang intact blijft, of de 'canal wall down' (CWD) procedure, waarbij de achterwand van de gehoorgang wordt weggeboord. Vaak is een tweede (een zogenaamde 'second look') operatie nodig, omdat een rest van het cholesteatoom achterblijft of weer terugkomt. Ook kan een tweede operatie tot doel hebben het gehoor te revalideren, bijvoorbeeld door het herstellen van de gehoorbeenketen als deze tijdens een eerste operatie onderbroken is. De laatste tijd wordt een verschuiving gezien naar een eenmalige operatie, waarbij het cholesteatoom verwijderd wordt en het rotsbeen (mastoid) geobliteereerd wordt. Dit zou de kans op terugkeer van het cholesteatoom verkleinen en zou de noodzaak voor een tweede operatie kunnen voorkomen. Hiervoor is een betrouwbaar diagnostisch middel voor het al dan niet aantonen van een recidief cholesteatoom erg belangrijk. **Hoofdstuk 2** beschrijft een systematische literatuurstudie naar de diagnostische waarde van een zogenaamde non-echo planar (non-EPI) diffusie gewogen MRI scan (DW MRI) voor de detectie van primaire (nog niet geopereerde) en postoperatieve cholesteatomen (na CWU chirurgie) bij volwassenen. Van de 779 gevonden artikelen werden 23 artikelen beoordeeld op relevantie en validiteit. Zeven artikelen voldeden aan onze criteria voor het postoperatieve cholesteatoom. Vier studies werden aanvullend geïncludeerd voor subgroep analyse voor het primaire cholesteatoom. Sensitiviteit, specificiteit, positief voorspellende waarde en negatief voorspellende waarde voor de gehele groep waren respectievelijk 43-92%, 58-100%, 50%-100% en 64%-100%. Resultaten van de subgroepanalyse van alleen het primair

cholesteatoom waren respectievelijk 83%-100%, 50%-100%, 85%-100%, en 50%-100%. Voor het postoperatief cholesteatoom alleen respectievelijk 80%-82%, 90%-100%, 96%-100% en 64%-85%. Klinisch toegevoegde waarde voor primair en postoperatief cholesteatoom was hetzelfde met een hoge voorspellende waarde van DW MRI. We zouden daarom het gebruik van non-EPI DWI aanraden in postoperatieve gevallen en bij twijfel over de juiste diagnose in een selecte groep patiënten met een primair cholestatoom.

In de cochlea (het slakkenhuis/gehoororgaan) wordt een geluidsgolf omgezet in een electrochemische stimulus, die via de gehoorzenuw zijn weg vindt naar de hersenstam. Pathologie van dit hele traject kan resulteren in sensorineuraal gehoorverlies (SNHL). Het afbeelden van de cochlea in meer anatomisch detail heeft zijn voordelen voor het stellen van de juiste diagnose, lokaliseren van de pathologie en het plannen van een chirurgische ingreep (bijvoorbeeld cochleaire implantatie). Met name het verkrijgen van normatieve metingen van de gezonde en pathologische cochlea kan helpen bij patiënten die in aanmerking komen voor een cochleair implantaat. Een andere toepassing van MRI voor het binnenoor is het afbeelden van endolymfatische hydrops (EH). De implementatie van 7.0 Tesla (7T) MRI voor klinisch gebruik heeft de potentie om de spatiële resolutie nog verder te verhogen dan op 1.5 Tesla of 3 Tesla. Hierdoor zouden we mogelijk de membraneuze structuren van het binnenoor beter kunnen afbeelden. Het is echter technisch lastig om het binnenoor af te beelden op 7T. De signaal-ruis verhouding neemt lineair toe met het verhogen van de veldsterkte. Maar de nabijgelegen liquor (ruggenmergsvocht) en bot kan leiden tot susceptibiliteitsartefacten en signaalverlies op de overgang van het binnenoor met de omgevende structuren. In **hoofdstuk 3** hebben we zowel een menselijk kadaverhoofd (ex vivo) als 2 vrijwilligers (in vivo) gescand op 7 Tesla MRI.
Het eerste doel was om te scannen op een zo hoog mogelijke resolutie, onafhankelijk van scan tijd. Het tweede doel was om de scantijd te reduceren. De laatste stap was het ontwikkelen van een scan protocol die toepasbaar is in de medische praktijk. Zowel ex vivo als in vivo konden de grotere structuren zoals de basale winding van de cochlea, het vestibulum en de semicirculaire kanalen goed worden afgebeeld. De zenuwen werden beter afgebeeld in de vrijwilligers. Het interscalaire septum was zichtbaar op alleen afbeeldingen. Bij een langere scanduur ex vivo konden de scala tympani en de scala vestibuli in meer detail worden weergegeven. De scala media was niet zichtbaar, ook niet bij maximale resolutie ex vivo.

In **hoofdstuk 4** hebben we 3 gezonde vrijwilligers gescand met zowel het nieuwe klinische protocol op 7 Tesla MRI als met het routine ziekenhuis protocol op 3 Tesla

MRI. Op 7 Tesla MRI is aan de kant van het te scannen binnenoor een diëlectrische vulling ('pad') tegen het hoofd gelegd om het beeld te optimaliseren. Daardoor verdubbelde de scantijd tot in totaal 15 minuten op 7 Tesla. De zichtbaarheid van 10 anatomische onderdelen van het binnenoor werden vervolgens gescoord op een 4-punts schaal door twee onafhankelijke radiologen. Het interscalaire septum, de macula van de utriculus en de zenuwbundels in de meatus acousticus internus werden duidelijker afgebeeld op 7 Tesla MRI. Hoewel het een uitdaging blijft om beeldartefacten te voorkomen, met name op 7 Tesla MRI, konden alle structuren die op 3 Tesla werden gezien, ook op 7 Tesla gezien. De beeldkwaliteit van enkele structuren was superieur op 7 Tesla tov 3 Tesla. Verdere verbetering van beeldkwaliteit zou bereikt kunnen worden door het ontwikkelen van specifieke oppervlakte spoelen en door technische verbeteringen in 'B1 shimming' en specifieke radiofrequente pulssequenties.

Maligne (kwaadaardige) KNO aandoeningen

In de tweede helft van dit proefschrift richten we ons op kwaadaardige KNO aandoeningen. Een larynxcarcinoom (kanker van de stembanden) ontstaat doorgaans vanuit het slijmvliesoppervlak. Het kan daarom gemakkelijk in beeld worden gebracht door middel van directe laryngoscopie (inspectie van de larynx met een flexibele of starre camera). De diagnose wordt bevestigd door middel van een endoscopisch biopt (weefselafname). De diepte uitbreiding van de tumor in de stemband zelf of in de omliggende weefsels kan alleen niet echt betrouwbaar worden geïnventariseerd. Het vaststellen van de tumoruitbreiding, ook in de diepte van de weefsels is echter van groot belang voor zowel de stadiëring van de tumor, het kiezen van een behandeling (laserresectie of bestraling van de tumor) en systematische vergelijking van data. In **hoofdstuk 5** onderzochten we de diagnostische waarde van MRI bij de stadiering van kleine (tumorstadium 1 en 2) larynxcarcinomen. We evalueerden systematisch de tot nu toe gepubliceerde data in een review. 7 van de 938 gevonden studies werden geïncludeerd. In deze studies werden in totaal 64 patiënten beschreven die voldeden aan onze inclusiecriteria. MRI overstadieerde 6% en onderstadieerde 13% van de klinische T1 en T2 tumoren. De gevonden data zijn echter erg heterogeen, erg beperkt en met name gebaseerd op een subanalyse van een klein aantal patiënten. De gebruikte MRI protocollen in de gepubliceerde studies zijn met name ontwikkeld voor de grotere (T2 t/m T4b) tumoren van de larynx en lijken suboptimaal voor kleine stembandtumoren. De waarde van MRI voor het inschatten van subtiele diepte invasie van de tumor in de stemband zelf of uitbreiding van de tumor naar anatomische subregio's binnen de larynx (oa laryngeale ventrikel, voorste commissuur etc) kon niet worden vastgesteld. Er zijn meer studies nodig om de waarde van MRI voor kleine stembandtumoren te onderzoeken.

In **hoofdstuk 6** hebben we een dergelijke ontbrekende studie opgezet. Het betrof een klinische prospectieve haalbaarheidsstudie naar de waarde van 3 Tesla en 7 Tesla MRI voor klinische T1 (tumorgrootte 1, het kleinst van alle stadia) kanker van de stemband. 20 patiënten ondergingen routinematige klinische diagnostiek bestaande uit flexibele larynoscopie (met stroboscopie) en CT van de larynx. Daarnaast werd een 3 Tesla MRI, speciaal ontwikkeld voor kleine larynxtumoren en een 7 Tesla MRI scan gemaakt. Patiënten werden gescand in een zogenaamd masker (wat beweging tijdens scannen tegen gaat). De beelden werden beoordeeld en gescoord door drie onafhankelijke beoordelaars op technische beeldkwaliteit en zichtbaarheid van de tumor. Na aanvullend onderzoek werd een routine starre microlaryngoscopie onder algehele narcose verricht met het opmeten van de tumor en het nemen van foto's. Slechts 2 van de 7 (29%) 7 Tesla MRI scans hadden een matige tot goede technische beeldkwaliteit. Na exclusie van 3 patiënten met slechts milde tot matige dysplasie (geen kanker) ten tijde van de MRI scan waren 13 van de 17 (76%) 3 Tesla MRI's van voldoende technische beeldkwaliteit. De tumor was voldoende zichtbaar in 8 van de 13 (62%) patiënten met een invasief plaveiselcelcarcinoom (kanker). Na exclusie van 4 MRI scans met bewegingsartefacten kon op 8 van de 9 (89%) patiënten met een plaveiselcelcarcinoom de tumor adequaat worden gezien. Bij patiënten met een carcinoma in situ (beginnende kanker) was dit slechts bij 1 op 4 (25%) van de scans het geval.
Concluderend was 7 Tesla niet 'feasible'/klinisch haalbaar. 3 Tesla MRI kan wel 'feasible' zijn bij selectie van de juiste patiëntengroep, namelijk exclusie van patiënten met claustrofobie en inclusie van patiënten met een bewezen invasief plaveiselcelcarcinoom (en niet met een carcinoma in situ).
Verdere verbetering van de beeldkwaliteit van MRI is nog te verwachten.

In **hoofdstuk 7** richten we ons op een andere modaliteit van de medische beeldvorming, namelijk de 2-[18F]-fluoro-2-deoxy-D-glucose (FDG)-positrion emissie tomography(PET)/ computed tomography (CT). FDG-PET/CT heeft verschillende toepassingen binnen de hoofd hals kanker. FDG-PET/CT is vooralsnog geen routine onderzoek bij de diagnostiek van een primair hoofd hals carcinoom, hoewel het wel wordt gebruikt bij patiënten met oa een verhoogd risico op afstandsmetastasen (in oa longen of botten). Bij patiënten die primair bestraald worden en die geen indicatie hebben voor een halsklierdissectie (het verwijderen van de lymfeklieren in de hals) kan de uitslag van een FDG-PET/CT niet worden bevestigd dmv histopathologisch onderzoek. Bij deze patiënten kan een lymfeklier op FDG-PET verdacht zijn voor een metastase, terwijl dit op de CT niet het geval is, of andersom. In deze gevallen moet er een compromis gesloten worden tussen het risico op overbehandeling (hogere dosis radiotherapie) en het risico op onderbehandeling met daarbij een grotere kans op regionaal recidief

(in de halsklieren zelf) of op afstand met als gevolg een evident slechtere prognose. Het gebruik van Intensiteits Gemoduleerde Radiotherapie (IMRT), een bestralingstechniek met het voordeel dat omliggende weefsels beter gespaard kunnen worden, kan wel leiden tot recidieven aan de rand van het bestralingsveld indien de aangedane klieren niet de juiste dosis ontvangen. We hebben een retrospectieve studie gedaan met inclusie van 283 patiënten met hoofd hals kanker die primair bestraald zijn tussen 2002 en 2010. Hierbij onderzochten we wat de invloed was van FDG-PET/CT versus CT alleen op de bestralingsdosis van de halsklieren en evalueerden de klinische lange termijn resultaten. Ook werden de lokaties van regionale recidieven (nieuwe uitzaaiingen in de halsklieren) vergeleken met de bestralingsdosis op het desbetreffende gebied. Bij 92 patiënten was er sprake van discordantie tussen de resultaten van de FDG-PET en de CT. Bij 33% veranderde de stadiering van de halsklieren ten gevolge van FDG-PET. Bij 24% leidde de resultaten van FDG-PET ook tot een verandering van de bestralingsdosis, waarbij 18% een hogere bestralingsdosis kreeg en 6% een lagere bestralingsdosis kreeg. In 8 van deze 92 patiënten trad een regionaal recidief op in de halsklieren. Slechts twee patiënten had een recidief in een 'discordante klier' (waarbij FDG-PET uitslag en CT uitslag niet gelijk waren). Beide patiënten hadden een hoge bestralingsdosis op deze klieren gekregen. De goede klinische lange termijn resultaten van het beleid, gebaseerd op informatie van zowel FDG-PET als CT, ondersteunen de toegevoegde waarde van FDG-PET/CT vergeleken met CT alleen voor het bepalen van de bestralingsdosis op de halsklieren.

CHAPTER 10

General discussion

Medical imaging is an important tool in daily otolaryngology practice. We encounter numerous clinical problems each day. First, accurate diagnosis and evaluation of the disease, is crucial for choosing a treatment strategy, together with the patient. A therapy, with the best curable intent, taking into account both physical comorbidities, morbidity of the treatment, expected treatment outcomes and patients preference.
For accurate diagnosis, both physical examination and diagnostic imaging can complement each other. In follow-up after treatment, imaging is also used to evaluated the treatment and screening for recurrent disease.
This thesis focuses on diagnostic imaging, MRI, CT and PET-CT. We evaluate its accuracy for three anatomical regions; The first half of this thesis focuses on anatomy and benign disease of the middle - and inner ear. The second half on malignant disease of the larynx (small laryngeal carcinomas) and the neck (for primary staging of neck metastases in head and neck cancer). Table 1 shows an overview of the diagnostic studies and the anatomical regions.

Table 1: Overview of performed studies and its anatomical region

	Inner ear	Middle ear cholesteatoma	Early glottic carcinoma	Neck metastases
CT				
3T MRI				
7T MRI				
DW MRI				
PET-CT				

Chapter 2
Chapter 3 and 4
Chapter 5 and 6
Chapter 7

BENIGN DISEASE; MIDDLE EAR AND MASTOID CHOLESTEATOMA

Our **clinical question** was to evaluate the diagnostic accuracy of DW for the detection of primary and/or residual or recurrent cholesteatoma. In the latter, DW MRI may avoid the need for second look surgery and advocate a one stage surgery including hearing restoration with or without mastoid obliteration.

Review of literature

EPI versus non-EPI sequences

In 2006, DW MRI was first described as a diagnostic tool for the depiction of middle ear cholesteatoma [1,2]. Since then, numerous studies have assessed the diagnostic performance of DW MRI. Earlier DW MRI consisted of echo planar imaging (EPI), including single shot or multi shot sequences. In this sequence, k-space (a graphic matrix of digitized MR imaging data) is traversed in one or a small number of RF excitations. EPI is the fastest acquisition method in MRI (100 ms/slice) but is prone to susceptibilty artefacts. Newer non-echo planar imaging (non-EPI) sequences use either multishot fast-spin echo or single shot turbo spin echo sequences. Although acquisition time of non-EPI sequences are longer than EPI sequences, they are less susceptible to magnetic interface artefacts compared to EPI sequences, especially at the air-bone interface in the temporal bone. Also, non-EPI sequences allow thinner sections, higher imaging matrices and greater spatial resolution. Two systematic reviews compared EPI and non-EPI sequences [3,4]. Ranges of sensitivity, specificity, positive and negative predictive values of EPI sequences were 12.5-100%, 60-100%, 80-100% and 47-100%, as evaluated by two systematic reviews. Sensitivity, specificity, positive and negative predictive values non-EPI sequences were 62-100%, 86-100%, 89-100% and 50-100%. Studies included MRI DWI for residual and recurrent cholesteatoma only.

Non-EPI DWI for primary cases

When discussing the value of DW MRI for the detection of middle ear cholesteatoma, a distinction has to be made between primary and post-operative cases, and both adult and pediatric disease. In primary cholesteatoma, the diagnosis is usually made clinically by otoscopy. In these cases, CT can usually adequately depict opacification of the middle ear in combination with associated bony and ossicular chain erosion. And provide the necessary information for surgical planning.

However, DW MRI does have good diagnostic performance in primary cases. A correlation of CT and EPI DWI with surgical outcome as a reference showed an accuracy of high resolution CT and EPI DWMRI of 67.8% and 88.1%, respectively [5]. For non-EPI

DWI, we found a sensitivity, specificity, positive and negative predictive value ranges of 83%-100%, 50%-100%, 85%-100%,and 50%-100%, respectively [6]. This is in concordance with a recent meta-analysis reporting a sensitivity of 92% (CI 86-95%) and a specificity of 97% (CI 22-100%) for primary cases [7]. In most cases, CT alone can provide sufficient information. However, DW MRI can be complementary to CT in selected primary cases, especially for the diagnosis of cholesteatoma in high-risk tympanic retraction pockets, in cases of hampered otoscopy as a result of stenosis or occluded ear canal or due to an abnormal opaque tympanic membrane, or in case of monitoring cholesteatoma in patients that are not candidates for surgery due to various reasons.

Non-EPI DWI for postoperative cases

Middle ear cholesteatoma surgery can be broadly classified as canal-wall-up (CWU) or canal-wall-down (CWD) surgery, depending on whether the posterior canal wall is preserved. After a CWD procedure, an open mastoid cavity remains which requires regular follow up visits for removal of wax accumulation. The cavity is usually easy to inspect and recurrent cholesteatoma can be detected and removed on clinical otoscopy. Adversely, after CWU surgery, the canal wall remains intact, preserving the anatomy, eg improving the fitting of hearing aids when required, but blocking the view of the middle ear and mastoid cavity. CWU cases are therefore associated with a higher risk of residual (up to 36%) and recurrent (up to 18%) disease than CWD cases [8]. Up to now, a total of 5 systematic reviews/meta-analysis have been published, including our own, evaluating the diagnostic performance of DW MRI for postoperative cases [3,4,67,9]. One of these studies included both primary and postoperative cases but did not perform a subgroup analysis [9]. Diagnostic performance of the remaining 4 systematic reviews is shown in table 2. Sensitivity of our systematic review is somewhat lower compared to other reviews. This can be due to the relatively low patient number. We could only plot two studies, since other studies analyzed both primary and post-operative cases and no subgroup analysis for post-operative cases only was possible. Jindal et al had larger patient numbers, but included studies in which not all patients underwent surgical intervention (to conform presence or absence of cholesteatoma) following DW MRI. Our systematic review selected studies including patients after CWU surgery only. All other reviews included studies with patients after both CWU and CWD procedures and subgroup analysis of CWU procedures was not done.

DW MRI in the pediatric population (excluded in our systematic analysis)

Cholesteatoma can occur in both adults and children. Cholesteatoma in children is more aggressive than adult disease with a higher rate of recurrent and residual disease following primary surgery [10]. Furthermore, some children need sedation to prevent

Table 2: Meta-analysis and systematic reviews on the diagnostic performance of non-epi diffusion weighted MRI in the detection of post-operative (residual and recurrent) cholesteatoma.

	Patients scanned (surgery)	Prior surgical procedure	Sensitivity (SD)/[CI]	Specificity (SD)	PPV (SD)	NPV (SD)
Jindal 2011	207 (185)	CWU and CWD	91%	96%	97%	85%
Van Egmond 2016	57 (57)	CWU	Range 80-82%	Range 90-100%	Range 96-100%	Range 64-85%
Muzaffar 2016	444 (444)	CWU and CWD	90% (12)	95%(6)	97% (4)	80% (20)
Lingam 2017	? (14 studies)	CWU and CWD	93% [84-97]	91% [85-94]		

degradation and misregistration of the acquired images. These factors may warrant a second look surgery , rather that follow up with DW MRI. Diagnostic performance of DW MRI both in adults and in children, however, does not differ. A large observation study showed that DW MRI is equally effective in children as in adults for postoperative disease [11]. Sensitivity, specificity, positive and negative predictive values were 97%, 95%, 97% and 95%, respectively. This study does have its limitations; only 54 out of 90 DW MRI examinations were followed by surgery. And patients under the age of 6 years were not included. A pediatric subgroup analysis of 4 studies, included in the meta-analysis of Lingam et al. showed a sensitivity of 86% (CI 60-96%) and a specificity of 94% (CI 82-98%) [7]. Sensitivity was somewhat lower and the confidence interval was wider compared to the adult population. This could be due to the smaller patient numbers in the pediatric group. When second look surgery is to be replaced by DW MRI, the more aggressive nature of cholesteatoma has to be taken into account. A more frequent follow up schedule with DW MRI can therefore be justified. And in very young children who will need sedation, a second look surgery may be a better option.

Study limitations

Studies investigating the diagnostic performance of DW MRI may have several limitations. A selection bias is often present, including patients with clinically a high suspicion of primary cholesteatoma or recurrent disease. Also, surgical verification of DW MRI data is more often done in case of a positive DW MRI (suspect for cholesteatoma). Second, a publication bias can hamper results of a systematic review, as smaller studies reporting lower sensitivity or specificity may be less likely to be submitted or accepted for publication, and the meta-analysis may have overestimated the sensitivity and specificity. Third, in post-operative cases, some studies do not

describe whether the cholesteatoma encountered was residual or recurrent. Residual lesions encountered during a staged second-look procedure are often much smaller compared to recurrent lesions. Studies have a various time interval between the first surgery and scan or between preoperative scan and (primary or follow up) procedure. In the first case, when scanned too early after surgery, a residual lesion may be too small to identify on DW MRI. In the latter case, a small cholesteatoma, too small to be detected on DW MRI might have grown in the time to surgery. Fourth, there is variation in scanning parameters, protocols and slice thickness. When comparing systematic reviews, inclusion criteria and critical appraisal for relevance and validity of studies can lead to inclusion of different studies, leading to different results.

Pittfalls and drawbacks of DW MRI

The main limitation of DW MRI is the decreased sensitivity for cholesteatoma which are smaller than 2-3 mm in size. Other causes of false negative DW MRI studies include larger cholesteatoma, which lack the necessary keratin to return the high DWI signal. Also, auto-atticotomy, in which the central keratin has discharged leaving only an epithelial empty sac or matrix can be false negative. Patient motion artefacts and the microsuction of cholesteatoma during surgery can also result in false-negative findings. False positive results are due to ear wax, non-specific inflammation, operative materials such as silastic sheet, calcified cartilage, dental brace artefacts, cholesterol granuloma and squamous cell carcinoma.

DW MRI had other drawbacks. In cases without macroscopic residue and without signs of residual or recurrent disease (both clinical and on DWI MRI), repeat follow up does show cholesteatoma in 31% of the patients [12]. Repeated follow-up DWI, performed 1 year and 4 years after surgery is therefore recommended to detect residual or recurrent disease before patients present with extensive disease which caused (further) damage to the middle ear. In this follow up period, patients can be lost to follow up, due to patient non-compliance or a lack of awareness of the limitations of DW MRI by both clinician and patient.

MRI sequences

Several different non-echo planar imaging (non-EPI) techniques have been developed by different vendors of MRI. These non-EPI techniques cover the Single Shot Turbo Spin Echo sequences (SS TSE), including Half-fourier Acquisition Single-shot Turbo spin Echo (HASTE) DWI and the Multi Shot Turbo Spin Echo sequences (MS TSE), including Periodically Rotated Overlapping ParallEL Lines with Enhanced Reconstruction (PROPELLER) DWI. The rationale behind the HASTE sequence, a single-shot technique, is that data from all of k-space is obtained at a single 90°- excitation pulse, which

reduces the echo train length. Furthermore, the Half Fourier method used in HASTE sequences takes advantage of certain 'mirror-image' properties of k-space and the MR signal, allowing only a little more than half of the k-space being directly collected. Both properties of the HASTE sequence reduce the time of image acquisition. The PROPELLER technique is a radial sampling method using rotating blades composed of multiple phase-encoded lines. One of the advantages is that the center of k-space (which contains the highest signal amplitude and contributes most to image contrast) is oversampled, meaning that the signal-to-noise ratio and the contrast-to-noise ratio will be high. A second advantage is that the data of each blade can be compared to the data from previous blades for consistency. If patients move, data can be corrected or discarded, resulting in less motion artifacts.

The temporal bone consists of air, bone and soft tissue which lie in close proximity to each other. This induces the risk for susceptibility artefacts. Susceptibility is the ability of substances to be magnetized. The different bonding properties of hydrogen protons in different tissues will cause local magnetic field inhomogeneity at the tissue boundaries. The resonance frequency at the boundaries has therefore changed and the protons involved will not be displayed. Turbo Spin Echo (TSE) sequences are less sensitive for susceptibility differences and are therefore especially useful in the skull base and temporal bone. Due to the oversampling of k-space, susceptibility artifacts are also slightly reduced in the non-EPI PROPELLER sequence. There is no additional improvement of the detection of small cholesteatomas (< 2-3 mm) when scanning is performed at 3T MRI (compared to 1.5T).

The main diagnostic criterion for the presence of cholesteatoma on DW MRI is a lesion hyperintensity on high b value images. Usually, this is assessed qualitatively. To optimize the diagnostic performance of DW MRI for cholesteatoma, specific cutoff values can be determined for signal intensity (SI) and signal intensity ratios (SIR). In a retrospective study with two blinded observers, a SI of 92.5 and a SIR of 0.9 resulted in a sensitivity and specificity of 100%. This study was done using a Turbo Spin Echo sequence at 3 Tesla MRI [13].

Future perspectives

DW MRI can be complementary to CT in operative planning and patient counselling. DW MRI appears to be more sensitive and specific for the detection of cholesteatoma. However, anatomic information is lacking. High resolution CT does have excellent spatial resolution and depiction of anatomical landmarks. Recently, two studies have been done with fusion of both CT and DW MRI in a small number (12 and 33) of patients [14,15]. In the first study, use of CT-MRI fusion had greater diagnostic sensitivity (0.88 vs 0.75), positive predictive value (0.88 vs 0.86), and negative predictive value (0.75 vs

0.60) than PROPELLER DW MRI alone. Image fusion also showed increased overall localization accuracy when stratified across 6 distinct anatomical regions of the temporal bone (localization sensitivity and specificity, 0.76 and 0.98 for CT-MRI fusion vs. 0.58 and 0.98 for PROPELLER DW MRI) [14]. In the second study, intraoperative findings coincided with fusion CT-MRI imaging in 31 out of 33 patients [15].

Factors influencing the surgical plan in cholesteatoma surgery

The ideal surgical treatment of cholesteatoma has been subject to discussion for years. The goal of cholesteatoma surgery is to create a safe ear by complete removal of the disease, with the lowest possible rates of residual or recurrent disease. Other goals are to create a hygienic status without the need for regular cleaning, and to maintain or restore hearing (including both ossicular chain reconstruction and the use of good fitting hearing aids).

The question remains whether the level of diagnostic accuracy of non-EPI DWI as evaluated in our review and in other literature, is sufficient to change the decision-making of clinicians, which may be influenced by other issues.

One factor is the location of the cholesteatoma in the middle ear/mastoid cavity. Independent prognostic factors associated with a statistically significant increased risk of recurrent or residual disease include location in the sinus tympani and the mastoid (hazard ratio = 1.7), and both stapes- and incus erosion (hazard ratio = 1.9) [16,17]. Furthermore, erosion of the posterior external auditory canal wall and incomplete removal of mastoid apex cells are well correlated with recurrence after CWU surgery (p=0.009) [18]. In CWD surgery, high risk factors include residual mastoid apex cells, posterior external auditory canal wall erosion and presence of residual facial ridge cells (p=0.0036) [18]. In case of a high risk of recurrence, location of the cholesteatoma can be expected to influence the decision for a second look or follow up by DW MRI. When the cholesteatoma is localized in an anatomical subsite which can have a large impact on clinical outcome if left untreated, like the stapes footplate, DW MRI will probably not avoid the need for a second look procedure. Another factor is the age of the patient. The age of 15 years or younger is stated to be an independent prognostic factor for recidivism (hazard ratio = 2.2) [17]. Other factors include general health status of the patient (including the ability for general anesthesia, regular out-patient visits etc) and his or her preferences. And last but not least the preference and experience of the surgeon.

As mentioned earlier, a recent shift is seen towards mastoid obliteration. A recent systematic review showed that the rate of recurrent and residual disease after the use of single-stage mastoid obliteration with either CWU or CWD tympanoplasty was qualitatively similar, if not better than previously reported rates for non-obliterative techniques [19].

Conclusions

All in all, DW MRI has a place in daily practice for selected primary cases, clinically suspect for cholesteatoma. It has a good diagnostic performance in the follow up of postoperative cases. However, sensitivity of cholesteatomas smaller than 3 mm in diameter is much lower. One-third of patients with a negative (postoperative) DW MRI and absence of clinical symptoms can still have residual or recurrent disease. Therefore, repeated follow up scans are recommended when a second look operation is to be replaced by DW MRI. The clinical decision to choose a single stage procedure with direct restoration of hearing (in case of ossicular chain discontinuity) and regular DW MRI follow up, or the decision to perform a second look surgery will depend on multiple factors.

Non-EPI DWI MRI has its greatest potential clinical impact and cost savings, in terms of reducing unnecessary surgery when negative, and when there is no other clinical indication for revision ear surgery, like ossicular chain reconstruction or myringoplasty.

INNER EAR ANATOMY AND CLINICAL APPLICATIONS

Our **clinical question** was if 7 Tesla MRI can result in a better depiction of the membranous structures of the inner ear, than 3 Tesla MRI, both ex vivo and in vivo.

Study results and review of literature

As mentioned in the introduction, the inner ear, including the cochlea and labyrinth, is a complex structure. Improved visualization with detection of endolymphatic vesicles of the inner ear might permit new insights in the diagnosis and treatment of labyrinthine disease and can be useful for clinical application in cochlear implantation. In daily practice, 1.5 Tesla and 3 Tesla MRI scans are used. These can grossly depict the osseous labyrinth (including semicircular canals and vestibule), the fluid in the cochlea (including cochlear modiolus and interscalar septum), and the four nerve bundles in the internal auditory canal. Although the basilar membrane is clearly visible, separating the scala tympani and the scala vestibuli, Reissner's membrane and scala media cannot be depicted on 3 Tesla MRI [20]. Our aims were to scan with ultrahigh resolution (7 Tesla), independent of scan duration. Second, to reduce scan duration. And finally, to develop a scanning protocol suitable for clinical practice. Clinical (in vivo) images at 7 Tesla were compared to those on 3 Tesla.

In our study, including ex vivo and in vivo imaging, all structures visible on 3T could be visualized on 7T. However, no additional membranous structures could be depicted on 7T. There are two other published studies evaluating 7 Tesla MRI in vivo. One study

included 13 patients with sensoneurinal hearing loss eligible for cochlear implantation. Significant differences in favor of the 7 Tesla images were found for the scala tympani and scala vestibuli in the second a third turns of the cochlea [21]. The scala media was identified in 7 of 52 and 21 of 52 ratings on 7T images, in the first and second cochlear turn, respectively. However, in 22 out of 28 ratings, visibility was scored as 'poor', in 4 out of 28 cases as 'adequate' and in only 2 out of 28 cases as 'very good'. In another study, 18 patients with idiopathic sensorineural hearing loss and 32 normal-hearing patients were scanned on 7 Tesla to compare the detection rates of the labyrinthine artery. In all patients and in all but one healthy volunteer, the labyrinthine artery could be depicted [22].

Technical challenges of MRI of the inner ear

The anatomy of the inner ear and its surroundings makes visualization on 3 Tesla MRI, but especially on 7 Tesla, particularly challenging. The to a number of MR properties, increasing with field strength, settings applied in 1.5T and 3T have to be strongly adjusted at 7T to optimize image quality.

The first difficulty is the size of the inner ear. The membranous labyrinth is only 12 mm high and can only be examined in detail when submillimetric images are used. A higher spatial resolution can be accomplished by a smaller voxel size, leading to a diminished signal to noise ratio (SNR). To compensate for this issue, the number of signal averages (NSA) can be increased, resulting in a longer acquisition time. At 7T, this can be a problem due to maximum specific absorption rate (SAR). The SAR, for which regulatory safety limits are defined, scales quadratically with field strengths. Because of radiofrequency (RF) standing wave properties in human tissue, the maximum applicable SAR value will depend heavily on the geometry of the part of the body that is exposed to the RF energy and on the exact location and geometry of the RF source. In our study, the initial voxel size of 0.15 mm in maximal resolution ex vivo diminished to an isotropic voxel size of 0.5 mm in vivo at 7T. Non-isotropic voxel size was 0.5 x 0.6 mm at 3T MRI. Kraff et al. has described depiction of the facial nerve close to the brain stem with 0.6 mm isotropic voxel size [23]. Vd Jagt et al used an isotropic voxel size of 0.6 mm on 3T and an isotropic voxel size of 0.3 mm at 7T [21]. In our study, the acquisition time in vivo varied between approximately 7 and 14 minutes, not including 2 to 3 minutes for proper adjustment of frequency, transmitter voltage as well as 3D shim, which had to be performed manually before each examination. Quality of images with different acquisition times was similar. Acquisition time of vd Jagt was similar with approximately 10 minutes. Another small difference in scan sequence found in the study of vd Jagt was a refocusing angle of 130°, instead of the regular 180°. A smaller angle theoretically results in a smaller SAR which can be beneficial at 7T.

The second difficulty is the variety of tissues within this small space. The inner ear fluids with its surrounding bone, in close proximity to the bony skull base and air-filled areas, can result in inhomogeneities in the static B_0 field. Furthermore, the radiofrequency field (B_1) is influenced by the elliptic shape of the head [24]. Both susceptibility (B_0) and B1+ variations will scale linear with the main magnetic field. Where the signal to noise (SNR) increase is a clear advantage, the sensitivity to field-induced artifacts makes visualization and localization challenging at 7T.
A third difficulty at 7T is the lateralized location (off the midline) of the inner ears. At 7T, wavelength shortens, decreasing from 52 cm at 1.5T to 12 cm at 7T, which is smaller than the diameter of the human head. This causes interference in RF, an intrinsic problem at 7T. Without adjustments, signal intensity concentrates in the center of the head, resulting in diminished visualization of the more laterally situated inner ears. The study by Brink et al used geometrically tailored dielectric pads to locally tailor the B1 distribution [25]. These improved contrast homogeneity and transmit efficiency in the region of the inner ear without increasing the specific absorption rate. With the use of a unilateral dielectric pad, we optimized the signal intensity laterally, with optimization of image quality of the unilateral inner ear. As a consequence, to scan both inner ears with optimal signal intensity, scan duration doubled, with a total scan time of 15 minutes. In the study of Brink et al, asymmetrically sized pads were required to compensate for the intrinsic asymmetry at B1, which is known to increase with field strength [25]. With the use of a unilateral dielectric pad, we did not have to correct for this problem. We used a 32-channel receive coil. Brink et al. described an improvement in contrast homogeneity at 7T, especially at the IAC, when using a 32-channel receive array instead of a single surface coil.

Future clinical perspectives of MRI for the inner ear

The scala vestibuli and scala tympani can be visualized on 3T and 7T in vivo. The scala media could be depicted in some cases on 7T in vivo. Further improvement of inner ear imaging at 7T could be achieved by developing dedicated surface coils for the inner ear region, reducing the distance between the coil and the inner ear, and gaining maximum SNR in the cochlea with reduction of overall SAR to the patient. In contrast to other subsites of the head and neck, the inner ear is not prone for motion artefacts (in contrast to the larynx for example).
An ex vivo study on ultra-high field strength (11.7 Tesla) was able to clearly visualize Reissner's membrane, the scala media, and the basilar membrane in the cochlea. In the vestibular labyrinth, the wedge-shaped crista ampullaris and the maculae of both the saccule and utricle were visible. Details of the endolymphatic sac and duct were also demonstrated [26]. In clinical practice (in vivo), question remains, whether scanning

with ultra-high field MRI can be feasible. Difficulties encountered with scanning on 7T will increase even further, including further increase of SAR.

In cochlear implantation, pre-operative planning is very important. Adequate visualization of the cochlear morphology directly influences choice of electrode carrier, location of cochleostomy and insertion depth, to achieve optimal electrode position and hearing outcome. Especially in cochlear implantation with hearing preservation, the outcome clearly depends on the length of the electrode as well as the size of the individual cochlea. Imaging can also be useful for postoperative verification of electrode position.
Since CT and MRI provide complementary information about temporal bone structures and pathology, image registration and fusion gains significant improvement over conventional images in depicting the relationship between bone and soft tissue. In 2005, accurate, reproducible registration and fusion method was described, accomplished in 13 minutes [27] . This, in combination with high field MR imaging, may result in new opportunities to for normative measurements, evaluate pathologic alterations and provide detailed pre-operative planning [28].
In the future, minimally-invasive procedures will gain in importance [29,30]. In 2009 robot guidance cochlear implant surgery was described in 10 cadaveric temporal bones [30]. In 2014 eight out of nine patients were successfully implanted minimally invasive image guided approach, which involved drilling a narrow, linear tunnel to the cochlea pre- and intraoperative CT planning [29]. Advantages might be a shorter duration of surgery, reduced insertion trauma as well as an exact intracochlear positioning of the electrode taking into account the individual anatomy For these purposes, adequate visualization of the anatomy is of paramount importance.
Over the last 15 years, MRI has also been evolving for the detection of labyrinthine disease. As mentioned in the introduction, endolymphatic hydrops (EH) may be present in Meniere's disease. It may also result from a number of processes such as viral infection, trauma, auto-immune disorders and electrolyte imbalance. Different MRI sequences have been developed for the detection of EH. Now, there are increasing data to validate the application of 3T MRI performed at 4 hours post-intravenous gadolinium with 3D-FLAIR sequences for the diagnosis of EH, associated with Meniere's disease. With further technological developments and validation of MRI techniques, it may be a helpful diagnostic tool to evaluate therapeutic success of MD and influence therapeutic decisions [31].

Conclusions

For now, the use of 7T MRI for the depiction of the inner ear is not superior to scanning with 3T. Scanning on 7T is technical challenging, and at this moment, not feasible for routine clinical practice.

Further improvement could be achieved by developing dedicated surface coils for the inner ear region. However, increase of SAR and prolonged scanning times can still be limiting factors, when scanning on higher field strengths.

EARLY GLOTTIC CARCINOMA

Our **first clinical goal** was to review the diagnostic value of (the currently used) 1.5 and 3 Tesla MRI in pre-therapeutic staging of primary early stage (T1 and T2) glottic carcinoma. **Second clinical goal** was to assess the feasibility of the clinical use of a dedicated 3 Tesla MRI protocol for small laryngeal lesions and a 7 Tesla MRI protocol, including structural assessment of technical image quality and visibility of the tumor.

Clinical outline and review of the literature

Few studies have addressed the diagnostic performance of MRI for early glottic carcinoma, as concluded in our review. Patient numbers are low and in most studies subgroup analysis might have influenced the results. We therefore developed a new MRI protocol for 3T MRI with a smaller slice thickness of 0.5 to 1 mm and a 7T MRI protocol with a slice thickness of 0.4 to 0.7 mm. 7 Tesla MRI was considered not feasible. 3 Tesla MRI, with clinical exclusion of patients with a history of claustrophobia, and with histologically proven invasive squamous cell carcinoma, can be feasible. Especially with further improvement of MR image quality. Carcinoma in situ lesions are characterized by the absence of invasive growth. This characteristic in combination with small tumor volume makes visualization difficult on MRI. Moreover, in the absence of invasive growth, MRI can be considered of no use, since submucosal spread and extension to other laryngeal subsites is not expected.

Technical challenges of MRI of the larynx

Standard larynx protocols apply a slice thickness of 3-4 mm. For small laryngeal lesions, with a possible craniocaudal diameter of 1-2 mm, this could give rise to large partial volume effects. However, a smaller slice thickness results in a diminished Signal to Noise Ratio (SNR).

To optimize the signal in the area of interest, we used neck receive coils close to the larynx. MRI protocols for laryngeal carcinoma are usually performed with the use of a commercial local surface coil. In our 3 Tesla protocol we also used a standard surface receive coil, consisting of two loops, centrally positioned on the larynx. Correct positioning of the coil is essential for scan quality. The variation in anatomy, eg thickness of the neck region, can make correct positioning difficult. Furthermore, the separate

loops are prone for displacement during scanning, which increases the patients handling time. Is the loops are too far apart, or when the patient has a large neck, this can cause signal voids within the larynx. If the loops are placed too close to each other, they can couple to one another, resulting in diminished signal-to-noise and in a field-of-view (FOV) , reduced penetration depth and poor parallel imaging performance (including fold back artifacts) [32]. A study group in Leiden recently developed a flexible dedicated radiofrequency coil receive array for 3 Tesla MRI, especially for the larynx which can fit different-sized necks, containing four identical loops. The use of multiple loops in a receive coil enables the use of SENSE (SENSitivity Encoding), resulting in significant reduction of scan duration. Also, its high sensitivity on the surface might be an advantage in the depiction of the anteriorly located larynx, especially in the absence of abundant subcutaneous fat. Drawback of multiple small elements can be an inhomogeneous field distribution. Besides a receive coil for signal reception, a transmit coil is necessary to efficiently distribute the radiofrequency field (B1) to the area of into the area of interest. The transmit coil in a 3 Tesla MRI is uniformly located in the MRI scanner itself.

At 7 Tesla, the Signal to Noise Ratio (SNR) increases linearly with field strength. However, the image homogeneity is generally less due to the smaller RF wavelength causing RF interferences. At 7 Tesla MRI, the transmit coil is not located in the MRI scanner and has to be individually applied, depending on the area of interest. A transmit coil is important to efficiently distribute B1 (radiofrequency field) into the neck. We used a dedicated neck transmit coil with 2 antenna's to homogenize the transmit field based on the principle of a dielectric wave guide [33]. For signal reception, two 15-element receiver arrays were used, one for each side of the neck, to maximize the signal intensity obtained from the glottic area [34]. The receive coils were placed on the mask, covering the region of the larynx. The penetration depth of each receive array in general is about 50-75% of the diameter of the loops. The use of 30 receive arrays in our study, each with a small diameter, resulted in a high sensitivity on the surface, which especially accentuated the subcutaneous fat. The Leiden study group included one T1-weighted Turbo Spin Echo sequence with SPIR (Spectral Presaturation with Inversion Recovery) fat suppression [31]. Disadvantage of an Inversion Recovery (IR) sequence is the higher SAR due to additional 180° pulses. At 7 Tesla, therefore, IR sequences can be problematic.
Another difficulty in scanning the larynx is patient related movement due to breathing, swallowing and pulsation in the blood vessels. Breathing causes movement of the vocal cords, swallowing causes movement of the whole larynx in craniocaudal direction up to several centimeters. These motion artefacts can severely degrade image quality on

3 Tesla, but were even more pronounced on 7 Tesla, due to the high sensitivity of the small surface coils in the 7 Tesla setup close to the surface. To minimize motion artefacts, all patients in our study were scanned in a 4-point immobilisation mask. Although this minimizes external movements of the head and neck, internal motion as a result of breathing and swallowing cannot be prevented. The same study group in Leiden implemented respiratory-triggered scans, on 3 Tesla MRI, to prevent motion artefacts. Images were only obtained during exhaling, ensuring a stable position of the larynx [31]. A belt on the abdomen censored the initial stage of exhalation, initiating data acquisition. Since swallowing usually occurs after exhaling, respiratory triggering simultaneously prevented these motions artefacts to occur.

Future perspectives

With technological advances in MRI scanning, especially prevention of motion artefacts, 3 Tesla MRI can be a complementary diagnostic tool for assessment of small laryngeal carcinomas. Diagnostic performance favorably has to be verified with histopathology following laser resection.

It is difficult to conceive whether 7 Tesla might be promising with the use of respiratory triggering. The influence of internal motion of the larynx due to breathing and swallowing is even more pronounced at 7T. Respiratory triggering could preempt that. Also, receive coils play an important role. In the optimal situation, the number of elements is high enough to optimize SNR and its diameter is small enough for optimize the signal in the region of the larynx without emphasizing the subcutaneous fat. As SAR becomes one of the limiting factors with increasing field strength, Inversion Recovery sequences , like fat suppression, can be problematic at 7 Tesla MRI.

Conclusions

7 Tesla MRI is not feasible for small laryngeal carcinoma at this point. 3 Tesla MRI is not yet superior to CT. However, adjusted scanning protocols at 3 Tesla MRI (with smaller slice thickness), together with respiratory triggering (to prevent motion artefacts) and the use of dedicated receive coils are promising. And in time, can be feasible in daily practice for accurate depiction of tumor extension, especially of depth invasion.

PET-CT AND PRIMARY STAGING OF HEAD AND NECK CANCER; NECK METASTASES

In patients with primary head and neck cancer, routine CT and in selected cases FDG-PET/CT is performed. In the clinical setting, the relevant **clinical question** remains which treatment is justified in case of discordance between FDG-PET and CT results. Should lymph nodes clinically suspect for metastasis on either FDG-PET or CT be treated with high dose radiation (boost). A compromise has to be made between the risk of false positive FDG-PET and the risk of delaying appropriate salvage intervention. Second, smaller radiation fields using IMRT, allow tissue sparing, but could also lead to more marginal failures.

Study results and review of literature

Three meta-analyses, published in 2008, 2013 and 2015, have evaluated FDG-PET (Kyzas 2008), or FDG PET-CT (Yonkui 2013 and Sun 2015) for the detection of regional node metastasis in patients with primary head and neck cancer [35-37]. Histopathological correlation was an inclusion criterion in all studies. 32, 14 and 24 articles were included respectively, covering a total of 52 unique articles. All articles included in the meta-analysis of Yonkui in 2008, were also included in the meta-analysis done by Sun in 2015.

Kyzas concluded a FDG-PET sensitivity of 79% (CI 72-85%) and specificity of 86% (CI 83-89%) for the whole patient group [35]. When compared to conventional CT, FDG-PET had a higher sensitivity and specificity of 82% vs 74% and of 86% vs 76% respectively. Combined PET-CT is almost certainly more accurate than FDG-PET alone. Sun showed pooled per-patient, per-neck-side and per-neck-level sensitivities/specificities for FDG-PET/CT of 91/87%, 84/83%, and 80/96%, respectively. When PET-CT was compared to conventional imaging in a sub analysis across 13 studies, per-neck-level sensitivity and specificity were 84% vs 63% and 96% vs 96%, respectively [37]. Conventional imaging consisted of CT, MRI and CT/MRI. No subgroup analysis was done for CT only.

FDG-PET-CT findings must be interpreted with caution. Reactive lymph nodes can have variable FDG avidity. And FDG PET-CT may fail to detect cystic necrotic lymph nodes, that can be more easily seen on CT or MRI.

However, with a high diagnostic accuracy and an improvement for per-neck-level sensitivity of 20% compared to conventional imaging, PET-CT thus might be beneficial for the initial staging of nodal disease. However, its role in routine clinical work-up is not yet established. In case of primary radiation, histopathological verification cannot be obtained. But correct judgement of nodal metastases remains of vital importance for nodal target volume definition. False-positive nodes lead to overtreatment, while false-negative nodes lead to regional recurrence or distant failure.

In our retrospective study, the introduction of FDG-PET, as an addition to conventional CT, led to an alteration in nodal treatment radiation in 24% of the cases, including a nodal upstage of 18% and a nodal downstage of 6%. This is in concordance with literature, reporting a PET/CT-based change in patient management in 6–31%.
Diagnostic performance of PET-CT in patients with a clinically negative neck (unremarkable clinical examination and cross-sectional imaging) remains questionable. In a subanalysis, done by Kyzas in 2008, for cN0 patients (with clinically negative cervical lymph nodes), sensitivity of FDG-PET alone was only 50% (CI 37-63%) and specificity was 87% (CI 76-93%) [35]. This was later confirmed in several studies, showing that FDG PET-CT in cN0 patients has a lower positive predicting value (PPV) of 58% and sensitivity of 50–71% [35,38-40], compared to a PPV of 80% and sensitivity 87% in N+ patients [35,38]. The failure of PET-CT in these studies was due primarily to undiagnosed small volume disease; in particular, nodes less than 5 mm in size. These nodes, would however, also be missed on conventional imaging. Reliable imaging for clinically negative necks is therefore still absent.

When discussing the complementary value of FDG PET-CT compared to CT alone, for initial staging of head and neck disease, additional advantages of FDG PET-CT must also be taken into account. In about 25% of patients with proven metastatic neck disease and Cancer of Unknown Primary origin (CUP), following routine clinical work-up, PET-CT can identify the primary tumor location [41]. In Intensity Modulated Radiotherapy (IMRT) planning, PET-CT decreases the inter- and intra-observer variability and increases the conformity to real tumor boundaries. It is able to achieve a more precise definition of Gross Tumor Boundaries [42]. FDG-PET/CT is also reported to have a beneficial effect for RT target definition in IMRT planning for primary disease, with a change in gross target volumes (primary and nodal GTV) in 57% [43]. In the majority of published studies, the FDG-PET based target volumes were smaller than CT-scan based ones with statistically significant differences [42]. Furthermore, a recent prospective cohort study has shown that FDG PET-CT has a significantly higher detection rate of distant metastasic disease and synchronous cancer than Chest X-ray or Chest CT in combination with MR imaging of the head and neck region [44]. ^{18}FDG-PET is also able to detect residual tumor disease or early recurrences. A pitfall, however, is the presence of inflammation, eg induced by radiation therapy, leading to false positive results.

Other (future) applications of FDG PET-CT

FDG-PET has a wide range of clinical applications. FDG-PET has been studied in HPV positive versus HPV negative oropharyngeal carcinomas. Both morphologic and glycolytic parameters measured on FDG PET-CT are significantly larger in HPV

negative oropharyngeal primary carcinomas. For nodal parameters, results between studies differ, but parameters tend to be higher in HPV positive oropharyngeal carcinomas[45,46].

FDG-PET is also used in the development of Adaptive Radiotherapy Planning (ART). This is based on reassessment of macroscopic tumor volume (GTV) and of organs at risk (OARs) - such as the salivary glands- during radiotherapy treatment, to allow optimization of the radiotherapy plan [42]. FDG-PET has the potential to detect vital cancer tissue before morphologic changes in tissue can be seen. Furthermore, FDG-PET can distinguish between radioresistant and radioresponder areas, leading to a FDG-PET uptake adapted dose distribution. The main problem of FDG-PET during radiotherapy are the possible false-positive results due to radiation-induced inflammatory areas, leading to incorrect target volume expansion. Although re-planning is time consuming, it is expected to result in a more individualized therapy with a decreased probability rate of recurrences and toxicity. However, small numbers of publications are published and there is no strong evidence for the use of ART yet. Especially timing and frequency of re-planning, re-planning procedures etc. are not clarified yet. More studies are needed to confirm its feasibility.

Conclusions

The diagnostic accuracy of FDG-PET/CT for clinically N0 neck patients is low, with the risk of overtreatment when boosting FDG positive lymph nodes. FDG-PET/CT, as opposed to conventional imaging such as MRI, CT or ultrasound is not considered routine practice. In case of clinically positive necks, sensitivity of FDG-PET/CT is higher than conventional imaging. Because patients received primary radiation and histopathology was lacking, we could not confirm the diagnostic accuracy of FDG-PET/CT compared to conventional imaging in our retrospective study. Although this probably resulted in some overtreatment, we reached a high regional control with boosting both PET-positive or CT-positive nodes. To put things in perspective, a 15% or higher chance of positive (metastatic) lymph nodes is considered to justify elective neck treatment. A neck node that is suspect for metastatic disease on FDG-PET or CT has a higher change of being truly positive. Besides the higher sensitivity for nodal disease, FDG-PET/CT has its additional benefits, such as the detection of a second primary cancer or distant metastatic disease.

GENERAL CONCLUSIONS

Medical imaging techniques have been evolving rapidly. Both acquisition and reconstruction of data are far less time-consuming, MRI units as high as 7 Tesla are in clinical use and new techniques, for example diffusion weighted MRI, are becoming standard of care for varying clinical indications. In this thesis, I evaluated its potential and clinical applications in otolaryngology and head and neck disease.

Imaging is used both in diagnostics and follow-up. Diffusion weighted MRI has a place in daily practice for the diagnosis of middle ear cholesteatoma in selected primary cases and in postoperative cases, in some of which a second look operation can be avoided. For middle and inner ear pathology, the use of 7 Tesla MRI does not have a benefit yet in comparison with the 1.5 and 3 Tesla. This also applies for small laryngeal carcinoma, in which 7 Tesla is not feasible yet and 3 Tesla MRI is not yet superior to CT. However we do see clinical potential in 3 Tesla MRI for small laryngeal carcinoma with further technical development of this technique.

FDG-PET/CT in primary head and neck cancer is complementary to routine diagnostics, also for staging of the neck. In case of pathological lymph nodes on PET and/or CT scan, in most cases a high nodal target volume is given.

REFERENCES

1. De Foer B, Vercruysse J-P, Pilet B, et al. Single-shot, turbo spinecho, diffusion-weighted imaging versus Spin-Echo-planar, diffusion-weighted imaging in the detection of acquired middle ear cholesteatoma. *AJNR*. 2006;27:1480–2.

2. Dubrulle F, Souillard R, Chechin D, et al. Diffusion-weighted MR imaging sequence in the detection of postoperative recurrent cholesteatoma. *Radiology* 2006;238:604–10.

3. Jindal M, Riskalla A, Jiang D, et al. A systematic review of diffusion-weighted magnetic resonance imaging in the assessment of postoperative cholesteatoma. *Otol Neurotol.* 2011;32:1243–9.

4. Muzaffar J, Metcalfe C, Colley S, Coulson C. Diffuion-weighted magnetic resonance imaging for residual and recurrent cholesteatoma: a systematic review and meta-analysis. *Clin Otolaryngol.* 2017;42(3):536-543.

5. Songu M, Altay C, Onal K, et al. Correlation of computed tomography, echo planar diffusion-weighted magnetic resonance imaging and surgical outcomes in middle ear cholesteatoma. *Acta Oncolaryngol*. 2015;135(8):776-80.

6. van Egmond SL, Stegeman I, Grolman W, et al. A systematic review of non-echo planar diffusion-weighted magnetic resonance imaging for detection of primary and postoperative cholesteatoma. *Otolaryngol Head Neck Surg.* 2016;154:233–40.

7. Lingam RK, Bassett P. A meta-analysis on the diagnostic performance of non-echoplanar diffusion weighted imaging in the detecting middle ear cholesteatoma: 10 years on. *Otol Neurotol.* 2017;38(4):521-528.

8. Tomlin J, Chang D, McCutcheon B et al. Surgical technique and recurrence in cholesteatoma: a meta-analysis. Audiol Neurotol. 2013;18:135-42.

9. Li PM, Linos E, Gurgel RK, et al. Evaluating the utility of non echo-planar diffusion-weighted imaging in the preoperative evaluation of cholesteatoma: a meta-analysis. *Laryngoscope* 2013;123:1247–50.

10. Nevoux J, Lenoir M, Roger G. Childhoof cholesteatoma. *Eur Ann Otorhinolaryngol Head Neck Dis*. 2010;127-143-50.

11. Nash R, Wong PY, Kalan A, Lingam RK, Singh A. Comparing diffusion weighted MRI in the detection of post-operative middle ear cholesteatoma in children and adults. *Int J Pediatr Otorhinolaryngol*. 2015;79(12):2281-5.

12. Steens S, Venderink W, Kunst D, Meijer A, Mylanus E. Repeated postoperative follow-up diffusion-weighted magnetic resonance imaging to detect residual or recurrent cholesteatoma. *Otol Neurotol*. 2016;37(4):356-61.

13. Özgen B, Bulit E, Dolgun A, Bajin MD, Sennaroglu L. Accuracy of turbo spin-echo diffusion-weighted imaging signal intensity measurements for the diagnosis of cholesteatoma*. Diagn Interv Radiol.* 2017;23(4):300-306.

14. Locketz GD, Li PM, Fischbein NJ, Holdsworth SJ, Blevins NH. Fusion of computed tomography and PROPELLER diffusion-weighted magnetic resonance imaging for the detection and localization of middle ear cholesteatoma. *JAMA Otolaryngol Head Neck Surg*. 2016;142(10):947-953.

15. Campos A, Mata F, Reboll R, Peris ML, Basterra J. Computed tomography and magnetic resonance fusion imaging in cholesteatoma preoperative assessment. *Eur Arch Otorhinolaryngol.* 2017;274(3):1405-1411.

16. Mc Rackan TR, Abdellatif WM, Wanna GB, et al. Evaluation of second look procedures for pediatric cholesteatomas. *Otolaryngol Head Neck Surg.* 2011;145(1):154-60.

17. Britze A, Møller ML, Ovesen T. Incidence, 10-year recidivism rate and prognostic factors for cholesteatoma. *J Laryngol Otol.* 2017;131(4):319-328.

18. Košec A, Kelava I, Ajduk J, et al. Significance of intraoperative findings in revision tympanomastoidectomy. *Am J Otolaryngol.* 2017;38(4):462-465.

19. van der Toom HFE, van der Schroeff MP, Pauw RJ. Single-Stage Mastoid Obliteration in Cholesteatoma Surgery and Recurrent and Residual Disease Rates: A Systematic Review. *JAMA Otolaryngol Head Neck Surg.* 2018;144(5):440-446.

20. Casselman JW, Offeciers EF, De Foer B et al. CT and MR imaging of congenital abnormalities of the inner ear and internal auditory canal. *Eur J Radiol.* 2001;40(2): 94-104.

21. Vd Jagt MA, Brink WM, Versluis MJ, et al. Visualization of human inner ear anatomy with high-resolution MR imaging at 7T: initial clinical assessment. *Am J Neuroradiol* 2015;36:378-83.

22. Sato H, Kawagishi K. Labyrinthine artery detection in patients with idiopathic sudden sensorineural hearing loss by 7T MRI. *Otolaryngol Head Neck Surg.* 2014;150:455-9.

23. Kraff O, Theysohn JM, Maderwald S, et al. High-resolution MRI of the human parotid gland and duct at 7 Tesla. *Invest Radiol.* 2009;44:518-24.

24. Sled JG, Pike GB. Standing-wave and electrodynamic analysis of MRI*. IEEE Trans Med Imaging.* 1998;17:653-62.

25. Brink WM, van der Jagt AM, Versluis MJ, Verbist BM, Webb AG. High permittivity dielectric pads improve high spatial resolution magnetic resonance imaging of the inner ear at 7T. *Invest Radiol* 2014;49:271-7.

26. Thylur DS, Jacobs RE, Go JL, Toga AW, Niparko JK. Ultra-High-Field Magnetic Resonance Imaging of the Human Inner Ear at 11.7Tesla. *Otol neurotol.* 2017;38(1):133-138.

27. Bartling SH, Peldschus K, Rodt T, et al. Registration and fusion of CT and MRI of the temporal bone*. J Comput Assist Tomogr.* 2005;29(3):305-10.

28. Counter SA, Damberg P, Aski SN, et al. Experimental fusion of contrast enhanced high-field magnetic resonance imaging and high-resolution micro-computed tomography in imaging the inner mouse ear. *Open Neuroimag J.* 2015;9:7-12.

29. Labadie RF, Balachandran R, Noble JH, et al. Minimally invasive image-guided cochlear implantation surgery: first report of clinical implementation. *Laryngoscope* 2014;124(8):1915-22.

30. Majdani O, Rau TS, Baron S, et al. A robot-guided minimally invasive approach for cochlear implant surgery- preliminary results of a temporal bone study. *Int J Comput Assist Radiol Surg*. 2009;*4*(5):475-86.

31. Lingam RK, Connor SEJ, Casselman JW, Beale T. MRI in otology: applications in cholesteatoma and Meniere's disease. *Clinical Radiology.* 2018; 73(35-44).

32. Ruytenberg T, Verbist BM, Vonk-van Oosten J, et al. Improvements in High Resolution Laryngeal Magnetic Resonance Imaging for Preoperative Transoral Laser Microsurgery and Radiotherapy Considerations in Early Lesions. *Front Oncol*. 2018;8:216.

33. Bluemink JJ, Raaijmakers AJE, Koning W, et al. Dielectric waveguides for ultrahigh field magnetic resonance imaging. *Magn Reson Med.* 2016;76:1314–1324.

34. Koning W, Bluemink JJ, Langenhuizen EAJ, et al. High-resolution MRI of the carotid arteries using a leaky waveguide transmitter and a high-density receive array at 7T. *Magn Reson Med*. 2013;69:1186–1193.

35. Kyzas PA, Evangelou E, Denaxa-Kyza D, Ioannidis JP. 18F-fluorodeoxyglucose positron emission tomography to evaluate cervical node metastases in patients with head and neck squamous cell carcinoma: a meta-analysis. *J Natl Cancer Inst.* 2008;100:712–20.

36. Yongkui L, Jian L, Wanghan Jingui L. 18FDG-PET/CT for the detection of regional nodal metastasis in patients with primary head and neck cancer before treatment: a meta-analysis. *Surg Oncol.* 2013;22:e11–16.

37. Sun R, Tang X, Yang Y, Zhang C. 18FDG-PET/CT for the detection of regional nodal metastasis in patients with head and neck cancer. A meta-analysis. *Oral Oncol*. 2015;51:314–20.

38. Ozer E, Naiboglu B, Meacham R, et al. The value of PET/CT to assess clinically negative necks. *Eur Arch Otorhinolaryngol* . 2012;269:2411–14.

39. Roh J, Park JP, Kim JS, et al. 18F Fluorodeoxyglucose PET/CT in head and neck squamous cell carcinoma with negative neck palpation findings: a prospective study. *Radiology.* 2014;271:153–61.

40. Lee HJ, Kim J, Woo HY, et al. 18F-FDG PET-CT as a supplement to CT/MRI for detection of nodal metastasis in hypopharyngeal SCC with palpably negative neck. *Laryngoscope* 2015;125:1607–12.

41. De Bree R. The real additional value of FDG-PET in detecting the occult primary tumour in patients with cervical node metastases of unknown primary tumour. *Eur Arch Otohinolaryngol.* 2010;267:1653-1655.

42. Farina E, Ferioli M, Castellucci P, et al. ^{18}F-Fdg-PET-guided planning and re-planning (adaptive) radiotherapy in head and neck cancer: current state of art. *Anticancer research* 2017;37:6523-6532.

43. Wang D, Schultz CJ, Jursinic PA, et al. Initial experience of FDG-PET/CT guided IMRT of head-andneck carcinoma. *Int J Radiat Oncol Biol Phys.* 2006;65:143–51.

44. Rohde M, Nielsen A, Johansen J, et. al. Head-to-Head Comparison of Chest X-Ray/ Head and Neck MRI, Chest CT/Head and Neck MRI, and ^{18} F-FDG PET/CT for Detection of Distant Metastases and Synchronous Cancer in Oral, Pharyngeal, and Laryngeal *Cancer. J Nucl Med*. 2017;58:1919-1924.

45. Tahari AK, Alluri KC, Quoon H, et al. FDG PET/CT imaging of oropharyngeal squamous cell carcinoma. *Clin Nucl Med.* 2014;39(3):225-231.

46. Kendi ATK, Magliocca K, Corey A, et al. Do ^{18}F-FDG PET/CT parameters in oropharyngeal and oral cavity squamous cell carcinomas indicate HPV status? *Clin Nucl Med* 2015;40(3):e196-e200.

APPENDICES

ACKNOWLEGDGEMENTS – DANKWOORD

Iedereen die heeft bij gedragen aan de totstandkoming van dit proefschrift ben ik dank verschuldigd, maar een aantal mensen in het bijzonder.

Geachte professor Grolman, beste Wilko. Jij stimuleerde me om tijdens mijn KNO opleiding te beginnen met wetenschappelijk onderzoek. Eerst op het gebied van de otologie, jouw interessegebied, waarna ik de kant van de hoofd-hals chirurgie op ben gegaan, het vak waar mijn hart ligt. Zonder jouw stimulans en praktische insteek was ik nooit aan dit proefschrift begonnen.

Geachte professor Terhaard, beste Chris. Je begon als begeleider van een artikel en werd gaandeweg mede-promotor van mijn proefschrift. Bedankt voor al je tijd, je inzet en je interesse precies op het juiste moment, ook na de afronding van mijn KNO opleiding in Utrecht. Mede door jou is dit boekje toch nog tot stand gekomen.

Dr. Janssen, beste Luuk. Je hebt me enthousiast gemaakt voor de hoofd-hals chirurgie binnen de KNO. Bedankt voor je tijd, je vertrouwen, alle leermomenten tijdens mijn opleiding in Utrecht, en bedankt voor je inzet en de begeleiding van mijn proefschrift als co-promotor.

Beste Hanneke Bluemink, bedankt voor al je energie en doorzettingsvermogen om de MRI scans voor de kleine larynxtumoren te optimaliseren. En bedankt voor je vrije tijd waarin je hebt gepoogd mij de beginselen van de moeilijke MRI materie bij te brengen.

Frank Pameijer en Jan Willem Dankbaar, bedankt voor jullie radiologische input, kritische houding en jullie tijd voor de beoordeling van de diverse scans.

Beste Bernard (Vonck), bedankt voor je hulp bij LOCATE studie tijdens mijn verlof en mijn vertrek naar het LUMC. Zonder jouw inzet bij de dagelijkse logistiek had ik de LOCATE studie niet goed kunnen afronden.

Geachte leden van de leescommissie, hartelijk dank voor de bereidheid dit proefschrift te lezen en zitting te nemen in de promotiecommissie.

Een woord van dank aan alle collega's in het Leids Universitair Medisch Centrum. Bedankt voor jullie steun bij de afronding van mijn proefschrift en voor het plezier waarmee ik iedere dag naar mijn werk ga.

Bedankt aan alle opleiders van het Antonius Ziekenhuis Nieuwegein, Ziekenhuis de Gelderse Vallei in Ede en Gelre Ziekenhuizen Apeldoorn voor jullie aandeel in mijn opleiding. Professor P.P van Benthem, beste Peter Paul, een speciaal woord van dank aan jou. Naast de inspirerende tijd in Apeldoorn zijn we nu beiden werkzaam in het Leids Universitair Medisch Centrum te Leiden. Ik denk dat we ons geen beter afdelingshoofd kunnen wensen.

Beste collega arts-assistenten KNO en stafartsen van de afdeling KNO-Heelkunde van het Universitair Medisch Centrum Utrecht, bedankt voor de fijne opleidingstijd die ik mede door jullie en met jullie heb gehad. De gezelligheid, de onderlinge saamhorigheid en de vele leermomenten. Ik had het niet willen missen!

Lieve Willemijn, collega AIOS, vriendin, List-vrouw en paranimf. Bedankt voor je hulp als vrijwilliger bij mijn onderzoek, voor je altijd positieve instelling en vrolijkheid, zowel tijdens de opleiding als daarna.

Ik bedank mijn vrienden. Met speciale dank aan mijn lieve vriendinnen van geneeskunde 2000 (Irma, Stef), lieve eetmeiden van culturele antropologie 1999 (Marjolein, Bregje, Lilian, Juletta, Anne-Floor), lieve Mo en Janneke, lieve Carlijn (helaas aan de andere kant van de wereld), wat krijg ik toch veel energie van onze gezellige momenten samen! Ondanks een druk leven kan ik er dan altijd weer tegenaan.

Lieve pap en mam. Bedankt voor jullie onvoorwaardelijke steun, vertrouwen en liefde. Lieve zus, lieve Fenny, wat ben ik blij dat jij mijn zus bent. En wat fijn dat jij als paranimf achter mij wilt staan op deze dag.

De laatste plaats in dit dankwoord is voor Arnoud, Janne, Casper en Cato. Lieve Arnoud, bedankt voor je liefde, je gedrevenheid en ons fijne gezin samen. Lieve Janne, Casper en Tootje, wat hebben jullie een energie en wat zijn jullie vrolijk. Wat een heerlijke afleiding van werk en wetenschappelijk onderzoek. Ik geniet elke dag van jullie!

CURRICULUM VITAE

Sylvia Louise van Egmond was born on September 14th 1981 in De Bilt, The Netherlands. She graduated from the Stedelijk Gymnasium Johan van Oldenbarnevelt in Amersfoort in 1999. In the following year, she studied Cultural Anthropology at Utrecht University. In 2000, she started her medical study at Utrecht University. During her medical study, she followed three internships in Africa (South Africa, Tanzania and Malawi) and she did a research project in Melbourne, Australia. The experience abroad, especially in Africa, inspired her to start a medical specialty in Tropical Medicine after her medical degree, which she received in 2006. During this specialty, she worked at the Surgical department, Gynecology department, and worked in a district hospital in Nickerie, Surinam, for 6 months.

For the long run, she wanted to pursue a career in otorhinolaryngology and she started her residency at the department of Otorhinolaryngology and Head and Neck Surgery of the University Medical Center Utrecht (UMCU) in 2009. During the third year of residency, a first article on 7 Tesla MRI for the inner ear was written, which was the beginning of this thesis. In 2015 she became a medical specialist in Ear Nose and Throat (ENT). Till 2018, she followed a fellowship in Head and Neck Surgery at Leiden University Medical Center and she is now one of the staff members there.